
Theses and Dissertations

Spring 2015

Towards an optimized low radiation dose quantitative computed tomography protocol for pulmonary airway assessment

Alexandra Lynae Judisch
University of Iowa

Copyright 2015 Alexandra Lynae Judisch

This thesis is available at Iowa Research Online: <http://ir.uiowa.edu/etd/1652>

Recommended Citation

Judisch, Alexandra Lynae. "Towards an optimized low radiation dose quantitative computed tomography protocol for pulmonary airway assessment." MS (Master of Science) thesis, University of Iowa, 2015.
<http://ir.uiowa.edu/etd/1652>.

Follow this and additional works at: <http://ir.uiowa.edu/etd>



Part of the [Biomedical Engineering and Bioengineering Commons](#)

TOWARDS AN OPTIMIZED LOW RADIATION DOSE QUANTITATIVE
COMPUTED TOMOGRAPHY PROTOCOL FOR PULMONARY AIRWAY
ASSESSMENT

by

Alexandra Lynae Judisch

A thesis submitted in partial fulfillment
of the requirements for the Master of Science
degree in Biomedical Engineering in the
Graduate College of
The University of Iowa

May 2015

Thesis Supervisor: Assistant Professor Jessica C. Sieren

Graduate College
The University of Iowa
Iowa City, Iowa

CERTIFICATE OF APPROVAL

MASTER'S THESIS

This is to certify that the Master's thesis of

Alexandra Lynae Judisch

has been approved by the Examining Committee for
the thesis requirement for the Master of Science degree
in Biomedical Engineering at the May 2015 graduation.

Thesis Committee:

Jessica C. Sieren, Thesis Supervisor

Joseph M. Reinhardt

Eric A. Hoffman

ACKNOWLEDGEMENTS

I would like to take this opportunity to thank the numerous individuals who have made this work possible. First I would like to thank my thesis advisor and mentor, Dr. Jessica Sieren. Her endless support and guidance are the reason I decided to pursue this incredible opportunity. She encouraged me to learn and challenge myself more than I ever have before. I would like to thank my committee members, Dr. Joseph Reinhardt and Dr. Eric Hoffman. Each helped me with different components of this project so as to allow me complete it to the best of my ability. I would like to thank the members of the Advanced Pulmonary Physiomic Imaging Laboratory (APPIL), including Krishna Iyer and Samantha Dilger for their input and feedback as I worked through the various components of the project. I would like to specifically thank Nicholas Stoyles and Emily Hammond, for allowing me to build off of their work with the lung fixation procedure, Kizhakke Puliyakote, for helping me develop the physical lung segmentation procedure, and Nicholas Koehn and Johanna Uthoff, for their help getting the final pieces put together when it was crunch time. All of their work was invaluable and immensely appreciated. I would also like to thank the members of the Small Animal Imaging Core Laboratory and the workers at Plexicraft. Finally, I would like to thank my family and fiancé for their unconditional love and support always.

ABSTRACT

Lung disease affects tens of millions of Americans, making it one of the most common medical conditions in the United States. Many of these lung diseases are classified as chronic airway disease. Because of this, it is important to identify its development early to begin treatment as soon as possible to delay and subsequently monitor that progression. One method of doing so is the use of quantitative computed tomography (CT). Study of the airway anatomy can be quantified using such measures as minor inner diameter (MinD), major inner diameter (MajD), wall thickness (WT), inner area (IA), and outer area (OA). Changes in these measures can then be tracked over time to determine how the disease affects the airways. The challenge with the desired longitudinal imaging is that cumulative radiation exposure over a lifetime could be dangerous to the patient. To make it more feasible, it is important to determine the quantitative measures that can reliably be made at different CT acquisition radiation doses. In so doing, it will be possible to optimize the CT protocol to minimize radiation dose exposure and still provide accurate quantitative assessment of the target lung structures.

Working to make this determination, three different CT acquisition protocols with decreasing radiation doses were tested to evaluate their quantitative outputs for the lung. A high dose (14.98 mGy), medium dose (6.00), and low dose (0.74 mGy) CT protocol were used to image six different porcine subjects. Images were collected at these doses both while the lungs were in-vivo and once the lungs had been fixed and excised ex-vivo. All of the scans were then processed using Apollo (VIDA Diagnostics). From the complete airway trees, quantitative measures were collected from thirty-five airways. For

the airway tree analysis, the high dose in-vivo scans were used as ground truth to assess MinD, MajD, WT, IA, and OA. In order to determine how well the CT measures represent the actual anatomy, a total of thirteen cube samples containing airways were segmented from one of the lungs (based on volume analysis of the lung pre- and post-fixation and visual inspection). The cubes were imaged in CT, to aid establishment of original location and study the effect of a narrowed imaging window, and microscopic CT (μ CT). Since μ CT can have a resolution on the scale of microns, the values measured in these images were considered ground-truth. The CT and μ CT cubes were then registered to the high dose ex-vivo scan so as to compare the cube values with the ex-vivo values from each of the three doses. The same five measures were collected and analyzed.

The MinD, MajD, WT, IA, OA were statistically analyzed between the three in-vivo radiation dose scan sets, the high dose in- and ex-vivo scans, and the μ CT cube, CT cube, and the three ex-vivo radiation dose sets. Results for the in-vivo scans show that the medium dose scans can reliably ($< 5\%$ error) be used to evaluate airways with MinD greater than 3.5 mm. The low dose scans had less reliable results for assessment of these larger airways ($< 10\%$ error), supporting the use of the medium (6.00 mGy) radiation dose when studying airway disease affecting airways with minor diameters greater than 3.5 mm. Comparison of the high-dose in-vivo and ex-vivo scans showed that the fixation and excision of the lungs did not significantly affect the ex-vivo lungs' ability to be used as a model for the in-vivo lungs. Finally, small airway analysis showed that the CT cube data best matched the μ CT, supporting their use in collecting quantitative data, and the in-vivo individual airways followed the same trends found in the airway tree.

PUBLIC ABSTRACT

Chronic lung airway disease affects millions of Americans. Because it is a permanent condition, it needs to be monitored over time. This can be done using computed tomography (CT) to track changes in lung airway measurements, such as minor inner diameter (MinD), major inner diameter (MajD), wall thickness (WT), inner area (IA), and outer area (OA). Since the radiation from doing repeated CT imaging over time could be dangerous to the patient, it important to determine the lowest CT radiation dose that yields accurate lung airway measurements.

Working to make this determination, three different CT radiation doses were tested on six pig lungs to compare the resulting CT derived airway measurements. This comparison was done between all of the scans of the entire airway tree in the lungs and individual airways that were removed from the lungs and re-imaged in CT and high resolution microscopic CT (μ CT). The MinD, MajD, WT, IA, and OA were found for each of the airways and compared to the values found in the scans with the highest radiation doses.

Results show that for certain airways, the radiation dose used does not change accuracy of the measurements. The results also showed that while removing the lungs from the body did cause some changes in lung structure, these changes are proportional and can be used as a surrogate for the in-vivo situation. Finally, assuming the values from μ CT are the true values, the measures from the identical samples imaged in CT accurately reflect the true values.

TABLE OF CONTENTS

LIST OF TABLES	viii
LIST OF FIGURES	x
CHAPTER 1 INTRODUCTION	1
CHAPTER 2 BACKGROUND	4
2.1 Lung Airway Disease	4
2.2 Pathology-CT Correlations	10
2.3 Registration	12
CHAPTER 3 METHODS	17
3.1 Physical apparatuses.....	17
3.1.1 Ex-Vivo Whole Lung Imaging System	18
3.1.2 Tissue Orientation Management System.....	19
3.2 Data Collection.....	21
3.2.1 In-Vivo Lungs.....	21
3.2.2 Ex-Vivo Lungs	22
3.3 Registration	28
3.3.1 Preprocessing.....	29
3.3.2 Registration Framework	30
3.3.3 Validation	34
3.4 Quantitative Measurement	36
3.4.1 Complete Airway Tree	37
3.4.2 Full-Width Half-Maximum	38
3.4.3 Statistical Analysis	41
CHAPTER 4 RESULTS	42
4.1 Airway Tree Data and Analysis	42
4.1.1 Whole Lung Datasets and Considerations.....	42
4.1.2 Airway Tree Comparison	45
4.2 Individual Airway Cube Data and Analysis.....	59
4.2.1 Single Airway Cube Registration Dataset	59
4.2.2 Individual Airway Comparison	63
CHAPTER 5 DISCUSSION.....	73

5.1 Whole Lung Airway Tree Analysis	73
5.1.1 Dose Effects.....	73
5.1.2 Physical distortion caused by fixation	74
5.2 Individual Airway Comparison.....	75
5.2.1 Method Validation	76
5.2.2 Ex-Vivo Small Airway Analysis	77
5.2.3 In-Vivo Small Airway Analysis	79
CHAPTER 6 FUTURE WORK	80
6.1 Introduction	80
6.2 Expanded Airway Assessment	80
6.3 Parenchyma Assessment	81
6.4 Fixation Refinement for Vascular Examination.....	83
APPENDIX.....	84
REFERENCES	111

LIST OF TABLES

Table 1. T-Test p values across all of the airways for each of the subjects by measure. The values above 0.05 show significance.....	58
Table 2. Correlation values across all of the airways for each of the six subjects by measure. A value of 1.0 would indicate a perfect correlation.....	58
Table 3. Registered images. The single slices from the registered high dose, medium dose, low dose, CT cube, and μ CT cube are shown for each of the thirteen samples.	61
Table 4. Sum of squared differences between the fiducial markers from the stereologically sampled cubes. The registered fiducials had a much small sum of squared differences value.	63
Table 5. Assessment of the FWHM measures. The actual values and calculated values are shown for each of the five measures of interest in addition to the percent errors of the calculated values with respect to the actual.	64
Table 6. FWHM results for the thirteen ex-vivo airways. The calculated values are shown in the one-dimensional values and two-dimensional values columns. Each of the sample types is shown: high-dose (high), medium-dose (med), low-dose (low), CT cube (CT), and μ CT cube (μ CT). The percent errors comparing each of the first four types to the μ CT are shown in the one-dimensional percent errors and two-dimensional percent errors columns. MinD is shown in blue, MajD is red, WT is green, IA is teal, and OA is purple.	65
Table 7. T-test values calculated between the μ CT measures and each of the other sample types' measures. Values of 0.05 indicate that there is not a statistically significant difference present.	69
Table 8. Correlation values between the μ CT measures and each of the other sample types' measures. Values close to 1.0 are desired.	69
Table 9. FWHM results for the five stereologically samples in-vivo airways. The calculated values are shown in the one-dimensional values and two-dimensional values columns. Each of the sample types is shown: high-dose (high), medium-dose (med), low-dose (low), CT cube (CT), and μ CT cube (μ CT). The percent errors comparing each of the first four types to the μ CT are shown in the one-dimensional percent errors and two-dimensional percent errors columns. MinD is shown in blue, MajD is red, WT is green, IA is teal, and OA is purple.	70
Table 10. Percent error values for dose comparison. Each table represents one dose compared with the 14.98 mGy scan as ground truth and values < 0.05 emphasized.	84
Table 11. Percent error values for in- to ex-vivo comparison. Each table compares the 14.98 mGy scans using the in-vivo as ground truth with values < 0.05 emphasized.	96
Table 12. Output values from the full-width half-maximum calculation on the ex-vivo airways. Each of the five locations is shown for each of the thirteen cubes.	102

Table 13. Output values from the full-width half-maximum calculation on the in-vivo airways. Each of the five locations is shown for each of the five.105

Table 14. Post-registration layering. Examples of the registered images are showed layered over one another. Note the distinct appearance of the μ CT cube airway in the images as opposed to the appearance of the CT cube airway. ..106

Table 15. Fiducial alignment pre- and post-registration. The images in the left column are aligned by their centers. The images in the right column are aligned according to the final registration transform.109

LIST OF FIGURES

Figure 1. Airway generations. The lung airway tree can be broken down based on generation (z values) and size (large and small) as seen in this figure from McNulty [2].	6
Figure 2. Registration framework. The two images cycle through the four registration steps until an optimizer stop condition is reached.	13
Figure 3. The ex-vivo whole lung imaging system (EWLIS). The foremost side displays the fifteen slits used to guide the physical segmentation of the lungs.	19
Figure 4. Tissue orientation management system (TOMS). The TOMS was designed to ensure the integrity of the tissue cube sample orientation between imaging systems (CT and μ CT).	21
Figure 5. Axial slices from chest CT data of subject 40016. Three different CT protocols were used (from L-R) high (14.98 mGy), medium (6.00 mGy), and low (0.74 mGy) radiation doses. Increased noise is evident in the heart and soft tissue of the thorax in CT data acquired at lower radiation dose levels.	22
Figure 6. In-vivo and ex-vivo lung comparison. The left image shows the lungs from subject 40016 in-vivo and the right image shows the same lungs ex-vivo. The method of fixation via the vascular system causes blood to be removed from the vessels and hence no longer appears radio-opaque in post fixation CT data.	23
Figure 7. Slicing and sampling of fixed lungs. The lungs were segmented to create axial slices of the lungs and representatively sampled to obtain the cubes.	25
Figure 8. Cube B8L7C2R4 imaged in CT. Each of the cubes was imaged in CT to acquire the highest resolution possible with the SOMATOM CT system. Note the brightness of the wall surrounding the airway.	27
Figure 9. Cube B8L7C2R4 imaged in μ CT. Each of the cubes was imaged in μ CT to use as the ground truth for the airways measures. Note the improved tissue contrast and resolution with comparison to the CT data.	28
Figure 10. Final registration framework. The registration pipeline consisted of a linear interpolator, normalized correlation metric, regular step gradient descent optimizer, and an affine transform.	30
Figure 11. Mode of operation of trilinear interpolation. The linear interpolator used, since applied in three dimensions, is a trilinear interpolator. The black dot represents the final calculated intensity value as explained further in [16].	32
Figure 12. Apollo airway tree. The Apollo software generates a model of the entire airway tree in addition to making measurements of the airways it models.	38
Figure 13. Explanation of collected airway measures. The airway measures collected were (a) minor inner MinD, (b) MajD, (c) IA (d) OA, and (e) WT.	39
Figure 14. Airway tree labels. The airway tree shown was generated by Apollo and the thirty-five airways used were labeled as shown.	43
Figure 15. In-vivo and ex-vivo airway trees. The high dose in-vivo and ex-vivo segmented airway trees are rendered for the six Yucatan miniature pig subjects studied. Note, while minor differences in the segmentation are	

	evident due to the process of fixation and the manual editing required to generate the ex-vivo airway segmentations, the overall integrity and structure of the airway tress is preserved.	44
Figure 16.	(Left) The average and standard deviation of the MinD values across the six subjects for the in-vivo, high CT dose quantitative airway measurements. (Right) Percent error in MinD for the airways measured in the whole lung compared to the high dose values. The standard deviations are shown.....	47
Figure 17.	(Left) The average and standard deviation of the MajD values across the six subjects for the in-vivo, high CT dose quantitative airway measurements. (Right) Percent error in MajD for the airways measured in the whole lung compared to the high dose values. The standard deviations are shown.....	48
Figure 18.	(Left) The average and standard deviation of the WT values across the six subjects for the in-vivo, high CT dose quantitative airway measurements. (Right) Percent error in WT for the airways measured in the whole lung compared to the high dose values. The standard deviations are shown.....	49
Figure 19.	(Left) The average and standard deviation of the IA values across the six subjects for the in-vivo, high CT dose quantitative airway measurements. (Right) Percent error in IA for the airways measured in the whole lung compared to the high dose values. The standard deviations are shown.....	50
Figure 20.	(Left) The average and standard deviation of the OA values across the six subjects for the in-vivo, high CT dose quantitative airway measurements. (Right) Percent error in OA for the airways measured in the whole lung compared to the high dose values. The standard deviations are shown.....	51
Figure 21.	(Left) The average and standard deviation of the MinD values across the six subjects for the in-vivo, high CT dose quantitative airway measurements compared to the ex-vivo measurements. (Right) Percent error in MinD for the airways measured in the ex-vivo lung compared to the in-vivo values.	53
Figure 22.	(Left) The average and standard deviation of the MajD values across the six subjects for the in-vivo, high CT dose quantitative airway measurements compared to the ex-vivo measurements. (Right) Percent error in MajD for the airways measured in the ex-vivo lung compared to the in-vivo values.	54
Figure 23.	(Left) The average and standard deviation of the WT values across the six subjects for the in-vivo, high CT dose quantitative airway measurements compared to the ex-vivo measurements. (Right) Percent error in WT for the airways measured in the ex-vivo lung compared to the in-vivo values.	55
Figure 24.	(Left) The average and standard deviation of the IA values across the six subjects for the in-vivo, high CT dose quantitative airway measurements compared to the ex-vivo measurements. (Right) Percent error in IA for the airways measured in the ex-vivo lung compared to the in-vivo values.	56
Figure 25.	(Left) The average and standard deviation of the OA values across the six subjects for the in-vivo, high CT dose quantitative airway measurements compared to the ex-vivo measurements. (Right) Percent error in OA for the airways measured in the ex-vivo lung compared to the in-vivo values.	57
Figure 26.	Location of sampled cubes in the whole ex-vivo lung. The whole ex-vivo lung is shown in (a) coronal view. Images (b), (c), and (d) show axial cross-sectional slices B8L7, B11L10, and B14L13 respectively.	60

Figure 27. Phantom to test the accuracy of the FWHM algorithm. The image is constructed of a white ring (pixel values 125-255) on a black background (pixel value 0) in order to mimic an ideal airway63

CHAPTER 1

INTRODUCTION

Lung disease lead to the deaths of 235,000 Americans in 2010 and cost the economy nearly \$106 billion. Of these deaths, 135,000 were due to chronic obstructive pulmonary disease (COPD) and 3,000 were due to asthma. While these two diseases are responsible for the deaths of many Americans, they are two of many and millions suffer from them. The number of people diagnosed with COPD in 2010 was 12.7 million and the number of people with asthma totaled 39.5 million [1]. Since many people will develop lung disease well before they are diagnosed, these numbers underestimate the actual rates of occurrence. Based on these statistics, it is clear that the detection, treatment, and monitoring of lung disease is very important. When not detected early and treated properly, acute lung diseases can cause permanent damage to the lungs and contribute to the development of chronic lung disease which can dramatically decrease the patient's quality of life. Airway diseases are commonly diagnosed with a combination of blood testing, pulmonary function testing, and computed tomography (CT).

Since CT offers the ability to study the actual anatomy of the diseased lung and make multiple different quantitative measurements, CT is becoming an ever more prevalent method of assessing lung airway disease, especially in the case of chronic airway disease. In order to use quantitative measurements to monitor airway disease, longitudinal imaging is necessary. Unfortunately, the use of longitudinal imaging risks exposing patients to ionizing radiation. With lifetime cumulative medical radiation exposure levels on the rise, due to increased clinical utility of CT to diagnose and monitor injury and disease, it is necessary to optimize CT acquisition protocols. For each

monitoring task, it is necessary to determine the lowest radiation dose that can be used to accurately assess disease. Quantitative CT measurements may require a different CT protocol than is required for qualitative assessment, but provide the added advantage of objective measures of change that can be tracked longitudinally. One method for approaching this for the airway trees in-vivo is by comparing the values obtained across multiple different radiation doses, making the assumption that the measures derived from the highest radiation dose CT protocol are the most accurate. To further expand the assessment, individual airways imaged in microscopic CT (μ CT) can be included. μ CT is the highest resolution CT currently available that can be used to study lung airways. The inclusion of the μ CT data means that all of the doses tested can be compared, for individual airways, to the μ CT measurements as ground truth and evaluated for their ability to represent the highest resolution quantifications. To ensure that the measures can be accurately compared, image registration can be used to align the images between CT and μ CT. Once aligned, the extracted measures can be assessed for similarity, determining which doses can be used to collect which measures for which airways. For this work, it was hypothesized that the increased image noise due to decreased CT radiation dose would have minimal effect on the measurements of the central airway tree. However, it is expected that airways at the segmental/sub-segmental level will be impacted by CT acquisition dose reduction. This study will reveal the relationship between radiation dose and quantitative measurement with comparison to μ CT acting as ground truth in a final assessment. It is the goal of this study to determine the degree of airway measurement error related to airway size, airway position and, CT acquisition

dose such that this data can be utilized to optimize imaging schemes and identify targeted airways for analysis for future studies.

CHAPTER 2

BACKGROUND

2.1 Lung Airway Disease

Lung disease affects tens of millions of people in the United States, making it one of the most common medical conditions today. According to the National Heart, Lung, and Blood Institute (NHLBI), 235,000 Americans died from lung disease in 2010, 135,000 of which were caused specifically by chronic obstructive pulmonary disease (COPD) [1]. Lung disease can be caused by any number and combination of factors including smoking, various infections, and genetics. Due to the variety of anatomic structures within lungs, lung disease can occur in three different locations: airway (including alveolar), tissue (including interstitial and pleural) and, vascular. While many lung diseases occur in some combination of the tree locations, the airways are often primary location. This is due to the fact that the airways are the mode through which air is introduced to and expelled from the body, making them the first area of exposure to the ill effects of airborne pollutants and/or pathogens.

The airways within the lungs are the pathway through which oxygen is introduced into the body and carbon dioxide is removed. They are essential to functionality of the lungs. Most airways range in size from 0.5 mm to 20 mm in diameter with wall thicknesses of approximately 0.5 mm to 2 mm. As can be seen in Figure 1, these airways can be identified by their generation. Typically, as the generation of the airways increase, their diameter and wall thickness decrease. Arranged in tree-like manner, they begin with the trachea, generation 0, the main airway that connects the rest of the lungs to the pharynx and larynx. As the trachea descends, it splits into the left and right bronchi,

generation 1, leading to the left and right lungs, respectively. From there, the bronchi continue to divide and narrow further and further, by each generation, leading to the various sub-lobes. The narrowest airways, the bronchioles, are at the very ends of the airways trees, superior only to the alveoli, the tiny air sacs that number in the millions, acting as the primary site of gas exchange between the respiratory and cardiovascular systems. While there are some differences in the structures of the human and porcine lungs, specifically the presence of an extra, sixth, lobe in the porcine lungs as compared to the five lobes in the human lungs, the airways and airway trees themselves are very similar. Given this and their physical size and shape similarities, it is appropriate to use the porcine lung as a model through which to study the human lung.

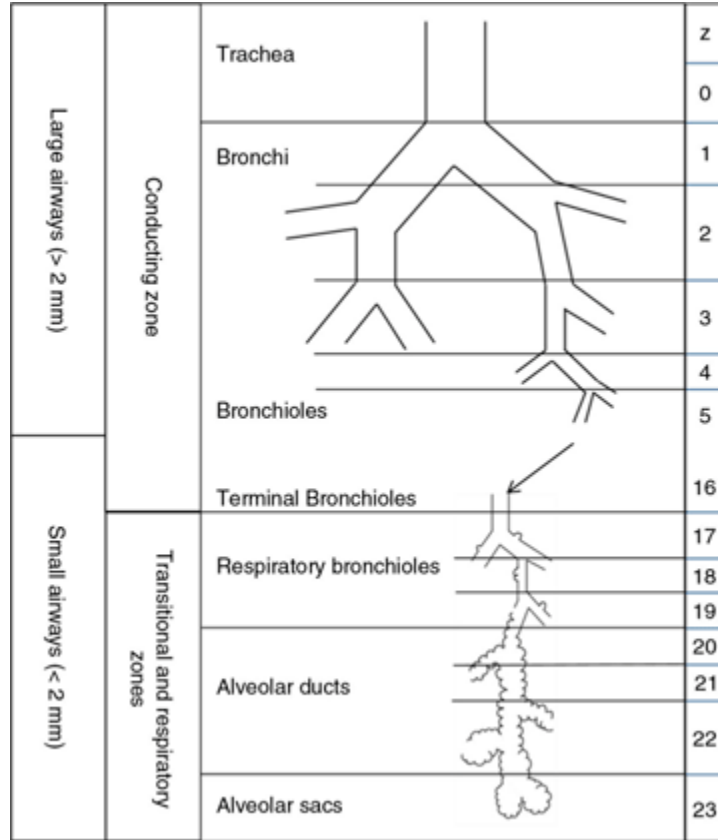


Figure 1. Airway generations. The lung airway tree can be broken down based on generation (z values) and size (large and small) as seen in this figure from West [2].

Damage of the airways can lead to chronic airways disease. One such disease is asthma. Asthma affects some 25 million people worldwide, 7 million of which are children. Asthma commonly affects the bronchi and bronchioles, generations 1-5+. At its core, asthma is an overreaction of these airways to various inhaled particulates due to a pre-existing inflammation of the airways. This reaction causes mucus to build up in the affected airways and can cause the muscles surrounding the airways to contract, further increasing the level of inflammation and mucus present, resulting in a narrowing of the airways. The narrowed airways can lead to the characteristic asthma symptoms of wheezing, chest tightness, short breath, and coughing. Aside from assessing symptoms,

asthma is often diagnosed using spirometry and peak flow tests, both of which make measurements based on the patient's ability to exhale. On occasion, CT scans are also done to evaluate the structure of the airways and identify regions of potential infection or other abnormality. Even though asthma's specific cause remains unknown, it has been determined that genetics, allergies, respiratory infections, and environment can all play roles in its development, and while it is not curable, there are many treatments available to effectively manage its symptoms. The inability to pinpoint the source of asthma or cure it entirely means that there is still much to learn about asthma to improve its diagnosis and treatment.

A second type of chronic airway disease is chronic obstructive pulmonary disease (COPD). COPD is a chronic progressive disease, meaning that it is a long-term disease with no cure that gradually gets worse over time. COPD is the third leading cause of death in America, and is confirmed to be affecting more than twelve million Americans [3]. The primary cause of COPD is smoking, with the majority of those afflicted being active or previous smokers, although there are other air pollutants that have been known to contribute as well as a rare genetic complication. COPD is a complex disease, both with relation to the proportion of emphysema versus bronchitis contributing to obstruction as well as the spatial distribution and variation in disease severity among the lobes of the lung. Spirometry, the clinical standard for COPD severity assessment, provides a quantified measure of overall airflow obstruction but does not indicate cause (emphysema, air-tapping, bronchitis) or distribution (i.e. single lobe disease versus uniform distribution across whole lung). CT can provide valuable insight into both cause and distribution of COPD. Due to the manner in which COPD develops, many people are

unaware of their condition while still in the earliest stages. In fact, it is entirely likely that there are millions of American's with yet-to-be-diagnosed COPD. This is especially concerning because the further along the disease progresses, the worse the patients' quality of life is. This makes early detection, perhaps through the use of CT screening, critical.

COPD is typically a combination of chronic bronchitis and emphysema. Chronic bronchitis is known to affect approximately 9.9 million Americans [4]. It is characterized by inflammation of the bronchi and bronchioles. As the inflammation fails to be corrected it leads to a more permanent thickening of the airway walls and an overproduction of the mucus that lines the airways. Chronic bronchitis cases often occur in current or previous smokers. While acute bronchitis, which can happen easily in conjunction with the common cold, is short in duration, chronic bronchitis is persistent. It is initially diagnosed when its symptoms are present for three or more months in two consecutive years. These symptoms include wheezing, chest tightness, excessive mucus production, and coughing. Over time, this can lead to scarring of the lung tissue and development of other chronic lung diseases. To diagnose chronic bronchitis a physician will assess medical history, smoking history, exposure to air pollutants, and the presence of wheezing. Diagnosis confirmation may then be done by mucus tests, blood tests, pulmonary function tests, and chest x-ray/CT. As mentioned with the previous diseases, early detection is absolutely necessary in extending and improving quality of the life for the afflicted.

Emphysema is a disease that arises from damage done to the alveoli, the tiny air sacs that are found in clusters at the ends of the bronchioles. This damage, often the byproduct of smoking, takes the form of the rupturing of the alveolar walls, resulting in

the clusters of alveoli becoming much larger air spaces. Since the alveoli are the sites at which the oxygen and carbon dioxide exchange between the lungs and the vasculature, rupturing of the walls reduces the amount of surface area present for the exchange to occur, limiting the amount of oxygen that can be delivered to and the carbon dioxide that can be retrieved from the rest of the body. This reduction leads to air trapping, the inability to properly expel carbon dioxide-rich air or bring in the necessary amounts of oxygen-rich air to replace it and often occurs in conjunction with the collapsing of small airways. The primary symptom that manifests is shortness of breath which can increase in severity over time, especially if the patient has a preexisting lung condition like asthma or has a history of smoking. To confirm a diagnosis of emphysema, CT, blood tests, and spirometry, can all contribute. If not monitored, other complications can develop such as pneumothorax, cor pulmonae, giant bullae, pulmonary hypertension, and recurring infections. Emphysema can only be managed, not cured, and if not caught early enough can have a significant impact on quality of life.

One final type of airway disease is cystic fibrosis. Cystic fibrosis is a genetic disease that affects both the pulmonary and digestive systems. It is estimated that 30,000 people in the United States suffer from it [5]. As with many lung diseases, the symptoms of cystic fibrosis include having a persistent cough, frequent lung infections, wheezing, and shortness of breath. These symptoms arise from genetic damage to cells that produce mucus. These cells then produce mucus that is abnormally thick and adhesive, leading to a buildup of it the airways, restricting airflow and increasing susceptibility to all manner of lung infections. The presence of the mucus and recurring infections permanently damages the lungs, leaving increasing amounts of scar tissue and cysts. In adults, cystic

fibrosis is commonly diagnosed using lung function tests, sputum cultures, organ function tests, blood tests, and imaging tests, such as CT and MRI.

2.2 Pathology-CT Correlations

CT is a common form of early detection, diagnosis, and progression monitoring for lung disease. Understanding of the quantitative and qualitative correlation between CT imaging and lung pathology is pivotal in the growing understanding of airway disease. Study of these correlations has been done extensively [6-13].

One class of correlation that has been explored is qualitative assessment. For example, one study by Hruban et al. analyzed the correlations between pathologists and radiologists when grading the emphysema present in the lungs on a scale of zero to one hundred, zero representing no detectable emphysema present and one hundred representing the lungs being entirely overrun with emphysema. The study was done on twenty autopsied patients, focusing on five areas of interest as viewed in axial slices of the lungs. The final results of the study showed a nearly perfect correlation between the radiologic and pathologic assessment, implying that the CT is an accurate physical representation of the lungs [8]. Another study, done by Remy-Jardin, showed a similar outcome with the added warning that in cases where the radiologic and pathologic evaluations do not agree it is mostly likely the case that the CT has underestimated the extent of the emphysema present. The study also found that ground glass attenuation, abnormal alveolar content (i.e. mucus, excessive macrophages), and inflamed alveoli are all readily identifiable in the lungs and correlate strongly with their observations in pathology [10].

Quantitative CT-pathology correlations have not been explored to the same extent in the past, but have become popular areas of interest in recent years due to the increased resolution available in newer CT scanners. The majority of quantitative studies done to date have focused on evaluating low attenuation areas to identify areas in the lung where air trapping is occurring, as in the case of emphysema. According to Coxson and Rogers, previous studies have shown that patients with centrilobular emphysema typically have high percentages of pixel values in the range of -900 to -1000 Hounsfield units (HU) and areas in the lungs that have air spaces of 5mm or greater in diameter have values around -910 HU. Coxson and Rogers also describe how another study concluded that areas in the lungs with values of -950 or lower can reliably be classified as areas of emphysema.

Airway-specific measures commonly collected are wall thickness, airway diameter, and airway area [7]. While these measures tend to correlate strongly between CT and anatomy, the error that is found in the values increases as the size of the airway decreases which further complicates things because Washko's work has shown that fifth and sixth generation airways are most representative of airway disease [13]. Work done by McDonough analyzed the relationship between small airways (<2 mm in diameter) and emphysema. He used μ CT to calculate the mean linear intercept of the airways, minimum diameters, and cross-sectional areas of terminal bronchioles and counted their frequency per mL of lung volume. His results concluded that there were both a loss in cross-sectional area in the airways (81-99.7%) and a reduction in their occurrence frequency (72-89% fewer) [9]. Finally, Hogg's paper suggests that COPD stage correlates strongly with and can therefore be predicted by the wall tissue volume, amount of mucus present, and number of immune system cells present in the airways [6]. As can

be seen from each of these studies, quantitative CT measurements of the airways, particularly small airways, looks to be the future of lung disease assessment. It is because of this that it is becoming more and more important to establish standards for the appropriate radiation dose needed to collect these quantitative measures in order to effectively monitor and diagnose lung disease without putting the patient at unnecessary risk.

2.3 Registration

Image registration is the process of creating a mapping of the each of the points in one image to the points in another image so that the features of one image are aligned with the corresponding features in the other image. This is done by applying a transform to one image to affect its features to establish the correspondence. The image undergoing the transformation is the moving image and the image to which it is being matched is the fixed image. Figure 2 presents the general components of an image registration framework. Registration can be used to solve all types of imaging challenges, whether the images differ in collection time, resolution, dimension, modality, or even image subject. Because each of these problems requires a unique approach, there are many different types of interpolators, metrics, optimizers, and transforms and combinations in which they can be used.

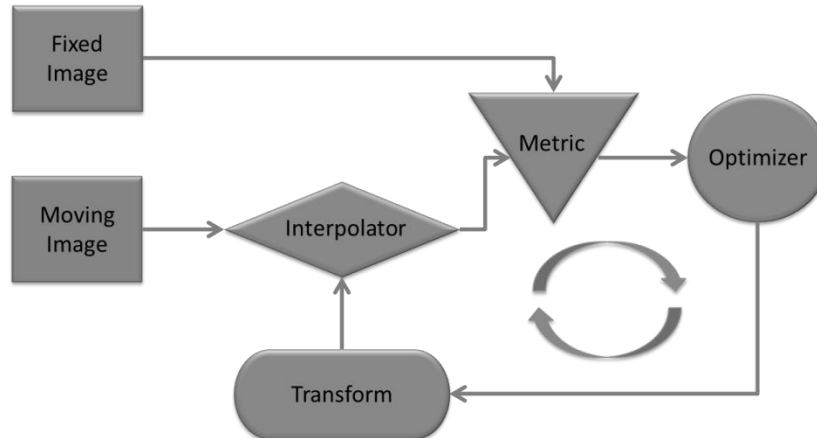


Figure 2. Registration framework. The two images cycle through the four registration steps until an optimizer stop condition is reached.

Image interpolation is the process of taking an image of one resolution and using its pixel intensity values to determine the appropriate corresponding pixel values for the same image at a different resolution. When the interpolation is being used to go from a higher resolution to a lower resolution it is known as image downsampling. When it is used to go from a lower resolution to a higher resolution it is known as image upsampling. There are several types of image interpolators that are commonly used: nearest-neighbor, linear, and B-spline. Nearest-neighbor interpolation is the simplest and fastest of the algorithms. Simply put, the nearest-neighbor algorithm determines the value of the new pixel by assigning it the value of the previously existing pixel that is closest to it. Linear interpolation determines the value of the new pixel by taking a weighted average (based on proximity) of the surrounding existing pixels. Linear interpolation is known as bilinear interpolation when applied to a two-dimensional image and trilinear interpolation when applied to a three-dimensional image series. This method of interpolation is more time-consuming than the nearest-neighbor approach but is also

much more accurate because it considers more neighboring points. B-spline (short for basis spline) interpolation uses a combination of the surrounding pixel intensity values, which are used as the discrete function coefficients, and a chosen continuous function to compute the intensity value of the new pixel. While this is by far the most costly of the three methods, it is also the best when dealing with more complex image problems. Choosing the best interpolator for the registration is necessary for ensure that the resolution changes made to each of the images are as accurate as possible to ensure that the final image is true to the original input images.

The second component of the registration is the metric. The metric is the measure of how well the fixed image matches the moving image. It is also known as the similarity metric. The three primary metrics are mean squares, normalized correlation, and mutual information. The mean square metric works by calculating the sum of squared differences between the pixel values in the images. The mean square metric is only effective for images of the same modality since the intensity values need to be within the same range for the sum of squared differences calculation to be as effective as possible. It is the simplest and least time-consuming metric. The normalized correlation metric works by calculating the correlation between the pixel intensity values in the two images and normalizing them based on the average and standard deviation of the intensity values in each image. This metric is useful when the pixel values do not fit within exactly the same range but are still related linearly. It is more costly and more accurate than the mean square metric. Mutual information is the metric most often used in complex registrations where there are significant differences in the intensity ranges of the two images. Mutual information relies on the calculation of the entropy of an image. To use mutual

information, the entropy of each image is calculated based on the probabilities of each of its intensity values and the joint entropy of the images together is based on their joint probabilities. The actual mutual information is then determined by subtracting the entropies of each of the images from the joint entropy. Since mutual information is the most costly metric, it is generally only used when the particular registration necessitates it, as is the case when different modalities are being registered.

Optimization is an essential part of image registration. The role of the optimizer is to adjust the values within the transform so that the alignment of the images will improve on the next iteration. The optimizer's manipulation of the transform is guided by the value of the metric, having an array of scales that can be adjusted so as to manually influence the transform's parameters. Examples of optimizers used for image registration include the Gaussian-Newton, Levenberg-Marquardt, and gradient descent. Gaussian-Newton optimizers are very fast and general optimizers, ideal for images that are collected from data that resembles a Gaussian curve. They typically sacrifice accuracy for speed. The Levenberg-Marquardt optimizer is an improvement on the Gaussian-Newton method, incorporating least-squares to make it more robust. The Levenberg-Marquardt method is slower than the Gaussian-Newton but also more accurate. A final example of a registration optimizer is the gradient descent optimizer. The gradient descent optimizer works by calculating the gradient and then taking a step in the direction of the greatest negative gradient. The gradient descent optimizer is one of the most common optimizers and tends to perform the best within a wide variety of registration problems. Selection of the most appropriate optimizer plays a significant role in determining the final accuracy and run-time of the registration.

The final component of the registration is the transform. Transformation is the method by which the moving image is altered to align with the fixed image. There are three overarching types of transforms. They are rigid, affine, and deformable. Rigid transforms involve rotation, translation, and scaling. They involve the least amount of change in the image, preserving lengths, angles, and parallel lines. This type of transform is most useful when there is little difference in the subjects of the images at the times of their collection and when it is necessary to preserve the original images as closely as possible. Affine transforms go one step beyond rigid transforms. In addition to rotation, translation, and scaling, they allow shearing. While still maintaining parallel lines, the lengths of the lines and the angles between individual pixels are no longer maintained. Affine transforms are ideal then the moving image has been uniformly deformed from the fixed image. When deformation of the image has not occurred in a uniform manner, then a more drastic transform is needed. This is done using a deformable transform. Of the different types of transforms, deformable is the most ill-defined. It is not restricted to maintaining parallel lines, line length, or pixel relational angles. Deformable transforms are necessary when significant deformation is present either because of different modalities, large growth over time, or any other large-scale change. The transform is the visible action of the registration, the image manipulation that results in the final registered image.

CHAPTER 3

METHODS

This study sought to establish a method of evaluating quantitative airway measures made using images collected with different doses in CT for the purpose of determining the dosage requirements for airways of various sizes. In order to do this, two physical apparatuses were developed for the purpose of segmenting lungs into cube samples and positioning those lung samples consistently between imaging. In-vivo and fixed, ex-vivo whole lung CT scans were collected at three different radiation dose levels. The ex-vivo lungs were then sectioned into cubes and scanned with a tightened field of view, and resolution, in CT and μ CT. To compare the airways in the lung samples with the airways in their original locations in the whole lungs, an image registration pipeline was created. Finally, statistical analysis was done on the individual airways to determine the relationships between the various doses and samples. The following sections describe the procedure used at each step in the data collection and processing. Ultimately, this pipeline was established to observe the impact of fixation on the airway structure and the relationship between CT acquisition parameters (particularly focused on radiation dose) and airway measurement.

3.1 Physical apparatuses

Accurate comparison of computed tomography scans begins with proper orientation management. For the purpose of this study, two different orientation management tools were created.

3.1.1 Ex-Vivo Whole Lung Imaging System

The first tool is the ex-vivo whole lung imaging system (EWLIS). It is a box in which the ex-vivo lungs are placed for the purpose of maintaining orientation between the collection of the CT scans and following physical segmentation of the lungs into slices (Figure 3). The EWLIS was designed virtually using Pro-E (Pro-Engineer, PTC, Needham, MA) and constructed with the help of Plexicraft in Iowa City, Iowa. It was built out of Delrin, a medical grade plastic that is radio-lucent, ensuring a lack of interference with the collection of the CT scans. Its dimensions are 44cm x 27.5cm x 38.5cm. These dimensions were determined based on the need to be able to comfortably hold the excised lungs while still allowing for enough room to completely surrounding the lungs with spray foam to secure them and small enough to fit into the bore of the CT scanner. The EWLIS is comprised of five individual pieces fitted together with fish tail grooves to form the four sides and bottom of the box. The ability to deconstruct it was designed for ease of removal of the lungs, collection of the cube samples, cleaning, and storage. The largest opposing sides contain fifteen opposing slits that run vertically. The slits were designed to act as a guide, allowing a 10in knife to pass through both sides and follow a straight path the height of the box, and are 2.5cm apart so that each slice is 2.5cm thick since the target size for the cubes was 2.5cm x 2.5cm x 2.5cm.



Figure 3. The ex-vivo whole lung imaging system (EWLIS). The foremost side displays the fifteen slits used to guide the physical segmentation of the lungs.

3.1.2 Tissue Orientation Management System

The second tool developed was the tissue orientation management system (TOMS). The purpose of the TOMS was to maintain orientation of the lung cubes samples between imaging in CT and μ CT. It was designed virtually using Pro-E and constructed with the help of Plexicraft in Iowa City, Iowa. The TOMS consists of three main components, the primary piece being the stand (Figure 4). The stand was made out of Plexiglass, a polycarbonate often used in medical imaging because of its complete lack of radio-opacity. This was especially important because μ CT is highly sensitive to the densities of materials near the sample, making it crucial to be aware of any potential

sources of beam hardening artifact. Its dimensions, 5.5cm x 10cm x 6.5cm, were chosen so that it would be small enough to fit in the bore of the μ CT scanner but still be large enough to clearly appear within the field of view of the CT scanner. The second component is three identical pieces. They are the pegs, specifically three drywall anchors. The pegs were inserted into the three slots in slanted component of the stand to act as skewers to hold the sample in place. They also were intended for use as fiducial markers since their angled positioning places them in slightly planes within the scans and their plastic composition makes them show up as bright spots within the scans. The final component is the stand-end, a piece made with Plexiglass that holds one extra peg. The stand-end slides onto the end of the stand and serves as a means of protecting the sample from coming into contact with the μ CT scanner and providing it extra physical support. The TOMS was specifically designed for use with the I-CLIC MicroCAT (*Siemens Medical Solutions, Erlangen, Germany*) system. Due to technical malfunctions in this μ CT system at the time of data collection, data was collected using a Siemens Inveon μ CT system (*Siemens Medical Solutions, Erlangen, Germany*) without incorporating the physical unit of the TOMS. However, the constraints used to design the stand were still applied in the collection of the images.

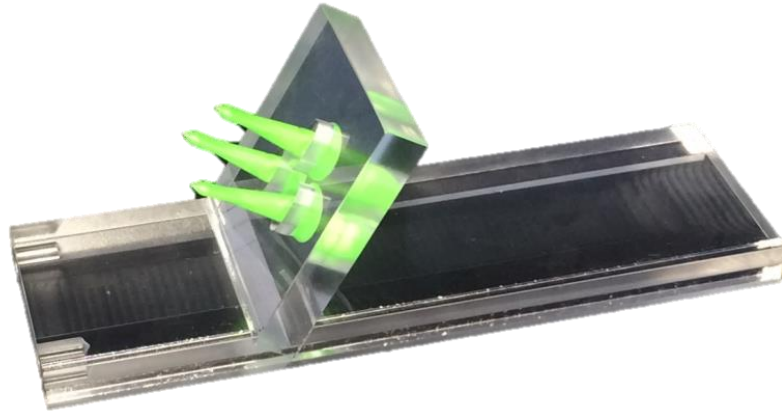


Figure 4. Tissue orientation management system (TOMS). The TOMS was designed to ensure the integrity of the tissue cube sample orientation between imaging systems (CT and μ CT).

3.2 Data Collection

Yucatan miniature pigs were used as the test subjects for this study, due to close similarity in physical size of the thorax and lungs to humans, and access to complete lung specimens for intra-thoracic lung fixation. A progressive pipeline was utilized to acquire CT data in-vivo, following lung fixation (ex-vivo), from isolated sections of the lung (slices and cubes) and with high resolution μ CT (cubes).

3.2.1 In-Vivo Lungs

The in-vivo CT scans used for this study were collected during the course of another study [14]. Prior to imaging, the subjects underwent anesthetization and intubation to allow for mechanical control of respiration and static lung volume during CT acquisition. Physiological monitoring (ECG, EtCO₂, SPO₂) throughout the study ensured appropriate levels of anesthesia and respiration were maintained. All scans were acquired with an enforced static inspiratory volume of 25 cmH₂O. A Somatom Definition CT (Siemens Medical Solutions, Erlangen, Germany) was utilized to gain chest CT data with three different protocols: high (14.98 mGy), medium (6.00 mGy) and

low (0.74 mGy) radiation exposure (Figure 5). Radiation exposure was adjusted by changing the effective mAs (222mAs, 89mAs, and 11mAs respectively) while the remaining acquisition parameters were held constant: 120kV, pitch of 1, 0.5sec rotation time. Data was reconstructed with 0.75 mm slice thickness using a medium iterative reconstruction kernel (I30).

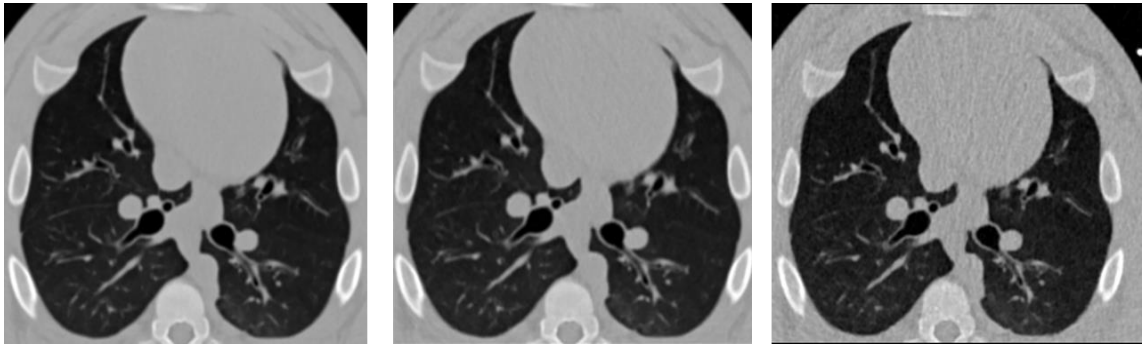


Figure 5. Axial slices from chest CT data of subject 40016. Three different CT protocols were used (from L-R) high (14.98 mGy), medium (6.00 mGy), and low (0.74 mGy) radiation doses. Increased noise is evident in the heart and soft tissue of the thorax in CT data acquired at lower radiation dose levels.

3.2.2 Ex-Vivo Lungs

After the in-vivo images were collected, the six sets of lungs were fixed and extracted from the subjects. This was done by first performing a tracheostomy so as to be able to continue mechanical ventilation maintenance done through endotracheal intubation. Then a median sternotomy was done to expose the lungs in the chest cavity. Upon exposure of the chest cavity, the lungs were isolated from surrounding anatomical structures and perfused with a flush solution of hespan and heparin, followed by a fixative solution of polyethylene glycol 400, formaldehyde, ethanol, and distilled water. When the perfusion was complete, the chest cavity was filled with excess fixative solution, so as to completely submerge the lungs, and closed, to continue to fix the lungs in a manner that was as structurally accurate as possible. After the completion of the final

in-vivo fixation step, the lungs were carefully removed from the body and dried at 27 degrees Celsius for 72 hrs. Once the lungs were dry, they were scanned in using the same imaging protocol as the in-vivo lungs (see 3.2.1 In-Vivo Lungs) (Figure 6). The optimal set of ex-vivo lungs was then selected for further evaluation based on the whole lung and lung tissue volume, as quantitatively compared to the corresponding high dose in-vivo lungs, in addition to qualitative assessments of the shape and tissue integrity.

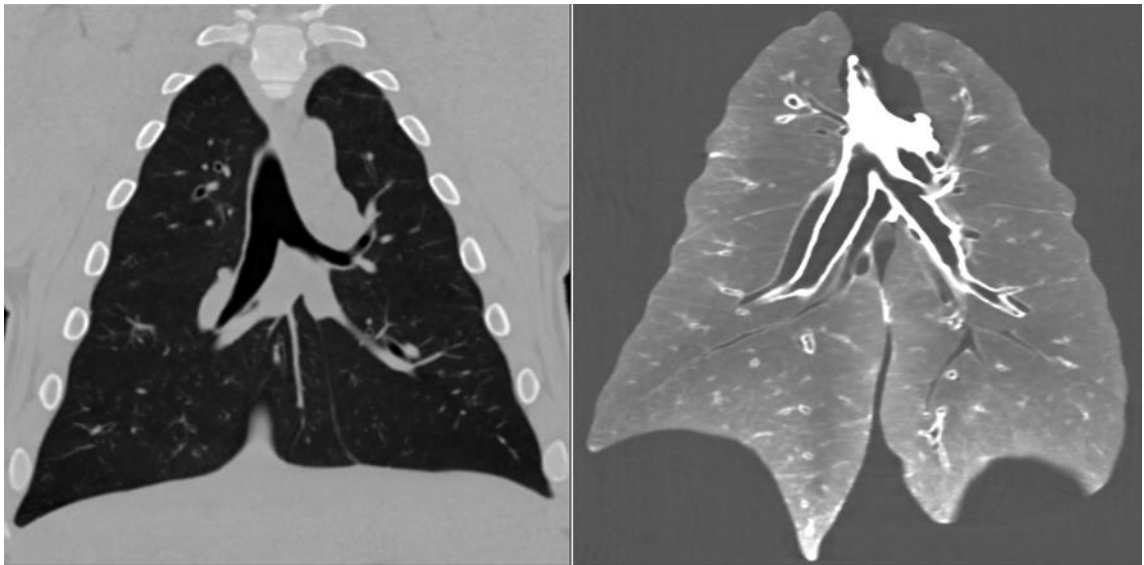


Figure 6. In-vivo and ex-vivo lung comparison. The left image shows the lungs from subject 40016 in-vivo and the right image shows the same lungs ex-vivo. The method of fixation via the vascular system causes blood to be removed from the vessels and hence no longer appears radio-opaque in post fixation CT data.

3.2.2.1 Sliced Lungs

To prepare the pair of lungs for sectioning, the trachea tube from the fixation procedure, was removed. The interior of the EWLIS was lined with parchment paper to ease the setting up and removal of the lungs. The bottom of the interior of the EWLIS was coated with a thick layer spray foam insulation so as to provide a place for the lungs to sit elevated from the base. The lungs were then wrapped in a thin layer of medical gauze so as to aid in the segmentation of the lungs from the foam since the densities of

the two are so similar. After wrapping the lungs, they were placed on top of the first layer of foam so as to have the base of the lungs aligned with one slit and resting in an orientation such that the slits in the opposing sides of the EWLIS line up with the lungs in such a manner that when the slices were made they would be axial, corresponding to the standard method for viewing and assessing lung CT images. Once the lungs were placed in the proper position, more spray foam insulation was added around the lungs, approximately up half of the height of the box, so as to provide the necessary support the lung from the sides. The foam was allowed to set up for six hours to ensure that it could expand maximally and dry. After the six hours, the remaining foam was added, fully covering the lungs. This was allowed to set up overnight, ensuring that everything would solidify properly. The following morning, the lung-foam block was removed from the EWLIS and scanned in CT.

Upon collection of the lung-foam block scan, the lungs were returned to the EWLIS. The lungs were then sliced using a 10-inch knife. The lungs and foam were cut at all fifteen slits resulting in sixteen 2.5cm slices with a total of nine containing lung tissue (Figure 7). The slices were named based on a two-part labeling system. The first part of the name specifies the location of the particular slice in relation to the front of the box and the second part of the name refers to its position relative to the first slice containing the trachea. This meant that the eighth slice in the box was labeled B8L7 (since the trachea began in the second slice). Basic stereological sampling methods were utilized to obtain samples representative of the whole lung, based on the volume of the lung and the size of the sample [15]. To determine which slices to include, a simple random number generator was used, resulting in the selection of the third lung slice

(B8L7). Due to the sampling pattern, the sixth (B11L10) and ninth (B14L13) lung slices were also used. The slices were then imaged in CT, temporarily removed from the foam, in the same orientation that they were in when imaged as part of the whole lung, using the high dose CT protocol described above (see 3.2.1 In-Vivo Lungs). These images were collected to use later as a reference to locate the cube samples for the purpose of initializing the registration.

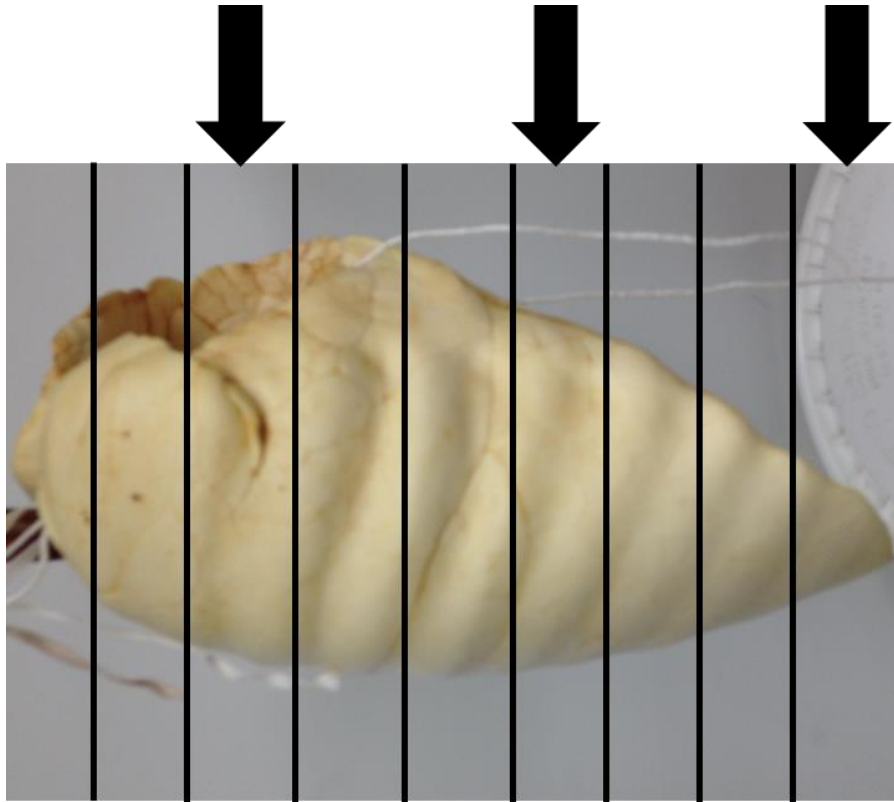


Figure 7. Slicing and sampling of fixed lungs. The lungs were segmented to create axial slices of the lungs and representatively sampled to obtain the cubes.

3.2.2.2 CT Cubes

The cubes were segmented from the three selected slices using one of the sides of the EWLIS. This was done for each slice as follows. The slice (both lung and foam) was laid on a sterile drape on the countertop. One of the slit sides of the EWLIS was placed on top so that the lines ran vertically down the length of the slice and one of the slits

aligned with the leftmost edge of the lungs. Strips were then made by running the knife along each of the slits, shifting the EWLIS side as needed to segment the entire slice. Without moving the strips, the slits were then rotated so as to place them perpendicular to their former position, now aligning one of the slits with the topmost point of the lungs. The same procedure was followed, dividing the strips from the previous step into the desired cubes. The cubes containing lung tissue were then labeled using a modification of the labeling system used for the slices. In addition to the original slice's box and lung locations, the column and row location of the cube within the slice is also included. So, the cube from slice B8L7 that was selected from column five, row three was designated as B8L7C5R3. Again, this is critical for determining the cube's original location within the whole-lung CT. A total of fifty-four cubes were collected.

Two cohorts of cubes were created for analysis: A) stereologically sampled cubes to be representative of the whole lung (n=10) and B) an additional airway targeted dataset (n=10). For the *stereologically sampled cohort*, the cubes were sampled in a similar manner to the slices. The cubes were lined up according to rows and then columns within rows. A random number generator was used to randomly select the forty-sixth cube. Since the literature encouraged the use of ten samples [15], every fifth cube was selected based on the first randomly selected cube. The *small airway targeted cohort* of samples was collected based on the identification of all cubes containing target sized airways ($\leq 2\text{mm}$ minor inner diameter) in the ex-vivo lung data. An example of one of the cubes collected can be seen in Figure 8.

Prior to imaging the stereologically sampled cohort, fiducial markers were inserted into the cubes. The fiducial markers were three small plastic sticks inserted at

varying angles and depths into the superior side of each of the cubes. To image the cubes in CT, the cubes were lined up one after the other, each laying supine with the superior side entering the scanner first, so that all of the cubes could be imaged at once. The data was acquired using the high dose CT protocol described above (see 3.2.1 In-Vivo Lungs) resulting in final dataset voxel size of 0.488 x 0.488 x 0.500 mm.

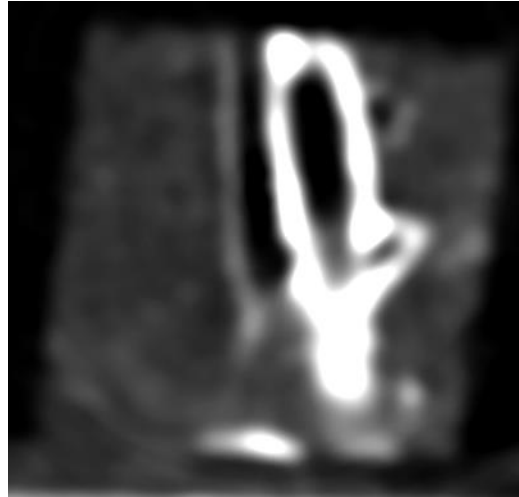


Figure 8. Cube B8L7C2R4 imaged in CT. Each of the cubes was imaged in CT to acquire the highest resolution possible with the SOMATOM CT system. Note the brightness of the wall surrounding the airway.

3.2.2.3 μ CT Cubes

The final stage of imaging was to image the lung cubes in the μ CT scanner. To do this, the cubes were each imaged supine with the superior side entering the scanner first. The scanner used was a small-animal Inveon PET/CT/SPECT imaging system (Siemens Medical Solutions, Erlangen, Germany). The CT function used was a cone beam with a variable focus x-ray source, a 165 mm detector, and a 10cm x 10cm field of view. It was run with a voltage of 80 kV and a current of 500 μ As. Because of the considerable time it took to run the scanner and reconstruction, and the size of the

resulting image size (1024 x 1024 x 1024) and voxel size (0.043 x 0.043 x 0.043 mm), the use of the μ CT scanner was the limiting factor in determining the number of cubes samples to image. One of the cubes imaged is shown in Figure 9.

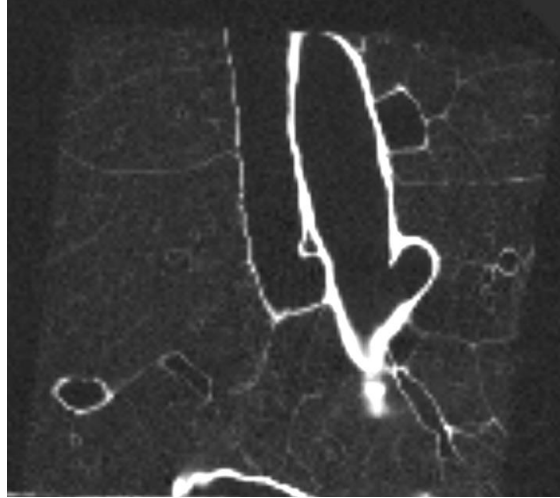


Figure 9. Cube B8L7C2R4 imaged in μ CT. Each of the cubes was imaged in μ CT to use as the ground truth for the airways measures. Note the improved tissue contrast and resolution with comparison to the CT data.

3.3 Registration

In order to be able to most accurately compare the quantitative measures of the airways extracted from the lung cubes and whole lungs, the images needed to be registered. The registration helped to manipulate the cube images in such a way as to reverse the changes that occurred in the process of sectioning the lungs. This includes the differences in imaging orientation and any slight deformation that may have happened at the edges of the cubes a result of the slicing with the knife.

3.3.1 Preprocessing

The CT cubes were processed in several stages using 3D Slicer (<http://www.slicer.org>). The first was to find the location of the cubes in the ex-vivo lungs, precisely the slice-determined cropped CT scans. Each cube was located in its corresponding CT crop based primarily on the labeling system, initially finding an area of approximately three cube-widths to ensure that the selected area included the cube. The area was then narrowed as much as possible using the airways and other anatomy. This was done for each of the cubes resulting in the selection of thirteen limited areas with which to register each of the cubes. The second stage of processing, done only on the stereologically sampled datasets of CT and μ CT cubes, was to create a cropped copy of the scans, eliminating the slices that contained the fiducial markers. This was done so that the registration could be done without the bright spots of the fiducial markers influencing the registration of the natural structures and so that the registration could later be evaluated by applying the output transforms to the fiducials. The next step done in the processing of all thirteen samples was to downsample and smooth the μ CT cubes. The cubes were downsampled using linear interpolation to a voxel size of $0.215 \times 0.215 \times 0.215$ mm, such that the resolution difference between μ CT and CT cube was 2 fold (as opposed to 10 fold). This was done because the higher resolution was not necessary for the registration to calculate the final transform, which could later be applied to the original image. Finally, masks of the thirteen airways were created. The masks were made using an Otsu threshold filter. The Otsu threshold filter was chosen because it uses a clustering algorithm to reduce a grayscale image, i.e. a CT scan, to a binary image. With the proper thresholds assigned, the filter can be used to automatically segment the

airway of interest from the rest of the lung tissue, as it was in this case. The resultant binary images were then used as masks so that the registration was based primarily on the airways and not the surrounding vessels. This preprocessed data was used to calculate the registration transform, such that the transform could be applied to the original, highest resolution μ CT data.

3.3.2 Registration Framework

The code for the registration was written using the Insight Segmentation and Registration Toolkit (ITK, Kitware, New York, USA). The registration used was a three stage multiresolution registration, adjusting the resolutions of the images each time, from the coarsest resolution to the finest, to improve the quality of the final registration. At the beginning of each stage, the output image from the previous stage is used as its initialization. Within each stage of the registration, each of the four major components of the framework, as pictured in Figure 10, are manipulated based on the resolution used at that stage.

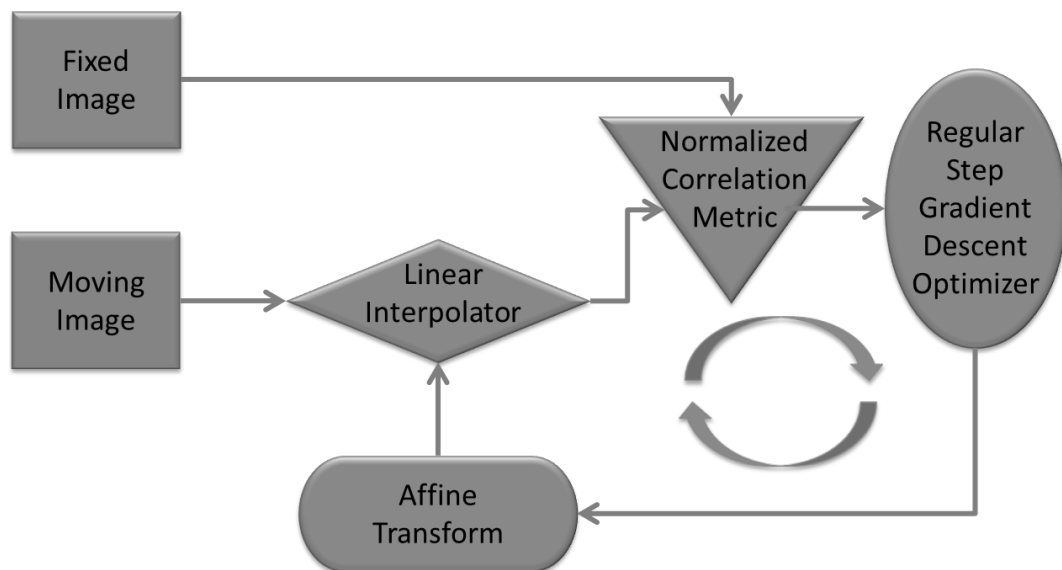


Figure 10. Final registration framework. The registration pipeline consisted of a linear interpolator, normalized correlation metric, regular step gradient descent optimizer, and an affine transform.

3.3.2.1 Interpolator

The registration algorithm used a three-dimensional linear interpolator, a trilinear interpolator (Figure 11). The interpolator was used to fill in the new pixel intensity values when the image resolutions were changed at the start of each stage of the registration. This was necessary because the images collected were discrete representations of a continuous scene, meaning that regardless of the initial resolution, there was data missing. So, to determine the missing values, the weighted average (based on proximity) of the surrounding preexisting pixels in the x, y, and z directions was calculated. At each stage of the registration, the linear interpolator was the first filter the images passed through. A linear interpolator was chosen because it is a commonly used interpolator for CT images since they are produced by linear systems and collected by linear detectors. The specific interpolator used was the `itkLinearInterpolateImageFunction`.

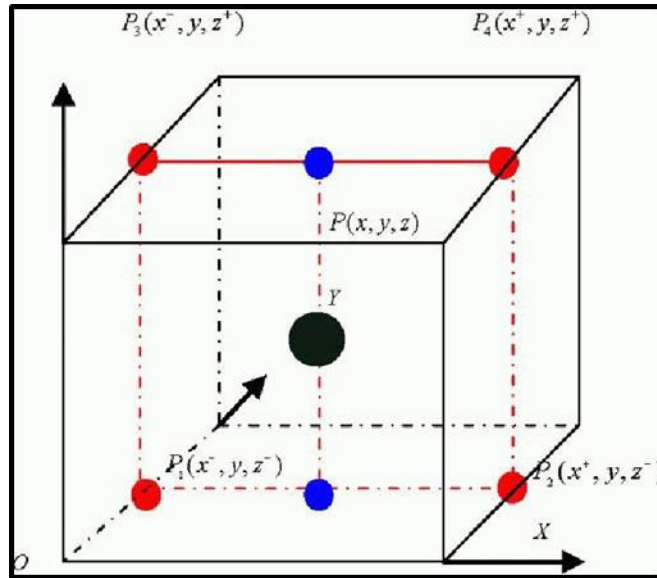


Figure 11. Mode of operation of trilinear interpolation. The linear interpolator used, since applied in three dimensions, is a trilinear interpolator. The black dot represents the final calculated intensity value as explained further in [16].

3.3.2.2 Metric

The purpose of the metric in the registration was to assess the alignment of the fixed image and the most recent transformation of the moving image. This evaluation was done after each new transform was applied to the image. The metric used for this registration was a normalized correlation metric (Equation 1). Normalized correlation is a commonly used metric for registration of CT images. This is because the pixel intensity values in CT are measured in Hounsfield units (HU). The use of HU ensures that the images, no matter where they fall on the scale, will be related linearly which is ideal for the use of normalized correlation. The differences in the ranges of intensity values in the images are first accounted for by normalizing the images based on their averages and standard deviations. Then, the correlation between the normalized images is calculated. The output value represents the quality of their alignment. The version of the metric used

from the ITK library, the `itkNormalizedCorrelationImageToImageMetric`, represents the value as a negative number so as to work with the minimization done in the optimizer.

So, a perfect correlation value would have been -1.

Equation 1. Normalized correlation (NC) equation. The moving image is represented by m , its average pixel value by \bar{m} the fixed image is represented by f , its average pixel value by \bar{f} , n is the number of pixels in the two images, σ is the standard deviation in the specified image, x is the x coordinate of the current pixel, and y is the pixel's y coordinate.

$$NC = \frac{1}{n} \sum_{x,y} \frac{(m(x,y) - \bar{m})(f(x,y) - \bar{f})}{\sigma_m \sigma_f}$$

3.3.2.3 Optimizer

The optimizer of the registration is the mode by which the metric is assessed and subsequently influences the manipulation of the transform parameters in the image registration. The optimizer used, the `itkRegularStepGradientDescentOptimizer`, was a gradient descent optimizer. The optimizer first calculated the gradient of the metric. Then, the optimizer took a step in the direction of the steepest negative gradient. The optimizer was the portion of the registration framework whose parameters were manually controlled the most. In this registration, there were 12 different optimizer scales that were manipulated, one corresponding to each of the parameters of the affine transform. In addition, the minimum and maximum step size and maximum number of steps taken were pre-set in order to strictly control the action of the optimizer to guide it to the best result as quickly as possible. This optimizer was chosen because it is a very commonly used optimizer and works extremely well with the normalized correlation metric chosen

since the metric is designed to output negative values to allow the optimizer to work towards minimization.

3.3.2.4 Transform

During each iteration of the registration, once the images had run through the interpolator, metric, and optimizer, they were passed into the transform. The first transform was initialized with a centered transform initializer. This aligned the centers of the images, based on their geometric centers. The transform itself was an affine transform, the `itkAffineTransform`. The affine transform allowed the image to be rotated, translated, scaled, and sheared. This ensured that the parallel lines within the image were maintained while allowing the lines to slide past one another. An affine transform is an intermediate between rigid and deformable transforms, accounting for restricted deformation to occur to align the images. This transform was chosen because the procedure to segment the cubes from the lungs may have caused slight shearing from the motion of the knife and compromised the orientation of the cubes in the images collected. An affine transform could correct these complications without altering the data unnecessarily, protecting the integrity of the data. Once the transform was determined, it was applied to the original (not downsampled) μ CT data, such that no loss of information was incurred.

3.3.3 Validation

It is important, when performing image registration, to have some mode of assessing the quality of the final image alignment. This can be done through any combination of qualitative and quantitative methods, as long as the baseline of what represents a successful registration is established.

3.3.3.1 Visual Assessment

Qualitative analysis of the registration framework was done using the layering tool found in Slicer. The layering tool allowed for the images to be overlaid on one another to form a composite image by altering the transparency of one image to show the second image behind it. This allowed for the images to be visually inspected and assessed by how visible physical structures aligned between the original fixed image and the final transformed moving image.

3.3.3.2 Metric Assessment

Quantitative analysis of the registration framework was done by calculating the sum of squared differences values for the fiducials in the five stereologically sampled datasets, making the comparison between the CT and μ CT images. Since both sets were registered to the ex-vivo, high dose, whole lung data, a successful registration algorithm would result in the alignment of their two independently registered sets since they contained the same airways. To compare the locations of the fiducials pre- and post-registration, the final transforms output from the registration were applied to the original images (the images as they were before the cropping done as described in 3.3.1). This transformed the fiducials in the same manner the rest of the cube had been during the registration. In order to compare the fiducials, the pre-transformation images first had to be aligned by their geometric centers. This was done because the original images did not overlap in their physical space coordinates, making it impossible to use them, as they were, as a basis of comparison. Since the registration transform was initialized by aligning the images by their geometric centers, this provided continuity in the assessment. Next, the fiducials in the untransformed and transformed images were identified

according to their centers. The centers of the fiducials were used due the differences in appearance of the fiducials in CT and μ CT. In the μ CT images, the fiducials are distinct and angular, just as they are physically. On the other hand, in CT the fiducials are ovular, with no visible corners, making it impossible to accurately identify anything other than their center. The x, y, and z components of the three fiducials markers' locations (in physical space coordinates) were compared between the CT and μ CT by calculating the squared difference for each and summing across all fiducials for each pair of cubes.

3.4 Quantitative Measurement

Five different quantitative measures were used to evaluate airway characterization: major inner diameter (MajD), minor inner diameter (MinD), wall thickness (WT), inner area (IA), and outer area (OA). These measures were collected in two different manners: A) The airway trees were analyzed using a pre-existing software package, Apollo (VidaDiagnostics, IA, USA) to explore the relationship between CT radiation dose level and airway measurement throughout the whole lung (pre and post fixation), and B) To explore the impact of CT radiation dose level on peripheral airways ($\leq 2\text{mm}$ MinD), the individual airways found in the collected samples were analyzed using a script written in MATLAB (MathWorks, Inc., Natick, Massachusetts, United States) based on the use of full-width half-maximum (FWHM) to make the necessary calculations. This was done to compare two datasets. The first was the ex-vivo dataset. For this assessment, the μ CT dataset was considered the gold standard to which the lower resolution CT data extracted values were compared. The second was the in-vivo dataset. For this assessment, the high dose CT dataset was used as the gold standard for which to compare the two lower dose datasets.

3.4.1 Complete Airway Tree

The processing of the in-vivo and ex-vivo whole lungs was done using Apollo with the intent to assess the impact of fixation on airway tree structure. Once the CT scan data were loaded in the Apollo workstation, the software automatically segmented the airway tree (Figure 12). Since Apollo is designed to process in-vivo lungs, they required little manual segmentation to supplement the initial automatic segmentation. However, due to the absence of the chest wall as a point-of-reference for the airway segmentation in the ex-vivo lungs, they required extensive manual segmentation to correct and expand the automatic segmentation. This involved correction of the trachea, since the trachea tube was left in the lungs during imaging, identification of the main bronchi, since the vasculature in the lungs had been emptied during fixation, causing it to appear air-filled in the same manner the airways do, and expansion of the peripheral airways. Following initial segmentation of the airway tree, the merging tool was used to refine each branch segment and unique airway labels were applied. Finally, the software was used to generate quantitative reports on the airway trees from the three in-vivo doses and the ex-vivo high dose. As mentioned above, the primary measures of interest extracted from these reports for later analysis were MajD, MinD, WT, IA, and OA.

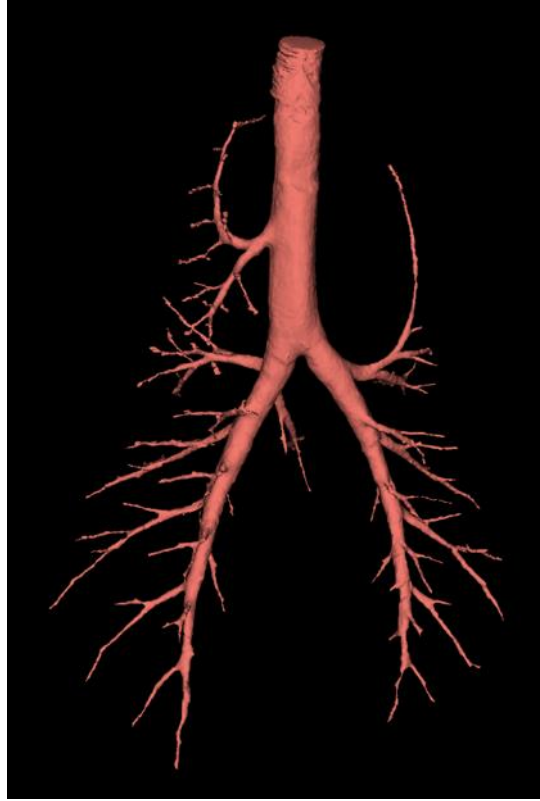


Figure 12. Apollo airway tree. The Apollo software generates a model of the entire airway tree in addition to making measurements of the airways it models.

3.4.2 Full-Width Half-Maximum

The full-width half-maximum (FWHM) algorithm was developed to assess the dimensions of airway structures in the registered, airway sample data (μ CT, cube CT and, ex-vivo CT). Since it relies only on the relationships between with pixel values within an image, the FWHM was chosen so that individual airways could be compared across doses and imaging modalities. Prior to measuring the airways, the FWHM was tested on a phantom. The phantom was a manufactured volume of a white ring (inner diameter = 360 pixels, outer diameter = 400 pixels) centered on a black background spanning three slices. The image was made to represent what a perfect airway sample would be, including the gradual decrease of the pixel intensity values from the center of the ring

wall. The first step in calculating the FWHM was to normalize the image so that minimum pixel value was mapped to 0 and the maximum value was mapped to 255. This ensured the integrity of the later calculations. The next step in testing the phantom was to trace the outer edge of the ring. The tracing was then used to calculate its center. Next the script was run, drawing rays from the centroid of the ring out to the edges of the image, crossing the inner and outer edges. Rays were drawn every 3 degrees around the centroid, resulting in a total of 120 rays in each slice and 360 rays total. Each of the rays was then plotted by distance from the centroid and pixel intensity. From the maximum pixel intensity, the half-maximum intensity was determined. On either side of the pixel at which the maximum value occurred, the pixel with the closest intensity to the half-maximum was located. These two pixel locations represent the start and end locations of the full-width. Using the pixel locations and the physical size of each pixel, the average MajD, MinD, WT, IA, and OA were calculated (Figure 13).

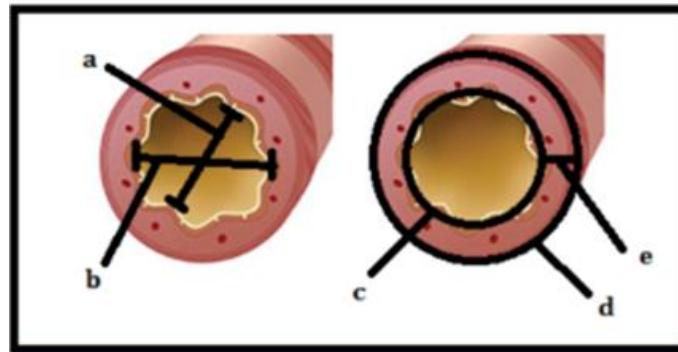


Figure 13. Explanation of collected airway measures. The airway measures collected were (a) minor inner MinD, (b) MajD, (c) IA (d) OA, and (e) WT.

3.4.2.1 Ex-Vivo Individual Airways

Upon confirmation that the FWHM algorithm could accurately measure the phantom, the ex-vivo airways were evaluated. The thirteen airways used, one from each

of the cubes, were selected by visually determining which airway in each of the cubes was most cross-sectional. Cross-sectional airways are the most circular and allow for the most accurate quantitative measurement collection. The thirteen airways were studied in the high dose, medium dose, and low dose CT scans as well as the CT cube and the μ CT cube, resulting in a total of sixty-five iterations of the FWHM for the ex-vivo dataset. For each of the iterations, this was done by first going through the scans so as to determine the three slices that show the airway most clearly, in order to be able to average the calculated values across multiple slices. Then the scan was cropped to include only the three selected slices. Once the airways were cropped, they were run through the FWHM code in the same manner the phantom had been. The use of this FWHM method for the dataset was necessary for making the quantitative measures for the individual airways because the Apollo software is designed to process the airway tree as a whole and cannot handle the images of the CT and μ CT cubes.

3.4.2.2 In-Vivo Individual Airways

As an extension of the in-vivo dose comparison mentioned in section 3.4, the FWHM calculations were also done on a subset of the cube airways as they appeared in-vivo. To do this, the five airways selected from the stereologically sampled cubes (as described in section 3.4.2.1) were located, as closely as possible, in the whole in-vivo lungs at all three doses. The resultant fifteen airways were run through the FWHM script in the same manner in the ex-vivo ones were. The use of this FWHM method for this dataset was done to expand upon the full airway tree assessment by looking at airways that are smaller than what Apollo can typically measure with accuracy in order to evaluate the dose effects for these airways.

3.4.3 Statistical Analysis

Statistical analysis of the quantitative measures was done using percent error and paired t-testing. Percent error was used to compare the values obtained during the multiple dose in-vivo scanning. The high dose, 14.98 mGy, scan was used as ground truth to which the medium, 6.00 mGy, dose and low, 0.74 mGy, dose were compared. A test of percent error reveals how close two series of values are in respect to the assigned expected value. A level of five percent error or less was desired. To assess the in-vivo and ex-vivo scan in addition to the CT and μ CT cube samples, a t-test was used. This t-test evaluated whether or not two datasets vary uniformly. This allows for the specific values within each set to differ from each other while still determining their relationship. Once again, the desired value was 0.05.

CHAPTER 4

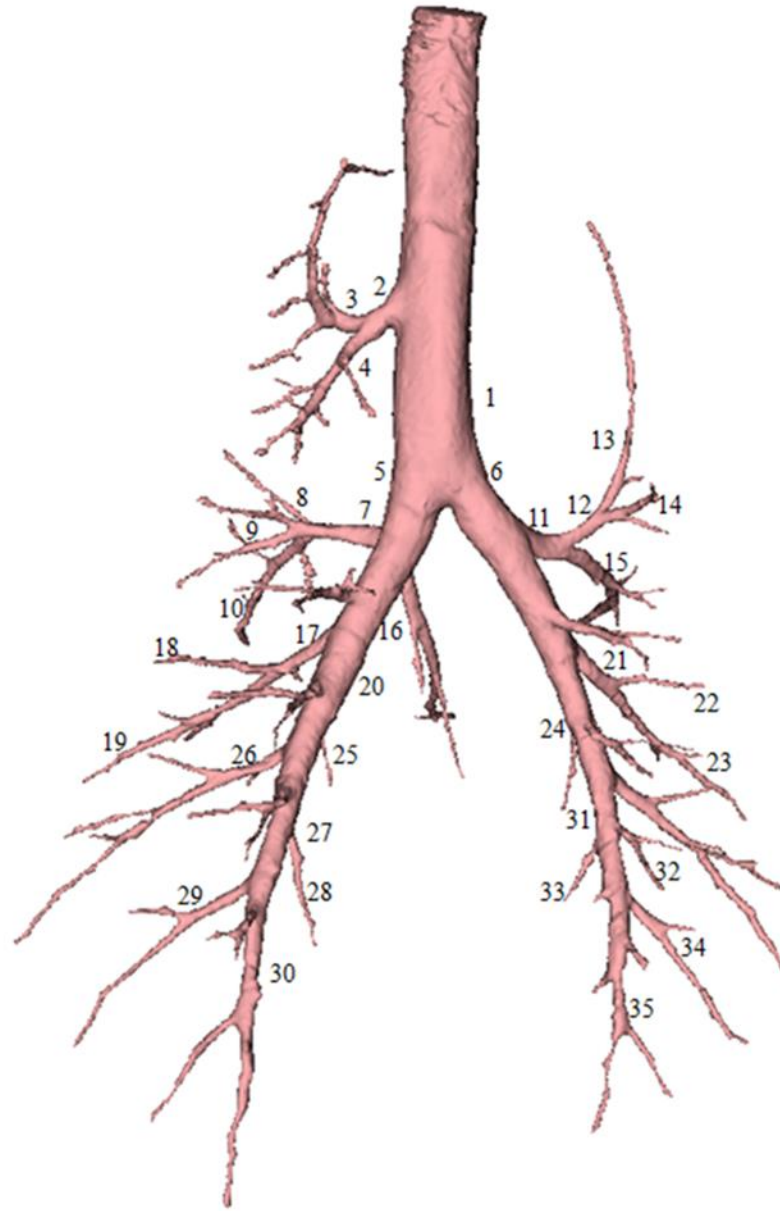
RESULTS

4.1 Airway Tree Data and Analysis

Each of the datasets used to produce the following results were collected from the lungs of six Yucatan miniature pigs. The subjects weighed an average of $33.3\text{kg} \pm 7.0\text{kg}$ and had an average lung volume of $1739.0\text{mL} \pm 133.9\text{mL}$.

4.1.1 Whole Lung Datasets and Considerations

There were four clusters of datasets used for the whole lung airway tree analysis. They were originally collected as part of the work done by Stoyles [14]. Prior to the fixation and excision of the lungs, each of the six subjects were imaged in CT per the procedure described in the methods section. These in-vivo images were collected at a high dose (14.98 mGy), medium dose (6.00 mGy), and low dose (0.74 mGy) for the purpose of establishing the relationship between the quantitative airway measures collected from each. Figure 14 shows the labeling system used to identify the airways. Following the fixation and excision of the lungs, they were imaged ex-vivo at 14.98 mGy. This dataset was then compared to the high dose in-vivo data collected. Figure 15 illustrates the segmented high dose in-vivo and ex-vivo airway trees for the six subjects. It should be taken into consideration that this data was collected as a part of Stoyles' study to establish the best fixation procedure to accurately model the lungs ex-vivo. Because of the changes that were made to the procedure regarding fixation time and lung environment, not every fixation was done identically.



1	T2
2	RB1-1
3	RB1-2
4	RB1-3
5	RMB
6	LMB
7	RB2-1
8	RB2-2
9	RB2-3
10	RB2-4
11	LB1-1
12	LB1-2
13	LB1-3
14	LB1-4
15	LB1-5
16	RMB-3
17	RB4-1
18	RB4-2
19	RB4-3
20	RB6
21	LB4-1
22	LB4-2
23	LB4-3
24	LMB-5
25	RMB-6
26	RB7
27	RMB-7
28	RB8-3
29	RB8-2
30	RB8-1
31	LB6
32	LB8-3
33	LMB-6
35	LB8-1
35	LB8-2

Figure 14. Airway tree labels. The airway tree shown was generated by Apollo and the thirty-five airways studied were labeled as shown.

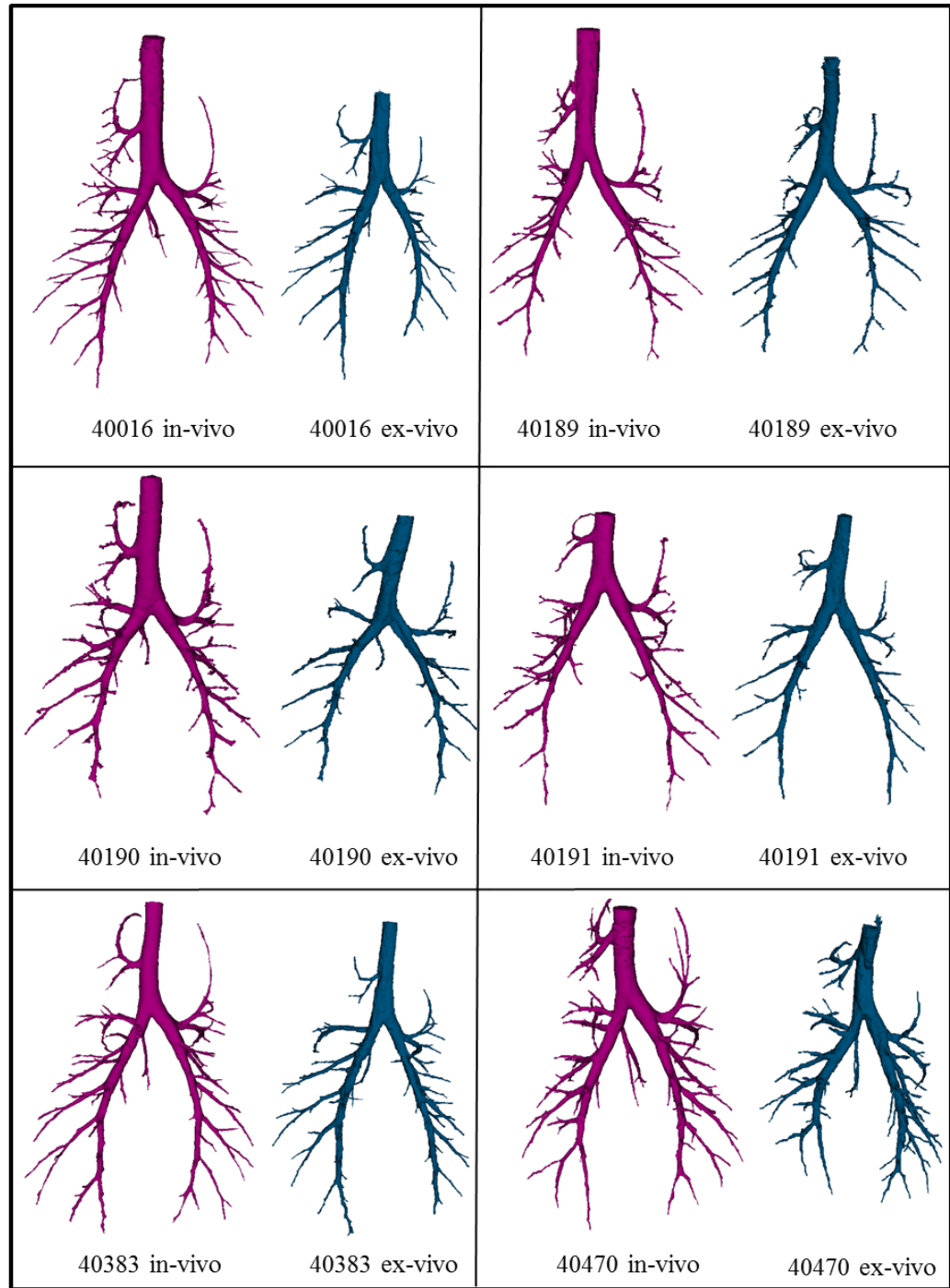


Figure 15. In-vivo and ex-vivo airway trees. The high dose in-vivo and ex-vivo segmented airway trees are rendered for the six Yucatan miniature pig subjects studied. Note, while minor differences in the segmentation are evident due to the process of fixation and the manual editing required to generate the ex-vivo airway segmentations, the overall integrity and structure of the airway trees are preserved.

4.1.2 Airway Tree Comparison

Airway tree comparison was done on the in-vivo and ex-vivo whole lungs for the purpose of comparing the quantitative measures collected across doses for the in-vivo scans and assessing the differences in the measures collected between the in-vivo and ex-vivo lungs.

4.1.2.1 Multiple Radiation Dose Apollo Comparison

Comparison of the quantitative in-vivo airway tree measures collected from the 6.00 mGy (medium) and 0.74 mGy (low) radiation dose CT scans was done by calculating the absolute percent error of the values based on the assumption that values from the 14.98 mGy (high) dose CT were ground truth. Figure 16, Figure 17, Figure 18, Figure 19, and Figure 20 demonstrate both the mean measurement value across subjects for each airway, and the percent error for the measurements made in the low and medium CT dose protocols for the five measures of interest: MinD, MajD, WT, IA and OA. Using the Apollo analysis software, airways ranging from 1.29-15.70 mm MinD and 2.01-38.91 mm MajD were assessed, with WT from 0.83-2.29 mm. When comparing the airways geometries between animals, relative consistency was found in the standard deviation of these airway measures with an exception being the RB1-1 airway branch. The RB1-1 airway is unique to the pig (apical lobe) and proved challenging to consistently delineate the start of this airway branch, resulting in higher standard deviation and error rates for this airway. Another factor contributing to the error in RB1-1 that caused error in other airways as well was a nearly perpendicular orientation with respect to the trachea. This could have caused problems since the airway trees are analyzed axially, so if an airway was not cross-sectional in that plane there was a greater potential for error. Analysis done

on the percent error values calculated (Table 10) revealed that airways with MinD greater than 3.5 mm can be reliably measured for all measures with both the 6.00 mGy ($< 5\%$ error) and the 0.74 mGy ($< 10\%$ error) dose with no consistent over- or underestimation of the 14.98 mGy measures.

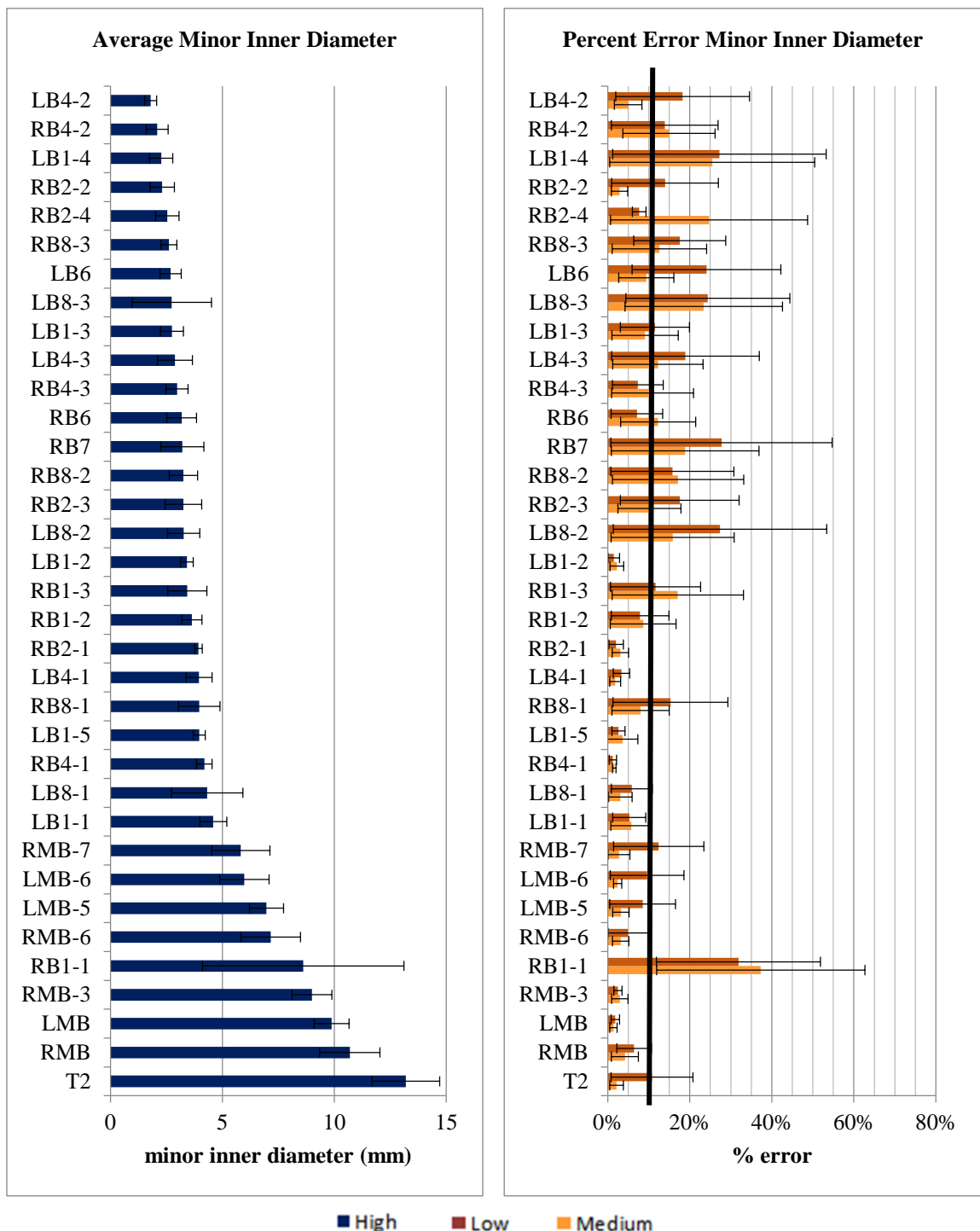


Figure 16. (Left) The average and standard deviation of the MinD values across the six subjects for the in-vivo, high CT dose quantitative airway measurements. (Right) Percent error in MinD for the airways measured in the whole lung compared to the high dose values. The standard deviations are shown.

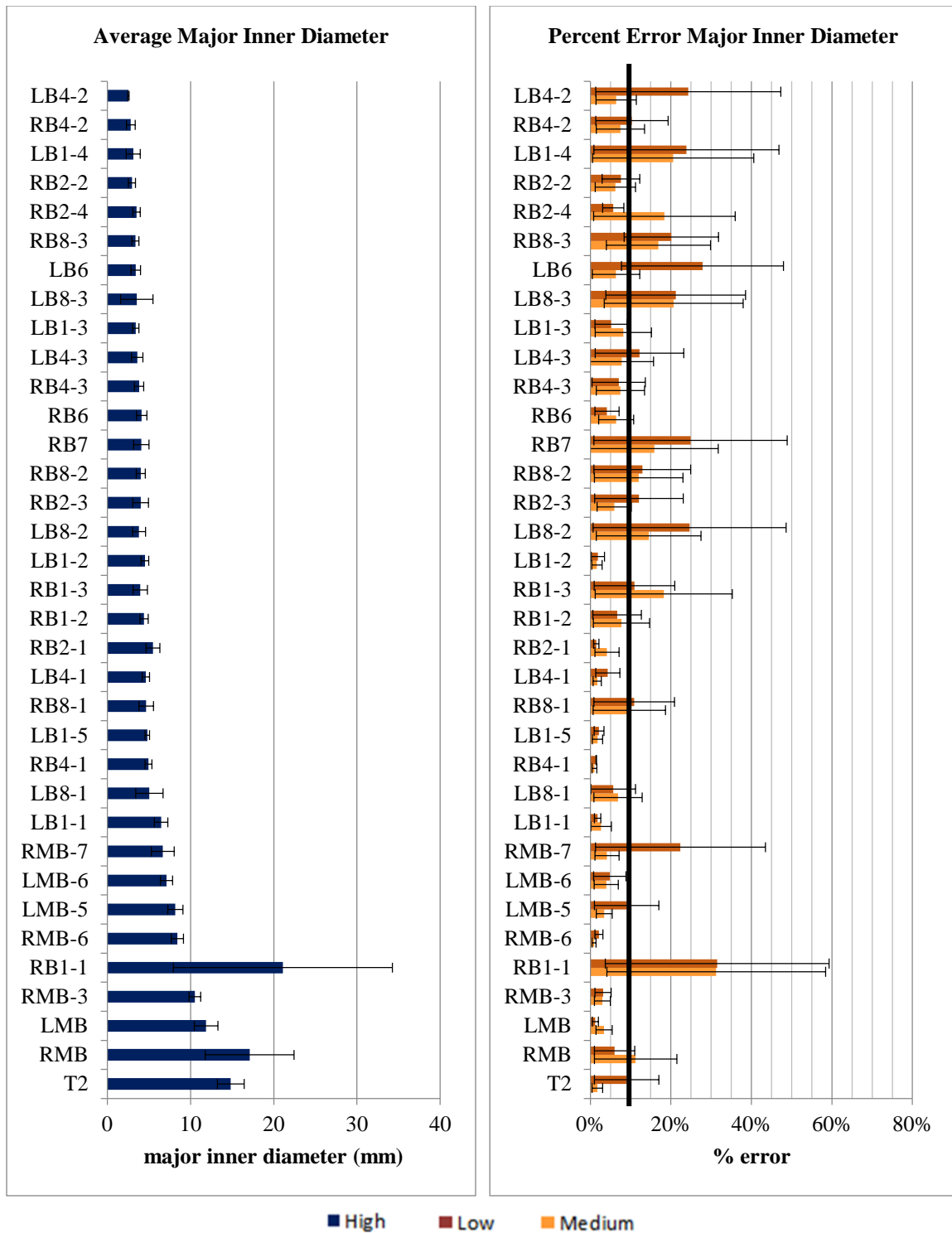


Figure 17. (Left) The average and standard deviation of the MajD values across the six subjects for the in-vivo, high CT dose quantitative airway measurements. (Right) Percent error in MajD for the airways measured in the whole lung compared to the high dose values. The standard deviations are shown.

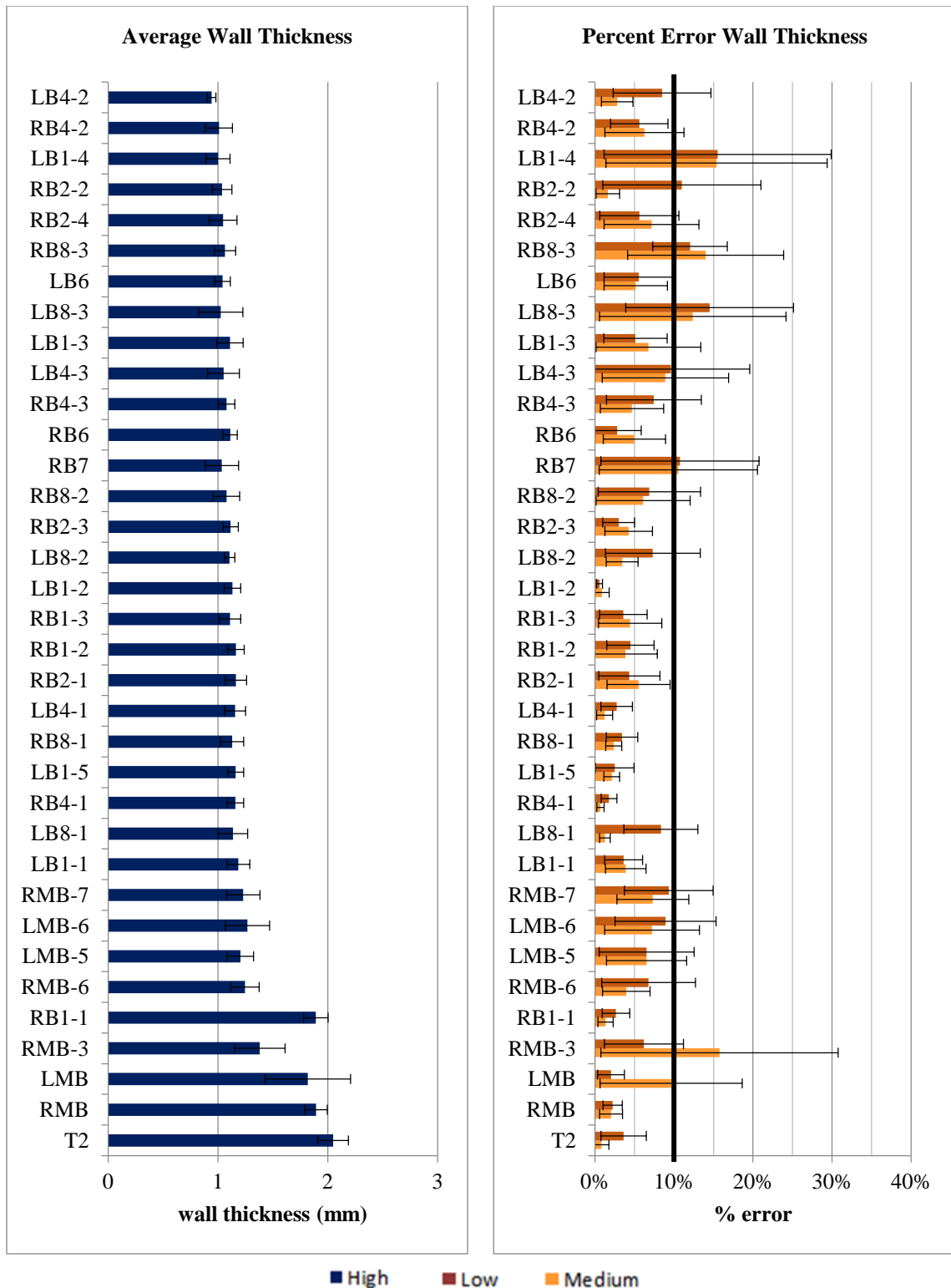


Figure 18. (Left) The average and standard deviation of the WT values across the six subjects for the in-vivo, high CT dose quantitative airway measurements. (Right) Percent error in WT for the airways measured in the whole lung compared to the high dose values. The standard deviations are shown.

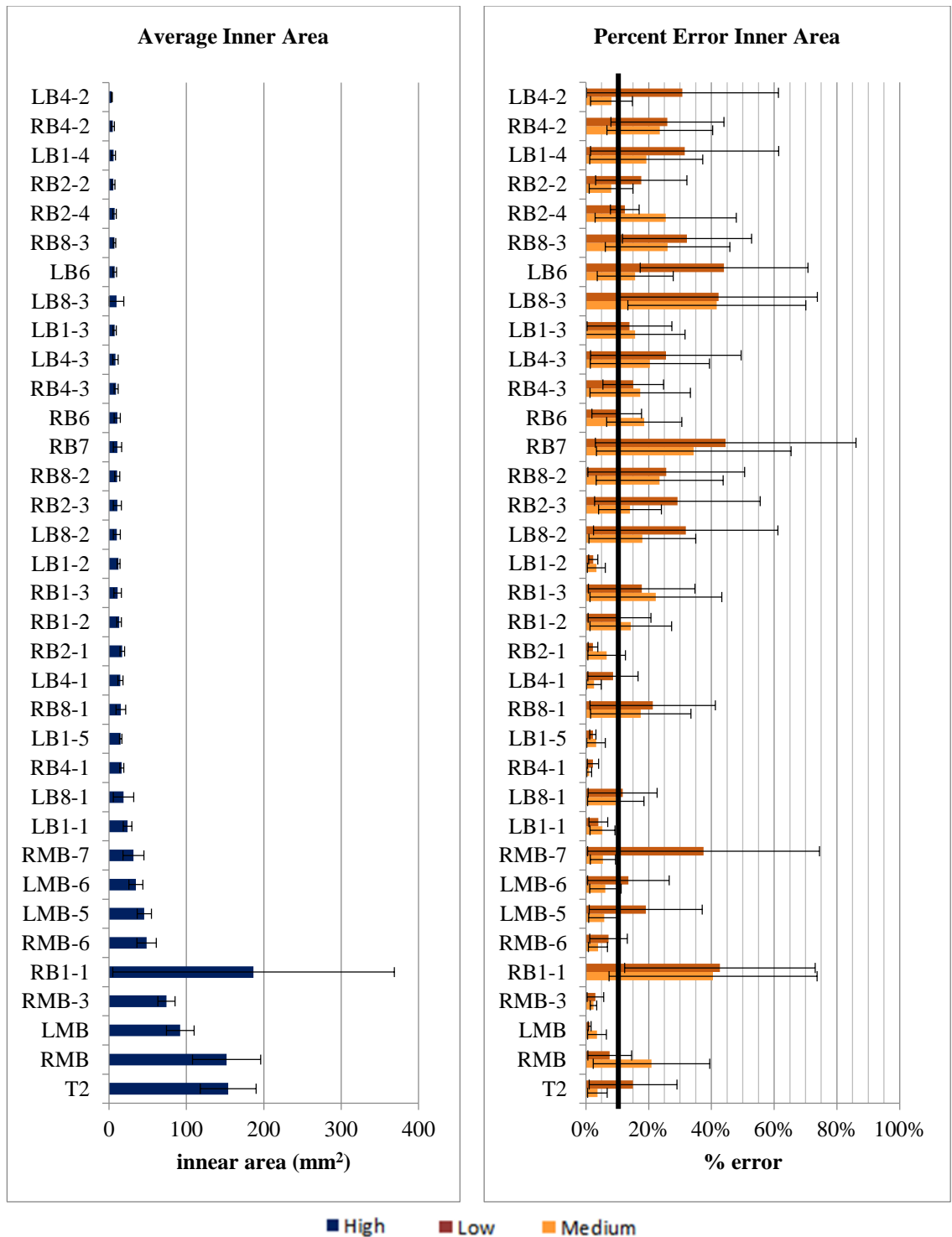


Figure 19. (Left) The average and standard deviation of the IA values across the six subjects for the in-vivo, high CT dose quantitative airway measurements. (Right) Percent error in IA for the airways measured in the whole lung compared to the high dose values. The standard deviations are shown.

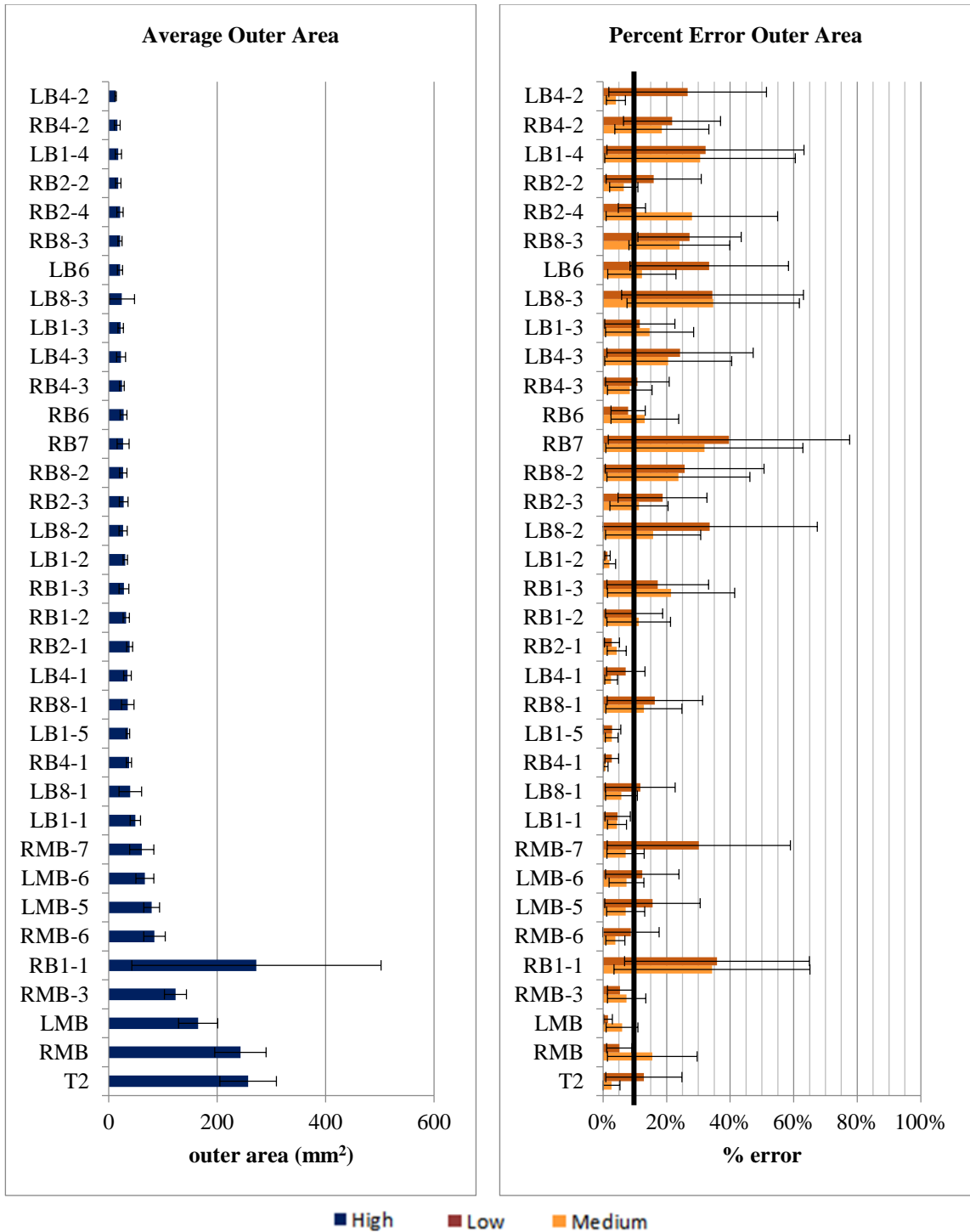


Figure 20. (Left) The average and standard deviation of the OA values across the six subjects for the in-vivo, high CT dose quantitative airway measurements. (Right) Percent error in OA for the airways measured in the whole lung compared to the high dose values. The standard deviations are shown.

4.1.2.2 *In-Vivo and Ex-Vivo Apollo Comparison*

It was expected that the process of fixation would have some impact on quantitative CT measurements, even though efforts were aimed at minimizing these (through the type of fixation fluid used, intravascular flushing of the fixation fluid, fixation of the lungs within the chest cavity etc.) [14]. This was confirmed with airway measurement comparisons (as in section 4.2.1) resulting in percent errors above ten percent (Figure 21, Figure 22, Figure 23, Figure 24, and Figure 25, Table 11). However, further analysis revealed that while the specific values collected were less alike than desired, the trends observed ex-vivo were similar to the ones observed in the in-vivo data. For example, the airways that resulted in the lowest error were often extensions of the main bronchi or direct branches. A t-test done on all of the main airways in the airway tree yielded no statistically significant differences between the in-vivo and ex-vivo measures for average MinD and average WT for three of the subjects, and average MajD, IA, and OA for all six subjects (Table 1). A correlation test done on all of the subjects revealed reasonably strong correlations between the in-vivo and ex-vivo values, with most reporting a correlation of 0.80 or better (Table 2). The strength of these relationships was the result of the consistent underestimation the ex-vivo values make with regard to the in-vivo values, most likely a consequence of the fixation. These relationships support the use of the ex-vivo fixed lungs to study the in-vivo lungs.

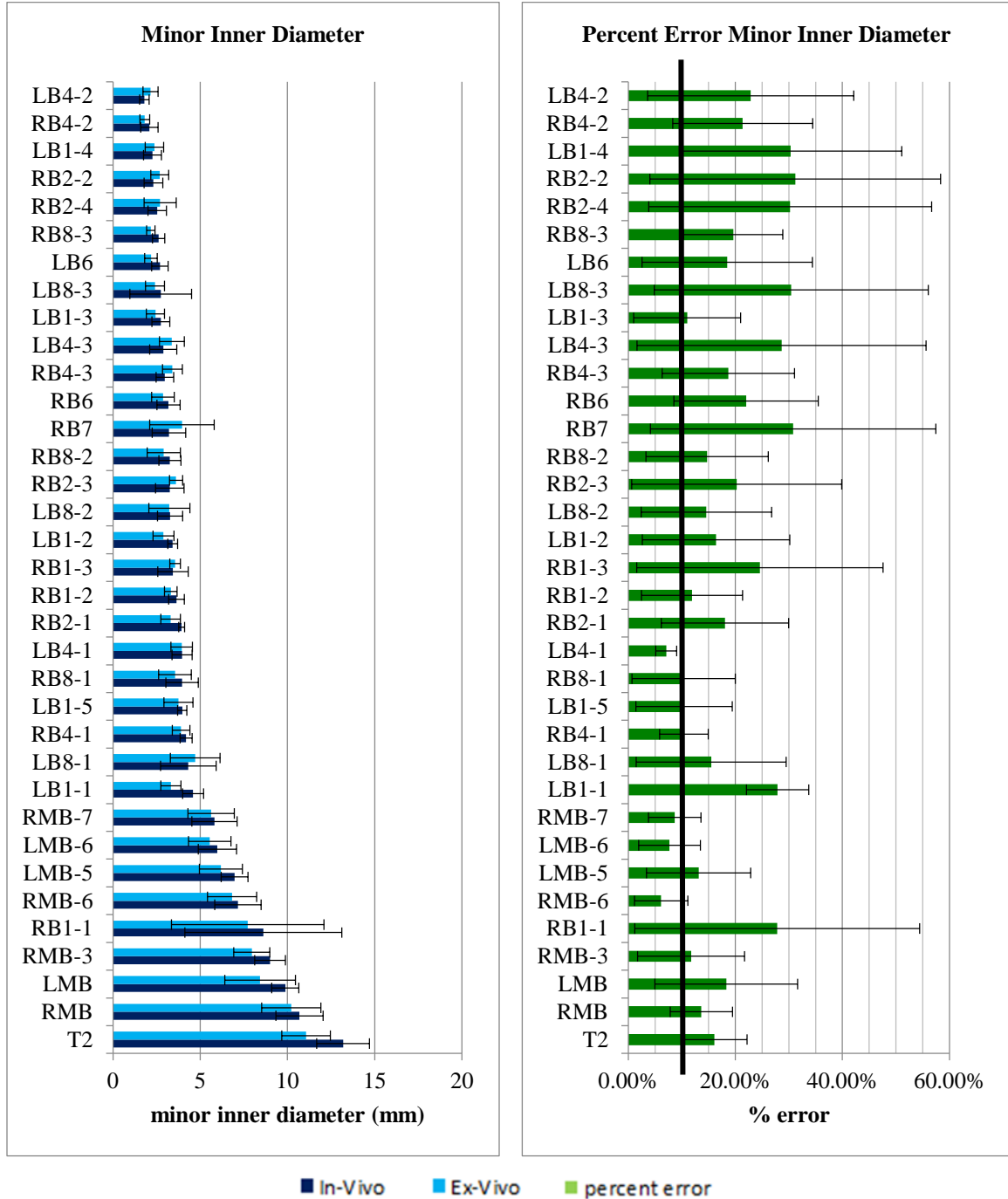


Figure 21. (Left) The average and standard deviation of the MinD values across the six subjects for the in-vivo, high CT dose quantitative airway measurements compared to the ex-vivo measurements. (Right) Percent error in MinD for the airways measured in the ex-vivo lung compared to the in-vivo values.

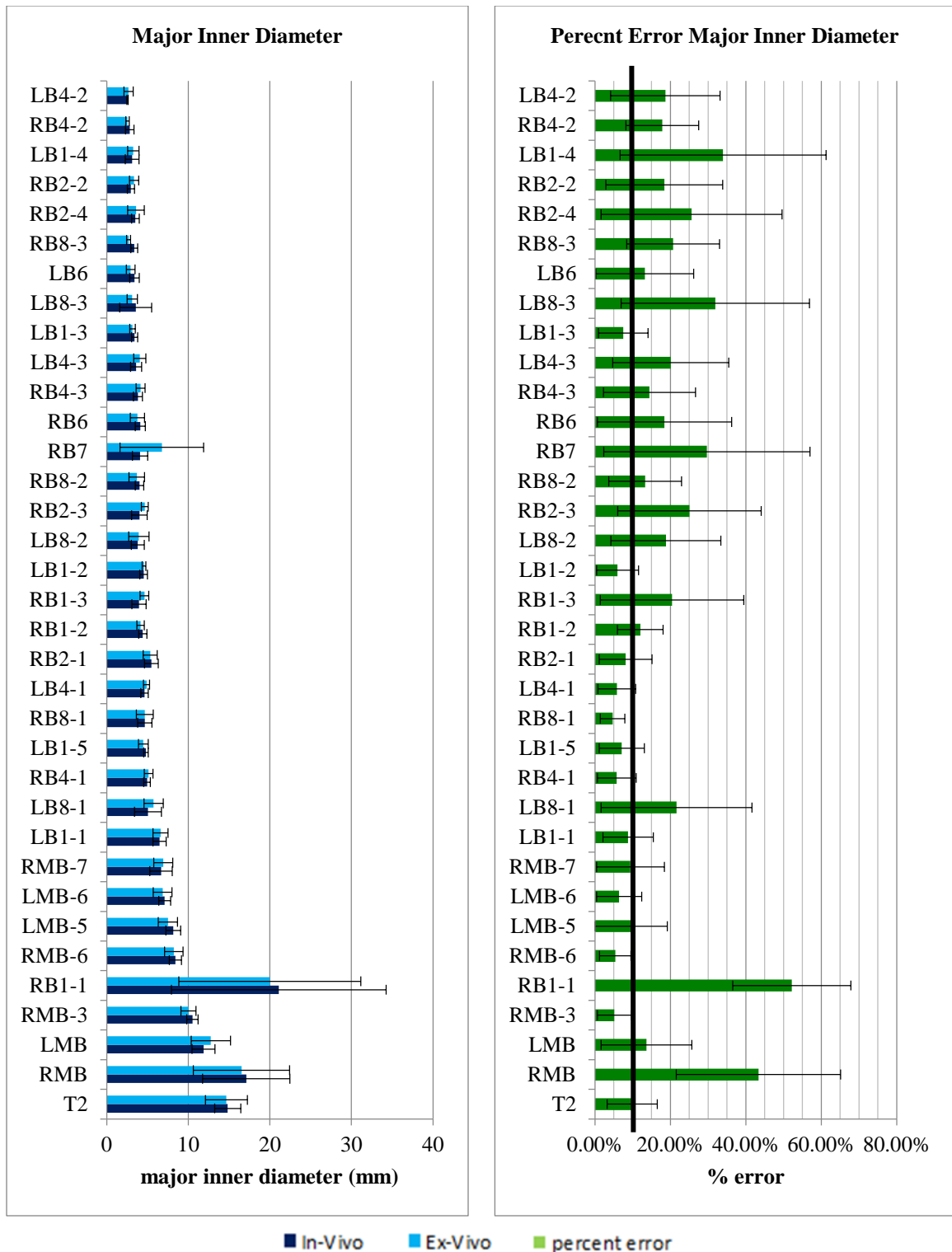


Figure 22. (Left) The average and standard deviation of the MajD values across the six subjects for the in-vivo, high CT dose quantitative airway measurements compared to the ex-vivo measurements. (Right) Percent error in MajD for the airways measured in the ex-vivo lung compared to the in-vivo values.

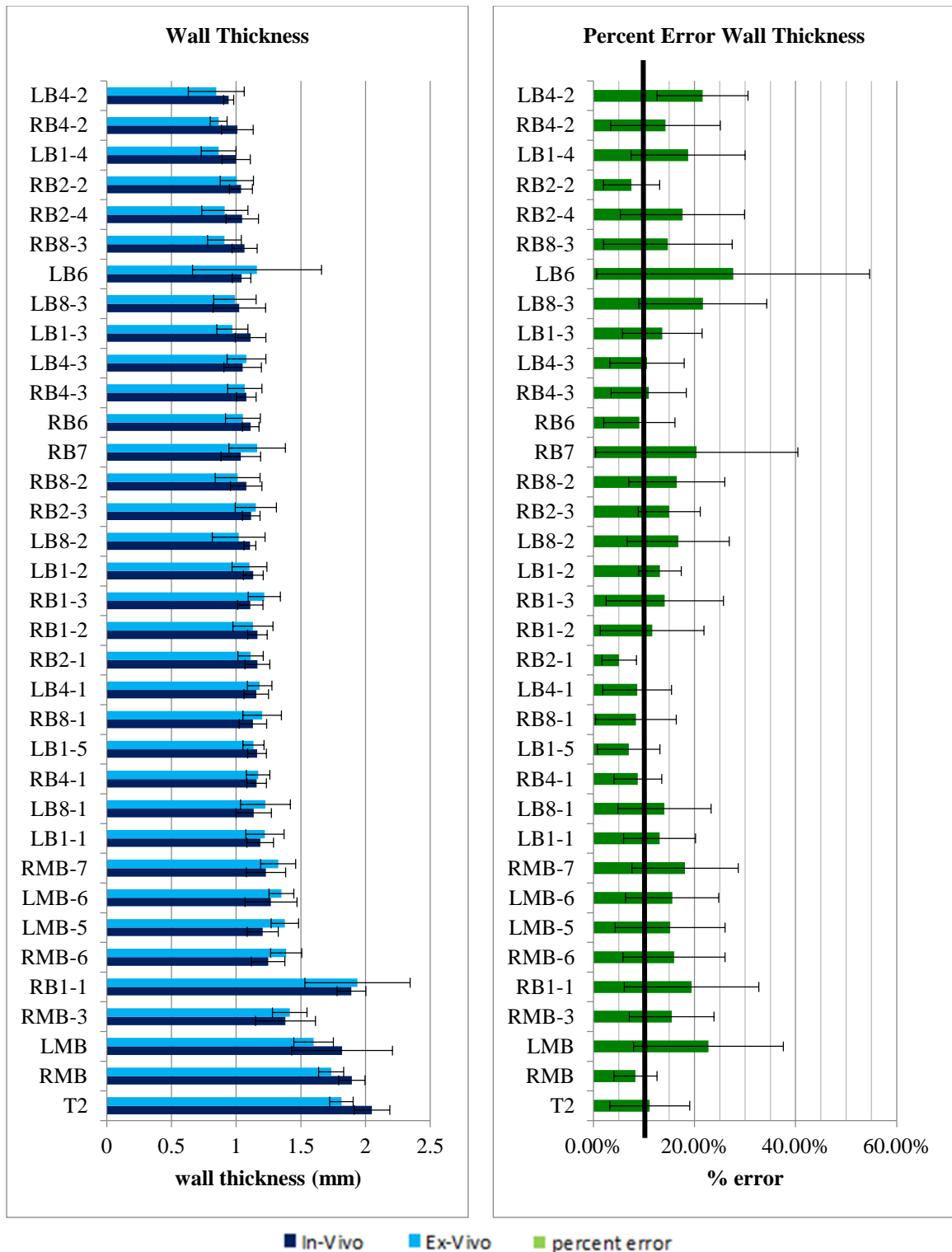


Figure 23. (Left) The average and standard deviation of the WT values across the six subjects for the in-vivo, high CT dose quantitative airway measurements compared to the ex-vivo measurements. (Right) Percent error in WT for the airways measured in the ex-vivo lung compared to the in-vivo values.

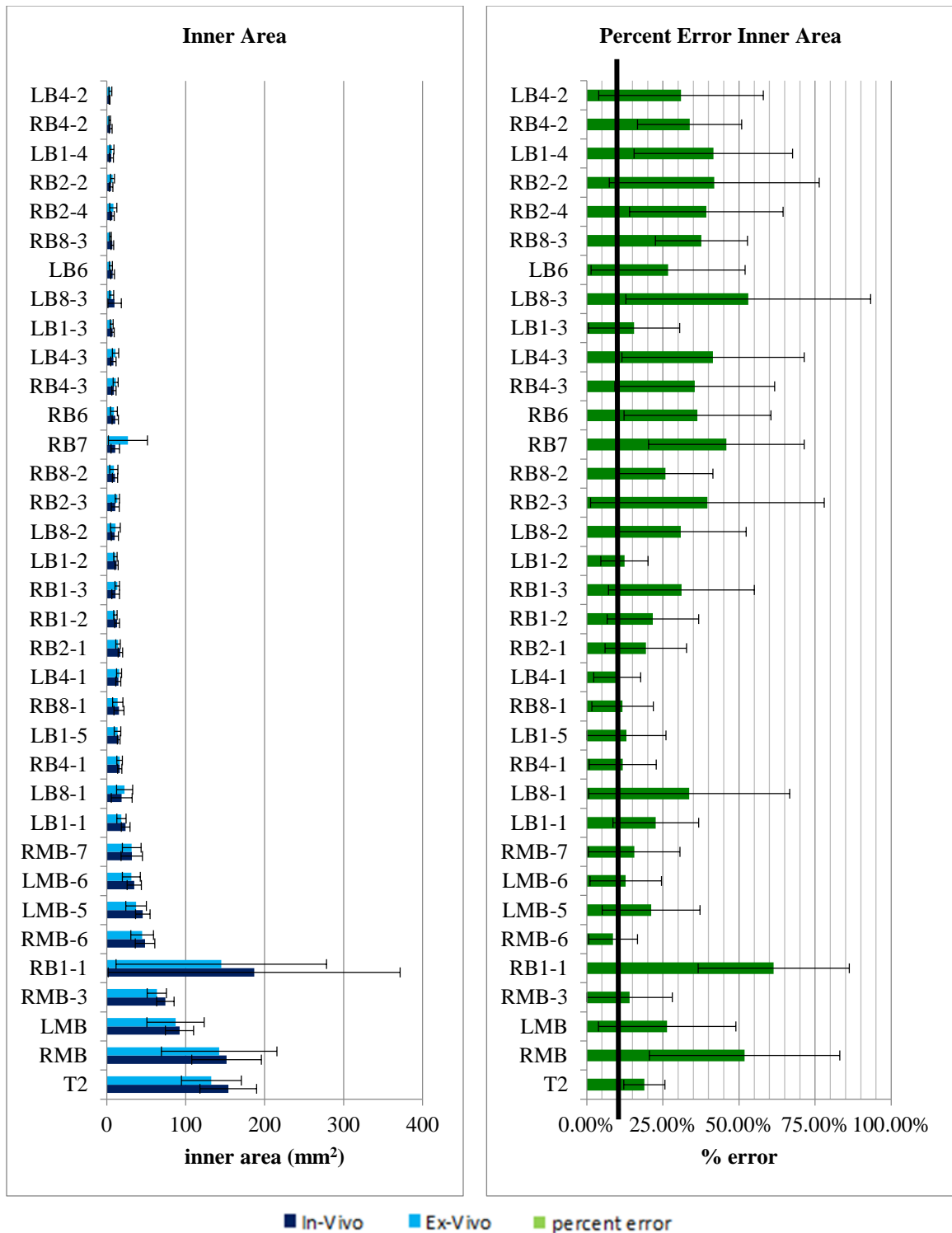


Figure 24. (Left) The average and standard deviation of the IA values across the six subjects for the in-vivo, high CT dose quantitative airway measurements compared to the ex-vivo measurements. (Right) Percent error in IA for the airways measured in the ex-vivo lung compared to the in-vivo values.

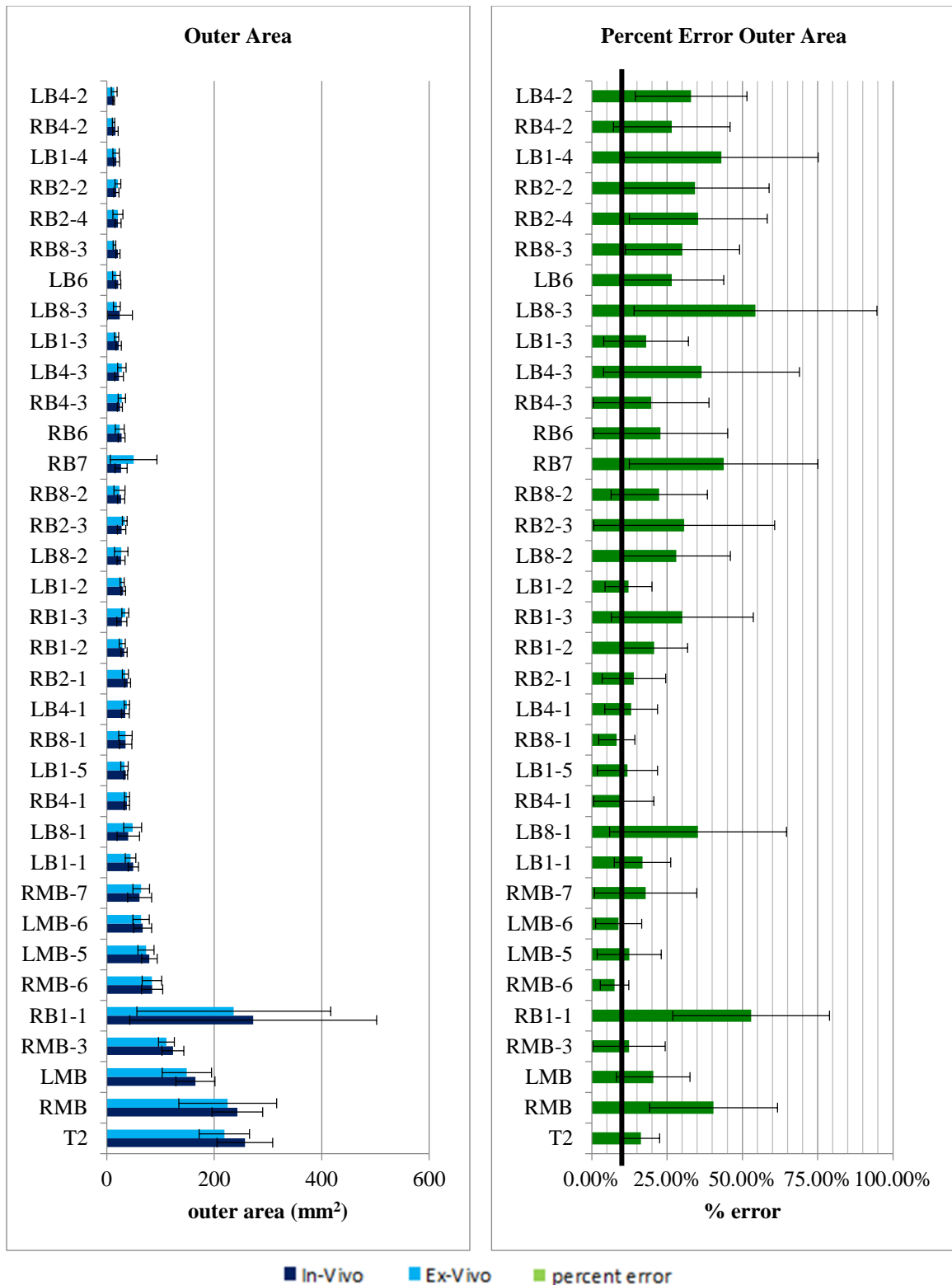


Figure 25. (Left) The average and standard deviation of the OA values across the six subjects for the in-vivo, high CT dose quantitative airway measurements compared to the ex-vivo measurements. (Right) Percent error in OA for the airways measured in the ex-vivo lung compared to the in-vivo values.

Table 1. T-Test p values across all of the airways for each of the subjects by measure. The values above 0.05 show significance.

Subject	Average MinD	Average MajD	Average WT	Average IA	Average OA
40016	0.06	0.79	0.00	0.31	0.23
40189	0.00	0.66	0.22	0.20	0.50
40190	0.60	0.23	0.75	0.09	0.25
40191	0.42	0.52	0.73	0.74	0.79
40383	0.57	0.12	0.00	0.25	0.17
40470	0.02	0.63	0.00	0.66	0.24

Table 2. Correlation values across all of the airways for each of the six subjects by measure. A value of 1.0 would indicate a perfect correlation.

Subject	Average MinD	Average MajD	Average WT	Average IA	Average OA
40016	0.78	0.81	0.81	0.64	0.72
40189	0.96	0.63	0.73	0.75	0.76
40190	0.93	0.94	0.81	0.96	0.95
40191	0.94	0.82	0.65	0.87	0.91
40383	0.89	0.74	0.83	0.62	0.72
40470	0.96	0.79	0.95	0.84	0.88

4.2 Individual Airway Cube Data and Analysis

The dataset used for the registration and subsequent individual airway analysis was collected from one of the subjects used in the whole lung airway tree comparison portion of the study, specifically subject AP40016. AP40016 weighed 41kg and had a lung volume of 1969.18mL.

4.2.1 Single Airway Cube Registration Dataset

The subject chosen for the individual airway analysis was selected due to the similarity in the lung volumes pre- and post-fixation (1969.18 mL and 2160.11 mL) as well as the similarity in lung shape and tissue integrity observed upon visual inspection. Thirteen cubes containing airway structures resulted from the combination of the stereological sampling and the specific airway selection cohorts described in the methods (section 3.2.2.2). The airway-containing sample cubes, originating from the locations pictured in Figure 26, were registered and their airways analyzed using the full-width half-maximum (FWHM) method. Example images from the high dose, medium dose, low dose, CT cube (post-registration), and μ CT cube (post-registration) scans are shown for each of the thirteen samples that were studied are shown in Table 3. Assessment of the registration was done qualitatively, by overlaying the fixed and moving images (Table 14), and quantitatively, by computing the sum of squared differences in the alignment of the fiducials, once initialized, pre- and post-fixation. The results of this testing are shown in Table 4 and Table 15.

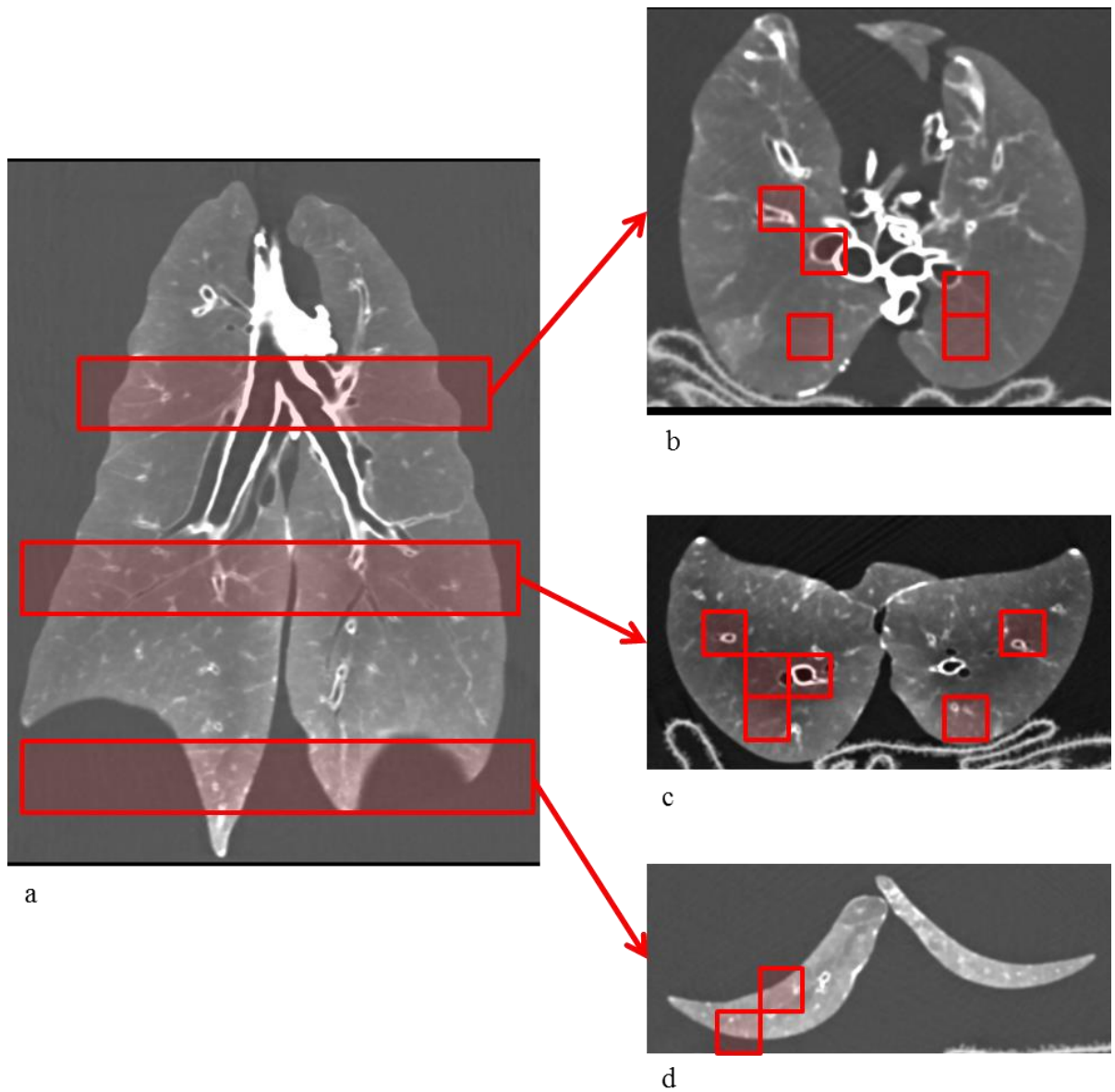


Figure 26. Location of sampled cubes in the whole ex-vivo lung. The whole ex-vivo lung is shown in (a) coronal view. Images (b), (c), and (d) show axial cross-sectional slices B8L7, B11L10, and B14L13 respectively.

Table 3. Registered images. The single slices from the registered high dose, medium dose, low dose, CT cube, and μ CT cube are shown for each of the thirteen samples.

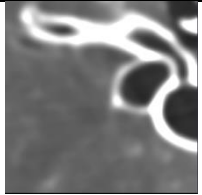
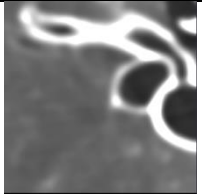
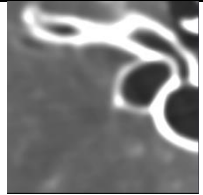
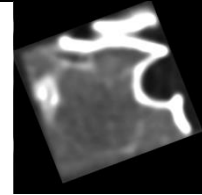
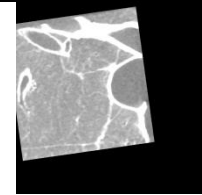
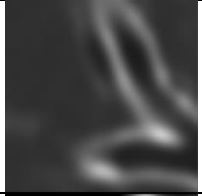
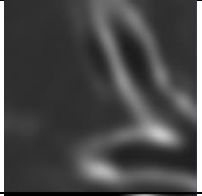
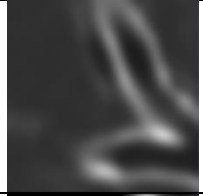
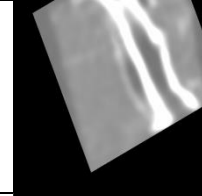
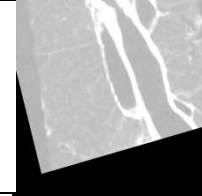
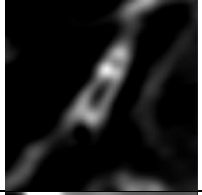
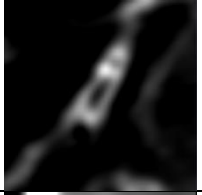
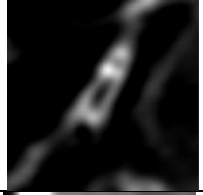
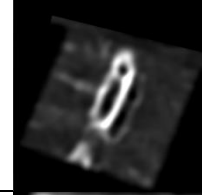
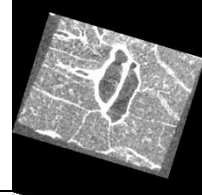
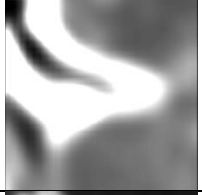
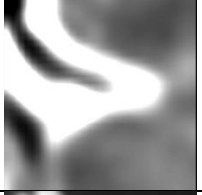

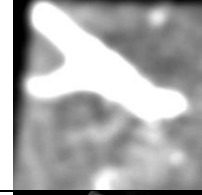
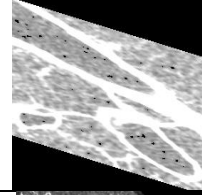
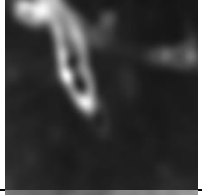


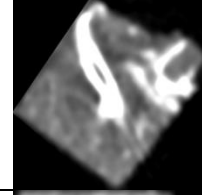
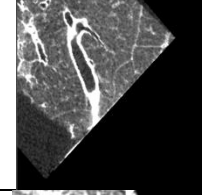

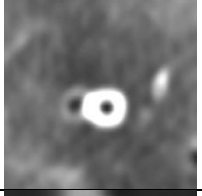
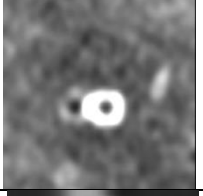
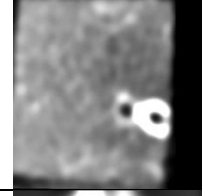
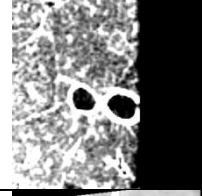
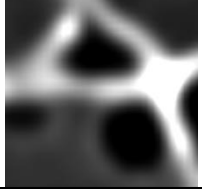
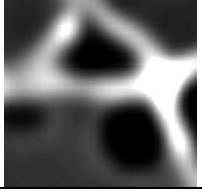
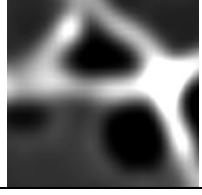
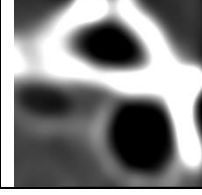
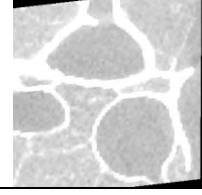
	High Dose	Medium Dose	Low Dose	CT Cube	μ CT
B8L7C2R3					
B8L7C2R4					
B8L7C2R5					
B8L7C5R3					
B8L7C5R4					
B11L10C1R3					
B11L10C2R2					

Table 3—continued.

	High Dose	Medium Dose	Low Dose	CT Cube	μ CT
B11L10C3R2					
B11L10C3R3					
B11L10C5R2					
B11L10C5R3					
B14L13C2R1					
B14L13C3R2					

Table 4. Sum of squared differences between the fiducial markers from the stereologically sampled cubes. The registered fiducials had much smaller sum of squared differences values.

	Original	Registered
B8L7C5R3	9.45	1.83
B8L7C2R5	26.21	2.16
B11L10C2R2	3.54	0.41
B11L10C5R3	9.31	0.78
B14L13C2R1	35.51	3.08

4.2.2 Individual Airway Comparison

Prior to using the FWHM method to assess the individual airways, it was tested on a phantom image (Figure 27). Since the image was constructed with the precise dimensions known, it was possible to conduct a percent error test to evaluate the FWHM generated measures with respect to the truth. The measures were shown to be accurate (Table 5) and testing moved to the actual airways.

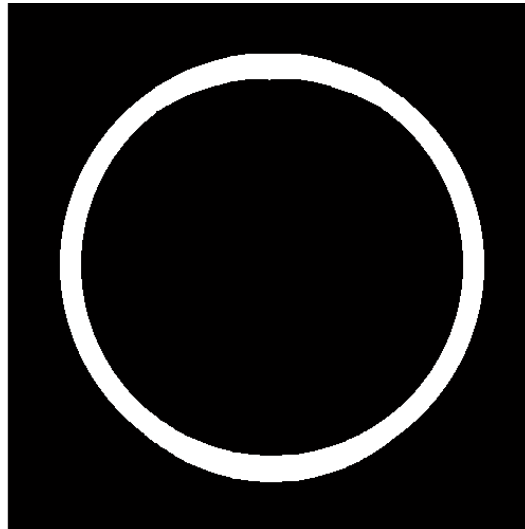


Figure 27. Phantom to test the accuracy of the FWHM algorithm. The image is constructed of a white ring (pixel values 125-255) on a black background (pixel value 0) in order to mimic an ideal airway.

Table 5. Assessment of the FWHM measures. The actual values and calculated values are shown for each of the five measures of interest in addition to the percent errors of the calculated values with respect to the actual.

	MinD	MajD	WT	IA	OA
Actual	360	360	20	1.02×10^5	1.26×10^5
Calculated	362	371	20	1.06×10^5	1.33×10^5
Percent Error	0.05%	3.05%	0.00%	3.92%	5.55%

4.2.2.1 Ex-Vivo Airways

Upon collection of the five measures of interest, using the FWHM approach on the registered ex-vivo lung dataset (Table 12), they were compared using a percent error, t-test, and correlation test to determine how well the values represented one another. In this comparison, the highest resolution data, the μ CT of the cube sample, was used as ground truth. Table 6 shows the collected values for all thirteen airways and their percent error comparisons to the μ CT values. The t-test and correlation values can be found in Table 7 and Table 8, respectively. The percent errors were high, 40% on average with values as high as 98%. The t-test and correlation values showed that CT cube values were representative of the μ CT values (there was only a statistically significant difference in the WT and the correlations were 0.75 on average), while all three doses from the ex-vivo whole lungs performed noticeably worse. Looking at the data further, patterns of over- and underestimation were discovered. All of the different CT measures of MinD were consistent overestimates, as was WT, and both IA and OA were consistently underestimated. The overestimation of the WT and the underestimation of the areas were expected due to the significant blurring of the airway wall in CT. The overestimation of MinD suggests that a greater amount of blurring occurs outside of the airway than inside, shifting the airway wall center as measured by the FWHM.

Table 6. FWHM results for the thirteen ex-vivo airways. The calculated values are shown in the one-dimensional values and two-dimensional values columns. Each of the sample types is shown: high-dose (high), medium-dose (med), low-dose (low), CT cube (CT), and μ CT cube (μ CT). The percent errors comparing each of the first four types to the μ CT are shown in the one-dimensional percent errors and two-dimensional percent errors columns. MinD is shown in blue, MajD is red, WT is green, IA is teal, and OA is purple.

	One-Dimensional Values	One-Dimensional Percent Errors	Two-Dimensional Values	Two-Dimensional Percent Errors
B8L7C2R3	<p>length (mm)</p>	<p>% error</p>	<p>area (mm²)</p>	<p>% error</p>
	<p>■ Minor Inner Diameter ■ Major Inner Diameter ■ Wall Thickness ■ Inner Area ■ Outer Area</p>			
B8L7C2R4	<p>length (mm)</p>	<p>% error</p>	<p>area (mm²)</p>	<p>% error</p>
	<p>■ Minor Inner Diameter ■ Major Inner Diameter ■ Wall Thickness ■ Inner Area ■ Outer Area</p>			
B8L7C2R5	<p>length (mm)</p>	<p>% error</p>	<p>area (mm²)</p>	<p>% error</p>
	<p>■ Minor Inner Diameter ■ Major Inner Diameter ■ Wall Thickness ■ Inner Area ■ Outer Area</p>			

Table 6—continued.

B8L7C5R3	<p>length (mm)</p>	<p>% error</p>	<p>area (mm²)</p>	<p>% error</p>
	<p>■ Minor Inner Diameter ■ Major Inner Diameter ■ Wall Thickness ■ Inner Area ■ Outer Area</p>			
B8L7C5R4	<p>length (mm)</p>	<p>% error</p>	<p>area (mm²)</p>	<p>% error</p>
	<p>■ Minor Inner Diameter ■ Major Inner Diameter ■ Wall Thickness ■ Inner Area ■ Outer Area</p>			
B11L10C1R3	<p>length (mm)</p>	<p>% error</p>	<p>area (mm²)</p>	<p>% error</p>
	<p>■ Minor Inner Diameter ■ Major Inner Diameter ■ Wall Thickness ■ Inner Area ■ Outer Area</p>			

Table 6—continued.

B11L10C2R2	<p>length (mm)</p>	<p>% error</p>	<p>area (mm²)</p>	<p>% error</p>
	<p>■ Minor Inner Diameter ■ Major Inner Diameter ■ Wall Thickness ■ Inner Area ■ Outer Area</p>			
B11L10C3R2	<p>length (mm)</p>	<p>% error</p>	<p>area (mm²)</p>	<p>% error</p>
	<p>■ Minor Inner Diameter ■ Major Inner Diameter ■ Wall Thickness ■ Inner Area ■ Outer Area</p>			
B11L10C3R3	<p>length (mm)</p>	<p>% error</p>	<p>area (mm²)</p>	<p>% error</p>
	<p>■ Minor Inner Diameter ■ Major Inner Diameter ■ Wall Thickness ■ Inner Area ■ Outer Area</p>			

Table 6—continued.

B11L10C5R2				
	<p>■ Minor Inner Diameter ■ Major Inner Diameter ■ Wall Thickness ■ Inner Area ■ Outer Area</p>			
B11L10C5R3				
	<p>■ Minor Inner Diameter ■ Major Inner Diameter ■ Wall Thickness ■ Inner Area ■ Outer Area</p>			
BB14L13C2R1				
	<p>■ Minor Inner Diameter ■ Major Inner Diameter ■ Wall Thickness ■ Inner Area ■ Outer Area</p>			

Table 6—continued.

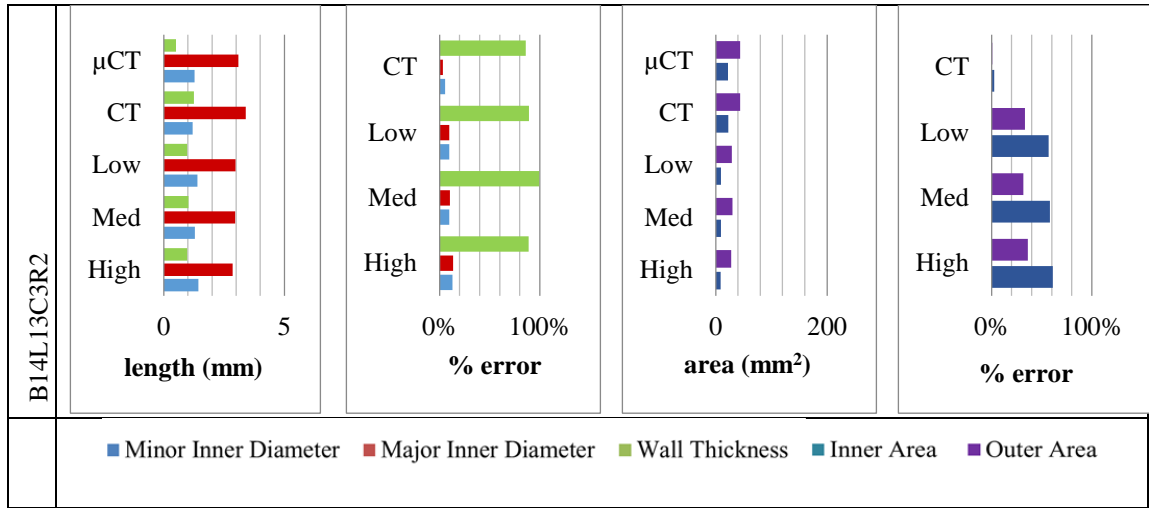


Table 7. T-test values calculated between the μ CT measures and each of the other sample types' measures. Values of 0.05 indicate that there is not a statistically significant difference present.

	MinD	MajD	WT	IA	OA
High to μ CT	0.44	0.09	0.01	0.00	0.02
Med to μ CT	0.27	0.20	0.01	0.00	0.01
Low to μ CT	0.30	0.15	0.00	0.00	0.03
CT to μ CT	0.84	0.21	0.00	0.34	0.884

Table 8. Correlation values between the μ CT measures and each of the other sample types' measures. Values close to 1.0 are desired.

	MinD	MajD	WT	IA	OA
High to μ CT	0.41	0.69	-0.21	0.65	0.55
Med to μ CT	0.30	0.65	-0.18	0.66	0.57
Low to μ CT	0.17	0.67	-0.14	0.65	0.50
CT to μ CT	0.50	0.75	0.64	0.93	0.96

4.2.2.2 In-Vivo Airways

Finally, collection of the five measures of interest was done using the FWHM approach on three different radiation doses from the in-vivo lung's stereologically sampled dataset. The resultant values (Table 13) were compared using percent error, as was done for the ex-vivo CT data (4.3.1). In this comparison, the high resolution data was used as ground truth. Seen in Table 9, the error values were very inconsistent across the airways, with errors ranging 0-87%, as was the case in the small airways in the full airway tree, and the average medium dose error values were lower than the low dose values (10% vs. 14%) and occurred in a smaller range (0-68% vs. 0-87%), with neither having a discernable pattern of over- or underestimation.

Table 9. FWHM results for the five stereologically samples in-vivo airways. The calculated values are shown in the one-dimensional values and two-dimensional values columns. Each of the sample types is shown: high-dose (high), medium-dose (med), low-dose (low), CT cube (CT), and μ CT cube (μ CT). The percent errors comparing each of the first four types to the μ CT are shown in the one-dimensional percent errors and two-dimensional percent errors columns. MinD is shown in blue, MajD is red, WT is green, IA is teal, and OA is purple.

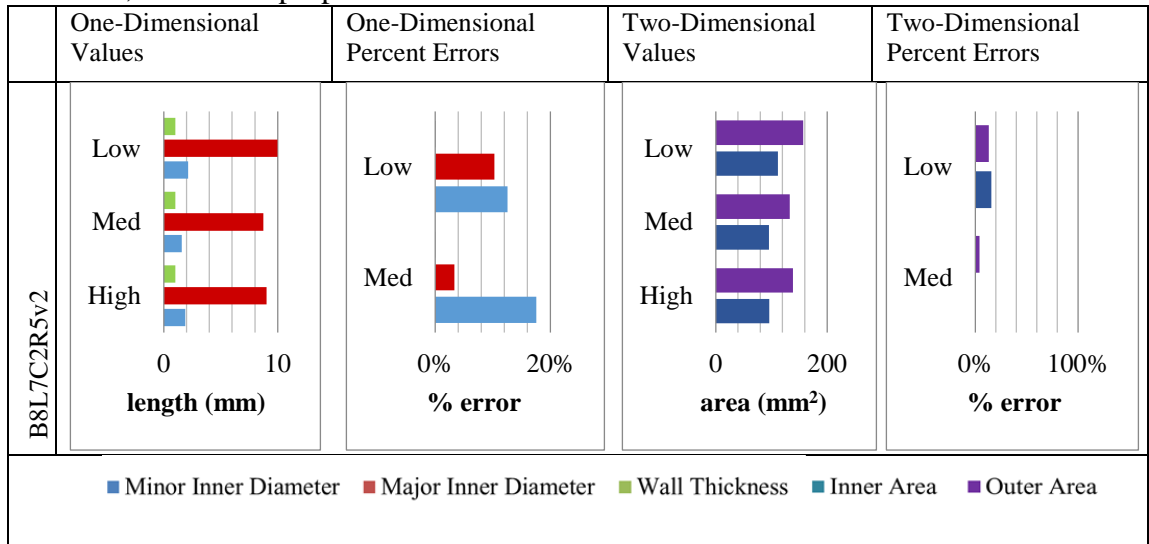


Table 9—continued.

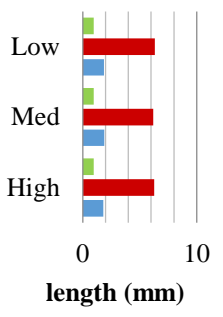
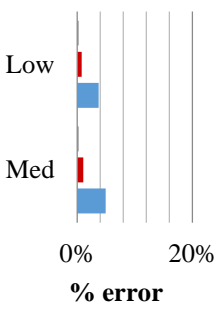
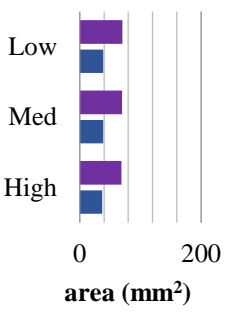
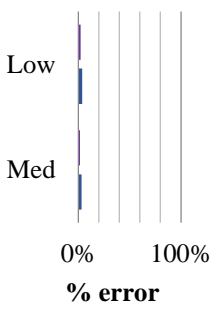
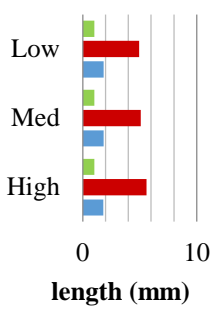
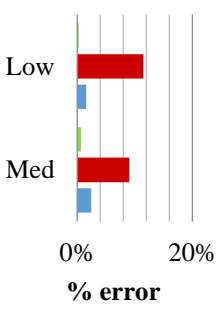
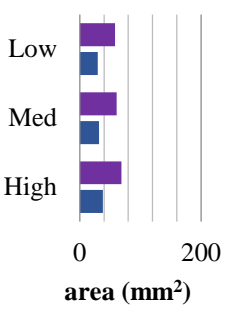
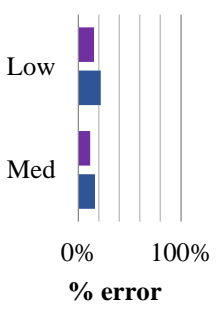
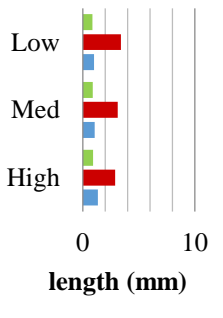
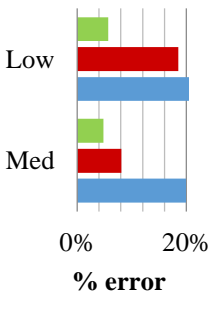
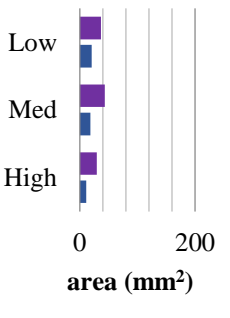
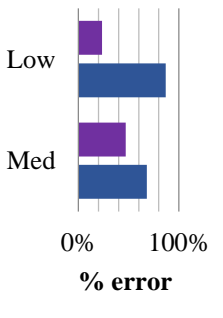
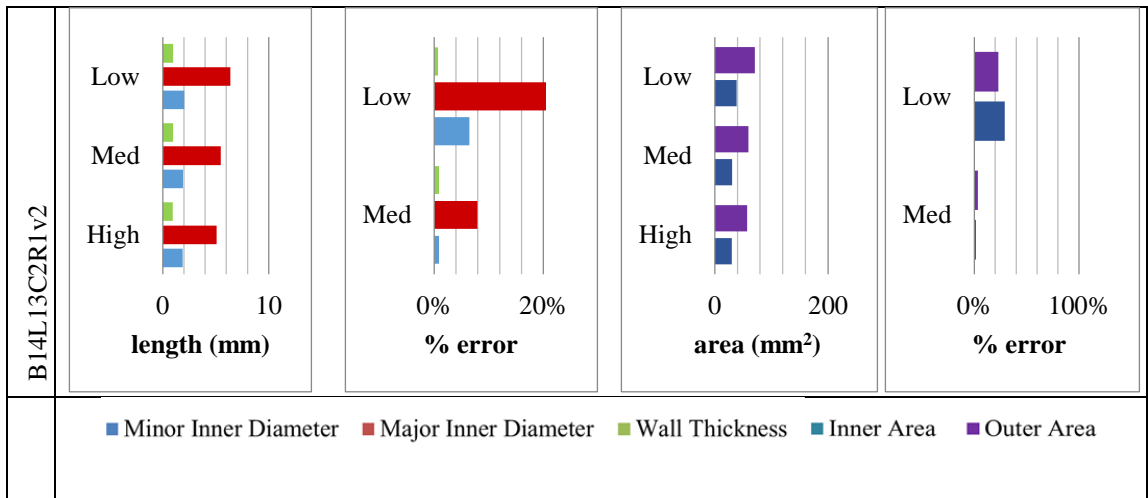
B8L7C5R3v2					<p>■ Minor Inner Diameter ■ Major Inner Diameter ■ Wall Thickness ■ Inner Area ■ Outer Area</p>
B11L10C2R2v2					<p>■ Minor Inner Diameter ■ Major Inner Diameter ■ Wall Thickness ■ Inner Area ■ Outer Area</p>
B11L10C5R3v2					<p>■ Minor Inner Diameter ■ Major Inner Diameter ■ Wall Thickness ■ Inner Area ■ Outer Area</p>

Table 9—continued.



CHAPTER 5

DISCUSSION

5.1 Whole Lung Airway Tree Analysis

In this study we developed a method of assessing quantitative CT airway measurements, scaling from in-vivo CT down to high resolution μ CT of isolated airway cube samples. In this dataset, we focused on studying the effect (error) of CT acquisition radiation dose on the quantitative measurements, MinD, MajD, WT, IA and OA. This was accomplished by comparing the measures collected from six porcine subjects across CT radiation doses, and pre-/post-fixation with increasing resolution.

5.1.1 Dose Effects

Three radiation doses were studied: high dose (14.98 mGy), medium dose (6.00 mGy), and low dose (0.74 mGy). Scans were collected and analyzed using Apollo at each of these doses for the six subjects. MinD, MajD, WT, IA and OA were measured for thirty-five of the airways. It was hypothesized for this study that decreased radiation dose would compromise the accuracy of airway measurements compared to the corresponding high dose CT data. It was expected that the increased image noise resulting from the low dose protocols would have minimal effect in the large central airways but significant percent error in the smaller airways, and that the effects in the medium dose data would exhibit a similar but moderated version of the low dose results. Based on the results from percent error statistical analysis of the airways between doses, airways with MinD less than 3.5 mm can be reliably measured (< 5% error) with the medium dose scans and can be somewhat less reliably measured (< 10% error) with the low dose scans. However, when measuring the WT of the airways there was very little difference observed in the

percent errors that resulted from the medium and low dose scans (< 5% error for both). This would imply that, should the goal be to assess airways with MinD above 3.5 mm, a medium dose scan would be best for making diameter and area measurements, but the low dose scan would be adequate for making and evaluating WT. The ability to use medium and low dose scans to study these airways means that longitudinal monitoring of the airway diseases affecting these airways is more feasible and much lower risk to the patient. However, smaller airways, those less than 3.5 mm in MinD will still need to be monitored using high dose CT, limiting the frequency of scans that can be collected.

5.1.2 Physical distortion caused by fixation

It was necessary in this study to isolate small regions of interest in the lung such that they could be imaged with very high resolution in μ CT (which has a restricted field of view for imaging). The lung is an air-filled organ with alveoli held open due to the negative pressure effects of the pleura and hence requires tissue fixation to maintain structure ex-vivo. We needed to understand the impact of lung extraction and fixation on airway structure. To do this we compared the in-vivo high dose (14.98 mGy) CT scans to ex-vivo data. Unlike with the comparison of the quantitative measurement from the in-vivo multiple CT dose data, percent error proved to be much greater between the in-vivo and ex-vivo airways because of the changes that the lungs underwent during fixation. However, even though the error values themselves were greater, they followed the same trend as the in-vivo data across the three doses. Just as the multi-dose data showed a large increase in error in MinD, MajD, IA and OA values when the airway MinD was less than 3.5 mm, so did the ex-vivo to in-vivo data. In addition, the error in the WT stayed relatively constant across all airways between ex-vivo and in-vivo data. To further study

the relationship between the ex-vivo and in-vivo airways, a t-test was done to identify statistically significant differences in the datasets and the correlation coefficients were found to quantify their relationship throughout the airway tree. Overall, the values showed that there were not statistically significant differences between the datasets and they correlated well with one another. In addition, the cases that showed statistically significant differences were not especially concerning because their correlation was typically still very strong. An important effect of the fixation that is important to note when considering the differences in the six lungs is the alterations made to the fixation procedure during its development. This is reflected in the t-test and correlation values. For example, subjects 40190 and 40191 have the most consistent values. When these two subjects were fixed they were left in the fixative solution for 60 minutes instead of 15 minutes as was done for the other subjects. This would imply that extended fixation time does a better job of preserving the airways. Regardless of this and any other changes made in the fixation procedure, the overall pattern in the data showed that the five measures of interest are related between the in-vivo and ex-vivo airways and therefore the ex-vivo can be used to derive and represent the in-vivo values.

5.2 Individual Airway Comparison

In order to most accurately evaluate the quantitative measures, a method of comparison was created to take advantage of the high-resolution capabilities of the μ CT scanner and use the measures extracted from these scans as a ground truth for comparison. One lung, subject 40016, was sampled to collect a total of thirteen cubes to conduct this comparison. This subject was selected based on the data that had been collected at the time, the visual inspection of the tissue integrity and the pre- and post-

fixation volume analysis. Subject 40016 was the best lung in these aspects. However, as can be seen in the results from section 4.2.2, this subject did not have the best ex-vivo airway tree. In continuing selecting lungs to sample in the future, the data from 4.2.2 will be considered in addition to the visual inspection and volume analysis so as to obtain the best possible airways for comparison (i.e. subjects 40190 and 40191).

5.2.1 Method Validation

Validation of the methods involved in conducting the individual airway cube comparisons was done in two stages. The first was the evaluation of the registration. This was done by computing the sum of squared errors between the fiducials used in the stereologically sampled dataset pre- and post-fixation. The exact points compared were the center of the fiducials since the actual fiducials were too small to fully resolve in the CT cubes resulting in their blurred oval appearance in contrast to their sharp and angular appearance in μ CT. While this is not ideal, qualitative assessment showed that they were aligned well and the quantitative assessment from comparing the identified center points confirmed this. The second stage was the evaluation of the full-width half-maximum (FWHM) output values (MinD, MajD, WT, IA and OA) using a phantom. Since the FWHM assumes that the greatest pixel intensities will occur at the center of the airway wall and then gradually decrease so that the values at the boundaries will be half of that maximum, the phantom was designed to fulfill this assumption. The values at the center of the phantom's airway wall were 255 (pure white) and gradually decreased out in both directions until they reached the boundary with the black (pixel value 0) background. The FWHM was then run on the phantom. The error between the calculated values and the predetermined truth values was insignificant ($< 5\%$ for all but OA which

was 5.55%). This supported the use of the FWHM in making quantitative assessments of the individual airways.

5.2.2 Ex-Vivo Small Airway Analysis

The thirteen samples collected from subject 40016 were imaged in both CT and μ CT. The samples were then registered to the high dose whole ex-vivo lung using the framework described in section 3.3.2. This registration was used to ensure that the airways present in the samples were aligned as well as possible with the original, whole ex-vivo lung airway tree. The whole ex-vivo lung airway tree was used as the fixed image in the registration so that both the sampled airways and the different dose whole ex-vivo airways could be related to the same image. The FWHM was then used to collect the measures for the airways from each of the different datasets (high dose ex-vivo whole lung, medium dose ex-vivo whole lung, low dose ex-vivo whole lung, CT cube sample, and μ CT cube sample).

The results showed some very distinct patterns. First, the MajD was often several times bigger than the MinD, which is surprising for cross-sectional airway measurements as these are expected to be closely circular in shape. The reason for this discrepancy comes from the FWHM evaluation of the airways. The FWHM required that three slices be used in making the calculations so that a total of 360 rays could be used to average the data. Given the resolution of the CT image, this created a complication for most of the airways because they often only had one or two slices that showed the airway isolated and cross-sectional. The other one or two slices used then included a bifurcation, with the airway emerging from a parent branch or diving into daughter branches. However, since the goal of this project was to evaluate the comparison of airways between datasets and

the same anatomical regions were used across datasets, this was determined to be an issue to address in future work but not for the scope of this work. Another pattern was the performance of the CT cube with respect to the airways in the whole ex-vivo lungs. The CT cube airway measures were consistently closer matched to the μ CT measures, having smaller percent errors for all of the values, fewer statistically significant differences, and greater correlations. This is mostly likely due to the fact that in the CT cubes the airways were imaged with a much smaller field of view, and hence (given a fixed CT slice array of 512x512 pixels) a higher spatial resolution. Another finding from the investigation was the large differences in measured WT between all CT images and μ CT. This difference is very evident in qualitative inspection of the airways since the μ CT airway walls appear much thinner and more well-defined. This can be contributed to the increased resolution present in μ CT. Increased resolution means that small structures can be resolved which means that the airway wall will not blur out in μ CT nearly as much as they do in CT. The final pattern that should be addressed is the similarity of the values between the airways in the high, medium, and low dose CT scans. Based on the results discussed previously, it would seem that the error should increase as the dose decreases which is not the case in our study. We believe the error increases as the dose decreases in the in-vivo data due to the presence of the chest wall. In-vivo, the lungs are surrounded by structures that attenuate the incoming radiation, limiting the amount that can reach the lungs, resulting in increased image noise. The ex-vivo lungs are totally exposed, with only the lung tissue itself contributing to attenuation and hence the image noise effects of CT radiation dose reduction are much less pronounced.

5.2.3 In-Vivo Small Airway Analysis

The five stereologically selected samples collected from subject 40016 were roughly located in the original in-vivo CT images for each of the three doses used to study the whole airway tree. This resulted in three in-vivo lung CT datasets of different doses containing those five airway locations. Since Apollo is not designed to assess small, individual airways, the FWHM was used to study the dose effects in these in-vivo CT airway regions. As was expected, since MinD of the airways were all less than 3.5 mm, the calculated error values were very different between airways although they did seem to follow the trend of the error being greater when the MinD was smaller. While the ex-vivo data showed a similar trend, the in-vivo data had even greater discrepancies in the MajD and MinD. The reason for this increase in error for the in-vivo data over the ex-vivo data is the appearance of the vessels that accompany the airways. Ex-vivo, the vessels are empty so they are less attenuating (low HU value) than the airway wall and do not contribute to the FWHM evaluation of the wall. In-vivo, the vessels are still fluid-filled which means they appear as very bright spots bordering the airways. These immediately neighboring bright spots extend the FWHM measure of airway wall out into the vessel, dramatically increasing the size of the calculated MajD. This is an area for future improvement. Relating directly back to the whole lung in-vivo data, two other trends were found in this analysis. This first is the low error observed for the WT and the second is the heightened error in the low dose data as compared to the medium dose data. These continuations of the major trends from the whole lung data show that the FWHM yields to similar results to Apollo and help to confirm the whole lung trends.

CHAPTER 6

FUTURE WORK

6.1 Introduction

The work done for this project laid the groundwork for many other potential future projects. They include the expansion and improvement of the current project to sample more airways in the lungs, the extension of the principles used in this project to the study the lung parenchyma in addition to the airways, and the improvement of the fixation procedure to replace the blood removed from the vasculature so as to study the vasculature as well.

6.2 Expanded Airway Assessment

In order to show proof of concept, the sampling procedure from [15] was adapted to collect ten samples from one set of lungs, selected according to qualitative tissue integrity assessment and quantitative volume assessment pre- and post-fixation. The first step in conducting future work on the airway study would be to reevaluate the method by which the lungs are selected for sampling. Since the airways would be the focus, it would be best to consider the data from section 4.2.2 so that the lungs with the best airway tree preservation could be chosen. The next step would be to expand the sampling procedure used. Due to the absence of visible airways in half of the initial stereologically sampled cubes in this study, the previously excluded samples from the three lung slices were searched to find any remaining samples containing externally visible airways. This resulted in the addition of eight new samples to the dataset, resulting in thirteen total samples. While the final dataset was more than the ten desired samples, it raises the question of whether or not the initial adaptation of the sampling procedure was ideal. To

improve the sampling of airways a new procedure should be adapted. First, the sampling of the lung slices should be eliminated; instead all slices should be included to make the cubes. Next, once all of the slices have been segmented into cubes, the set of cubes to sample from should be selected based on the desired external visibility of the airways. Finally, the resulting dataset should be composed of every third cube being selected based on the random number generation. This new sampling should be used on three of the lungs from the dose study so as to have samples from multiple lungs studied. While the size of the datasets may vary some between lungs, they would be much more representative of the airway tree as a whole and the inclusion of samples from multiple lungs would be more representative of the porcine population. The final change that would be made would be to improve the FWHM algorithm. The algorithm would be adapted so that the number of slices used would be determined by the airway that is to be segmented. So, instead of requiring three slices and 120 rays from each slice to reach the desired 360 rays, it could run with only one slice. In that case, the algorithm would then create rays every degree resulting in 360 rays all from one slice. This adjustment would make it easier to ensure that only isolated cross-sections of the airways would be used for the calculations.

6.3 Parenchyma Assessment

Lung disease affects not just the airways but the parenchyma as well. Because of this, to expand the clinical relevance of the work done here, it would be desirable to extend it to study of the parenchyma. According to Matsuoka [17], the diagnosis of chronic obstructive pulmonary disease (COPD) relies greatly on the use of quantitative CT assessment of the parenchyma. The specific values often used are relative low-

attenuation area (the percentage of lung tissue that attenuates at a lower value than the designated threshold) and frequency-attenuation distribution percentile (the percentile assignment based on the relative low-attenuation area). Given the proper threshold, typically around -950 HU, the quantification of areas affected by emphysema strongly correlates with the results of any pulmonary function testing (PFT) done. In addition, new techniques to determine the size and number of specific low-attenuation clusters show promise in better quantifying the extent of emphysema present in the lungs [17]. Guo's work [18] describes further analysis that can be done using lung segmentation, smoothing, and histogram analysis. The histogram analysis is used to determine such measures as grey level mean, skewness, and kurtosis in order to study the intensity value patterns present in the parenchyma [18]. Yet another method of parenchyma assessment is mean chord length. As described by Knudsen [19], mean chord length describes the mean free distance in the peripheral air spaces of the lungs. Essentially, it works by determining how far apart the walls of the alveoli, or alveolar clusters, are along a straight line. The larger the mean chord length, the larger the airspaces are and the greater the likelihood that there is emphysema and COPD present [19]. Lung parenchyma assessment has also been done on the microscopic scale. The work done by Vasilescu [20] compared tissue volume fractions, alveolar surface area, and number of alveoli in whole mice lungs as measured in μ CT to the same measures determined histologically. His results showed that the values from μ CT correlated well with the histological values, suggesting that imaging could be used to accurately assess the lung parenchyma, at least at small scales [20].

The development of these and other new techniques to quantitatively assess the lung parenchyma in the presence of lung disease once again poses the question of the influence of radiation dose on the calculated measure. Radiation dose has the ability to greatly affect the intensity values in an image. That being said, it is important to understand to what extent that changes the derived parenchyma measures. Understanding how the accuracy and repeatability of these measures is affected by acquisition radiation dose will help to determine what doses are needed to best represent the physiology of the lungs in order to better diagnose and monitor lung disease.

6.4 Fixation Refinement for Vascular Examination

The fixation procedure used to obtain the ex-vivo lungs used in this study utilized the pulmonary vasculature to deliver the fixative to the lung tissue. Because of this, at the end of the fixation process, the blood vessels were empty. This meant that the vasculature was no longer representative of the in-vivo state. In the CT images, the vessels appeared very similar to the airways since they are tubular airspaces as well. Emptying the vessels in this manner complicates the potential assessment of the vasculature ex-vivo since it is not safe to assume that the absence of fluid in the vessels has not compromised their structure in any way. Aside from changing the fixation technique entirely, one method of improving this would be the exploration of a replacement material to fill the vessels. This material could then be introduced to and sealed in the vasculature once the fixative has been flushed from the vessels at the end of the fixation. This would require a study to determine what new material would best mimic the blood without altering the vessels in any way, the best method of filling the vasculature with said material, and the optimal mode of sealing off the vessels to hold the material.

APPENDIX

Table 10. Percent error values for dose comparison. Each table represents one dose compared with the 14.98 mGy scan as ground truth and values < 0.05 emphasized.

Subject 40016, Percent Error Comparison of 6.00 mGy and 14.98 mGy					
Airway	MinD	MajD	IA	WT	OA
T2	2.31%	3.00%	0.39%	6.16%	4.65%
RB1-1	71.57%	43.20%	0.82%	78.93%	70.97%
RB1-2	1.36%	0.99%	0.32%	1.72%	0.86%
RB1-3	0.01%	2.07%	0.29%	3.23%	2.47%
RMB	2.14%	0.93%	2.40%	1.05%	0.46%
LMB	2.33%	1.97%	55.27%	1.68%	22.73%
RB2-1	3.20%	0.93%	3.78%	0.46%	3.20%
LB1-1	0.27%	4.40%	4.64%	3.72%	0.34%
RB2-2	9.10%	1.94%	4.32%	9.35%	7.60%
RB2-3	17.44%	9.26%	10.56%	20.22%	20.17%
RB2-4	5.86%	3.46%	1.11%	6.03%	3.21%
LB1-2	2.38%	0.81%	0.30%	2.75%	1.74%
LB1-3	1.46%	0.63%	0.05%	1.41%	0.42%
LB1-4	60.98%	56.30%	44.60%	49.14%	71.64%
LB1-5	3.24%	4.16%	0.03%	4.29%	2.58%
RMB-3	1.60%	1.10%	0.19%	0.81%	0.65%
RB4-1	1.55%	1.33%	0.53%	2.05%	2.26%
RB4-2	19.80%	13.64%	21.08%	32.30%	32.58%
RB4-3	19.92%	18.13%	11.92%	32.18%	26.02%
LB4-1	1.25%	0.22%	1.02%	0.03%	0.66%
LB4-2	1.36%	4.13%	2.20%	7.03%	0.74%
LB4-3	0.82%	3.44%	0.59%	3.83%	2.77%
RB6	2.05%	0.18%	2.92%	1.59%	2.97%
LMB-5	15.25%	13.95%	4.29%	31.04%	25.18%
LB6	18.93%	17.74%	14.52%	36.99%	34.85%
LMB-6	7.40%	13.95%	0.91%	22.60%	14.99%
RMB-6	0.61%	0.67%	11.79%	2.29%	4.05%
RB7	1.77%	0.66%	0.33%	2.44%	2.03%
RMB-7	1.08%	0.80%	0.31%	0.56%	0.70%
RB8-1	33.17%	26.92%	4.78%	51.64%	39.17%
RB8-2	50.91%	37.85%	5.79%	59.43%	66.62%
RB8-3	3.93%	6.04%	26.54%	6.77%	14.04%
LB8-1	0.24%	0.51%	1.12%	1.82%	1.70%
LB8-2	74.33%	76.16%	18.04%	62.92%	80.01%
LB8-3	53.37%	54.59%	20.34%	78.25%	68.25%

Table 10—continued.

Subject 40016, Percent Error Comparison of 0.74 mGy and 14.98 mGy					
Airway	MinD	MajD	IA	WT	OA
T2	5.39%	1.60%	3.90%	5.91%	5.74%
RB1-1	62.92%	80.04%	4.01%	93.51%	86.24%
RB1-2	0.76%	1.10%	0.21%	0.69%	0.58%
RB1-3	1.88%	1.24%	0.12%	0.31%	0.24%
RMB	0.13%	1.91%	2.72%	0.34%	0.96%
LMB	3.70%	0.77%	0.67%	0.76%	0.67%
RB2-1	5.72%	0.35%	5.30%	3.54%	1.33%
LB1-1	1.60%	2.61%	3.33%	2.92%	4.03%
RB2-2	20.20%	15.62%	27.51%	34.62%	38.16%
RB2-3	42.71%	24.21%	0.87%	76.42%	36.44%
RB2-4	4.48%	8.09%	15.82%	11.23%	5.95%
LB1-2	4.48%	1.49%	0.52%	0.54%	0.56%
LB1-3	3.19%	2.12%	0.59%	4.40%	1.61%
LB1-4	58.23%	55.67%	40.96%	53.54%	61.15%
LB1-5	1.11%	2.54%	0.41%	2.13%	1.85%
RMB-3	1.60%	0.28%	0.22%	2.29%	1.82%
RB4-1	2.43%	4.41%	0.53%	5.49%	4.66%
RB4-2	15.46%	1.81%	9.67%	15.44%	15.71%
RB4-3	19.06%	14.51%	7.20%	29.95%	21.16%
LB4-1	0.42%	0.27%	0.60%	1.72%	1.22%
LB4-2	20.10%	6.20%	17.22%	27.24%	26.68%
LB4-3	38.48%	38.94%	20.05%	61.43%	51.69%
RB6	6.83%	0.60%	5.08%	8.59%	8.63%
LMB-5	15.10%	17.30%	4.03%	34.90%	27.96%
LB6	34.72%	44.19%	10.09%	52.49%	65.38%
LMB-6	10.42%	13.49%	0.38%	23.79%	15.78%
RMB-6	3.27%	2.23%	15.29%	1.37%	8.24%
RB7	73.53%	70.46%	17.68%	93.53%	81.13%
RMB-7	45.02%	42.19%	12.05%	68.57%	58.10%
RB8-1	31.94%	27.37%	5.42%	50.44%	38.57%
RB8-2	51.89%	38.78%	11.54%	81.75%	73.01%
RB8-3	5.63%	0.68%	2.50%	1.67%	1.01%
LB8-1	0.04%	1.68%	1.03%	0.78%	0.78%
LB8-2	74.30%	73.35%	26.90%	200.53%	139.65%
LB8-3	54.42%	54.18%	21.88%	78.55%	68.86%

Table 10—continued.

Subject 40189, Percent Error Comparison of 6.00 mGy and 14.98 mGy					
Airway	MinD	MajD	IA	WT	OA
T2	1.70%	1.02%	0.62%	2.59%	1.78%
RB1-1	11.25%	3.06%	2.08%	11.60%	8.60%
RB1-2	1.28%	1.61%	3.24%	1.59%	3.60%
RB1-3	6.67%	17.17%	0.29%	26.23%	16.69%
RMB	1.98%	29.28%	3.55%	41.85%	34.17%
LMB	1.27%	0.10%	0.20%	0.05%	0.03%
RB2-1	0.28%	0.32%	2.33%	0.22%	1.92%
LB1-1	0.28%	0.66%	0.39%	0.30%	0.05%
RB2-2	1.49%	1.95%	1.38%	1.84%	3.47%
RB2-3	1.53%	0.37%	0.14%	0.08%	0.36%
RB2-4	32.41%	33.17%	20.60%	50.51%	44.01%
LB1-2	0.50%	2.21%	0.31%	0.66%	0.34%
LB1-3	8.90%	0.13%	14.78%	10.57%	18.41%
LB1-4	7.83%	7.37%	9.89%	1.64%	7.82%
LB1-5	1.29%	2.33%	0.08%	0.53%	0.26%
RMB-3	0.23%	1.30%	0.31%	0.12%	0.28%
RB4-1	1.32%	1.29%	0.56%	1.14%	1.06%
RB4-2	16.92%	21.01%	6.40%	45.46%	33.83%
RB4-3	5.84%	1.32%	1.37%	10.14%	6.59%
LB4-1	2.76%	1.95%	0.00%	2.95%	2.12%
LB4-2	12.02%	5.06%	1.24%	1.40%	0.60%
LB4-3	5.00%	13.35%	13.51%	21.36%	24.21%
RB6	18.50%	12.25%	6.84%	36.86%	27.48%
LMB-5	0.56%	1.03%	4.77%	1.12%	3.25%
LB6	2.46%	1.04%	12.50%	3.84%	6.96%
LMB-6	0.53%	0.03%	0.64%	0.36%	0.66%
RMB-6	0.16%	0.93%	0.01%	2.26%	1.82%
RB7	69.89%	24.62%	16.44%	68.64%	77.81%
RMB-7	0.89%	1.07%	4.08%	0.15%	2.28%
RB8-1	9.16%	23.66%	1.64%	38.51%	23.81%
RB8-2	13.95%	15.15%	13.75%	32.68%	32.31%
RB8-3	3.39%	5.89%	0.39%	9.97%	6.23%
LB8-1	0.35%	3.49%	1.05%	2.50%	1.22%
LB8-2	0.29%	0.04%	0.49%	1.07%	0.42%
LB8-3	13.84%	6.66%	1.39%	21.59%	11.09%

Table 10—continued.

Subject 40189, Percent Error Comparison of 0.74 mGy and 14.98 mGy					
Airway	MinD	MajD	IA	WT	OA
T2	52.41%	48.05%	9.42%	73.63%	62.25%
RB1-1	9.86%	0.48%	0.19%	12.80%	8.78%
RB1-2	2.84%	2.25%	2.90%	4.95%	5.45%
RB1-3	5.80%	7.03%	0.08%	13.26%	8.51%
RMB	9.93%	5.86%	0.08%	4.43%	2.91%
LMB	2.11%	2.25%	0.18%	0.49%	0.38%
RB2-1	0.77%	0.97%	0.69%	0.88%	0.25%
LB1-1	2.53%	2.53%	0.41%	0.53%	0.27%
RB2-2	43.68%	11.10%	25.36%	39.65%	38.51%
RB2-3	24.72%	34.77%	1.08%	51.61%	37.01%
RB2-4	7.12%	6.25%	13.46%	11.54%	17.76%
LB1-2	0.18%	0.72%	0.14%	0.70%	0.29%
LB1-3	11.67%	0.11%	0.36%	8.93%	4.30%
LB1-4	1.87%	6.23%	11.23%	2.79%	8.30%
LB1-5	3.44%	3.44%	0.96%	1.86%	1.73%
RMB-3	0.32%	0.62%	2.30%	1.06%	1.53%
RB4-1	0.67%	3.03%	0.48%	2.94%	2.31%
RB4-2	1.72%	28.22%	8.88%	37.12%	29.09%
RB4-3	10.34%	3.06%	11.45%	14.58%	0.44%
LB4-1	1.74%	0.62%	0.41%	4.17%	2.44%
LB4-2	20.17%	8.84%	1.11%	3.86%	2.47%
LB4-3	8.54%	8.51%	0.14%	18.54%	10.98%
RB6	1.09%	1.22%	0.07%	0.28%	0.20%
LMB-5	33.56%	31.25%	1.29%	73.91%	52.64%
LB6	95.94%	84.27%	4.18%	79.57%	54.78%
LMB-6	39.57%	11.03%	4.95%	48.37%	35.75%
RMB-6	1.73%	0.56%	5.23%	1.78%	3.59%
RB7	66.19%	23.64%	16.32%	63.45%	74.98%
RMB-7	19.41%	52.58%	14.71%	95.44%	75.07%
RB8-1	46.35%	25.77%	14.45%	56.86%	46.53%
RB8-2	30.03%	25.84%	14.88%	65.12%	52.65%
RB8-3	16.35%	24.90%	13.21%	39.08%	32.91%
LB8-1	10.21%	5.57%	14.76%	15.39%	24.00%
LB8-2	49.71%	53.52%	1.75%	126.96%	67.33%
LB8-3	7.54%	7.37%	16.59%	11.99%	5.14%

Table 10—continued.

Subject 40190, Percent Error Comparison of 6.00 mGy and 14.98 mGy					
Airway	MinD	MajD	IA	WT	OA
T2	0.68%	1.66%	2.91%	2.06%	0.67%
RB1-1	57.55%	79.28%	1.62%	90.69%	82.04%
RB1-2	3.70%	8.76%	2.36%	12.84%	6.65%
RB1-3	4.38%	9.05%	1.55%	14.96%	10.54%
RMB	3.97%	1.90%	0.28%	3.97%	3.47%
LMB	0.46%	12.62%	1.14%	11.64%	7.80%
RB2-1	1.14%	2.37%	10.02%	3.57%	8.83%
LB1-1	1.47%	1.25%	3.50%	0.41%	2.29%
RB2-2	3.37%	18.60%	2.82%	26.81%	11.63%
RB2-3	20.94%	4.16%	13.61%	22.22%	22.92%
RB2-4	9.30%	3.14%	3.47%	12.84%	10.70%
LB1-2	1.64%	0.38%	2.89%	2.18%	0.78%
LB1-3	20.03%	23.72%	12.57%	35.97%	30.77%
LB1-4	0.57%	1.85%	0.18%	2.36%	1.51%
LB1-5	0.72%	1.84%	3.30%	0.43%	1.92%
RMB-3	0.05%	0.02%	31.17%	0.04%	16.74%
RB4-1	1.35%	0.50%	0.47%	0.09%	0.40%
RB4-2	34.18%	5.86%	3.23%	40.41%	33.00%
RB4-3	4.00%	2.96%	1.62%	7.52%	2.77%
LB4-1	2.91%	6.85%	0.45%	7.13%	5.05%
LB4-2	5.43%	21.61%	2.09%	22.18%	13.00%
LB4-3	61.18%	22.34%	24.00%	64.02%	75.60%
RB6	23.37%	6.83%	11.29%	30.10%	26.39%
LMB-5	2.07%	4.02%	0.26%	1.84%	1.53%
LB6	16.35%	3.57%	0.52%	19.65%	9.69%
LMB-6	0.15%	1.04%	20.65%	3.16%	8.24%
RMB-6	0.68%	0.76%	6.47%	1.37%	2.43%
RB7	5.75%	6.39%	14.73%	14.24%	19.73%
RMB-7	8.16%	2.05%	5.60%	10.86%	11.08%
RB8-1	0.18%	1.10%	0.12%	3.32%	2.40%
RB8-2	23.90%	8.32%	2.32%	26.53%	19.22%
RB8-3	2.68%	7.31%	18.71%	12.20%	23.56%
LB8-1	8.91%	5.35%	0.95%	12.17%	8.10%
LB8-2	17.34%	8.01%	0.35%	20.96%	12.99%
LB8-3	25.41%	27.64%	20.15%	58.45%	52.04%

Table 10—continued.

Subject 40190, Percent Error Comparison of 0.74 mGy and 14.98 mGy					
Airway	MinD	MajD	IA	WT	OA
T2	1.02%	0.75%	2.45%	1.68%	0.48%
RB1-1	51.58%	49.65%	1.61%	73.77%	64.44%
RB1-2	33.72%	31.15%	17.61%	54.45%	46.62%
RB1-3	4.49%	10.17%	0.80%	13.96%	9.16%
RMB	8.01%	1.77%	2.33%	2.35%	1.68%
LMB	1.28%	0.77%	1.71%	0.04%	0.76%
RB2-1	2.15%	2.35%	9.82%	0.66%	6.73%
LB1-1	1.56%	1.45%	2.20%	1.06%	2.13%
RB2-2	1.74%	7.13%	9.56%	6.73%	3.68%
RB2-3	24.13%	2.52%	2.25%	23.01%	14.87%
RB2-4	9.28%	1.13%	3.10%	8.97%	8.33%
LB1-2	1.00%	1.99%	0.75%	3.07%	1.47%
LB1-3	8.60%	4.75%	0.61%	8.66%	4.65%
LB1-4	7.32%	4.43%	0.26%	8.87%	5.11%
LB1-5	2.14%	1.18%	1.15%	0.65%	1.29%
RMB-3	1.70%	0.02%	32.41%	0.60%	17.76%
RB4-1	0.04%	0.44%	8.46%	1.23%	6.40%
RB4-2	40.18%	23.26%	4.60%	54.98%	47.84%
RB4-3	8.16%	5.59%	0.91%	14.07%	7.37%
LB4-1	2.82%	1.01%	2.89%	1.73%	3.20%
LB4-2	7.25%	27.91%	14.11%	38.49%	37.15%
LB4-3	57.16%	19.74%	24.35%	100.53%	74.56%
RB6	7.63%	0.56%	8.44%	7.42%	10.75%
LMB-5	0.08%	1.38%	0.20%	0.53%	0.38%
LB6	43.37%	20.21%	12.57%	73.88%	52.43%
LMB-6	2.09%	0.08%	19.41%	2.37%	8.33%
RMB-6	14.03%	8.83%	13.53%	25.36%	26.54%
RB7	0.69%	3.30%	0.38%	5.19%	2.41%
RMB-7	7.31%	33.23%	1.87%	53.05%	37.27%
RB8-1	3.71%	0.33%	0.05%	3.72%	2.36%
RB8-2	3.08%	3.65%	13.40%	9.19%	16.67%
RB8-3	0.75%	7.79%	13.96%	5.63%	8.41%
LB8-1	21.95%	17.69%	10.23%	43.91%	36.19%
LB8-2	29.85%	13.24%	13.08%	36.63%	31.42%
LB8-3	27.23%	31.99%	15.14%	63.95%	50.16%

Table 10—continued.

Subject 40191, Percent Error Comparison of 6.00 mGy and 14.98 mGy					
Airway	MinD	MajD	IA	WT	OA
T2	1.62%	0.49%	0.27%	1.47%	1.10%
RB1-1	52.04%	9.32%	0.29%	24.16%	15.98%
RB1-2	41.36%	31.39%	13.13%	59.83%	47.42%
RB1-3	89.00%	72.37%	20.28%	79.37%	70.86%
RMB	0.62%	4.04%	0.02%	3.94%	2.52%
LMB	0.61%	1.09%	0.66%	1.16%	0.54%
RB2-1	9.76%	15.79%	12.06%	27.23%	7.83%
LB1-1	3.83%	0.93%	2.41%	1.24%	0.44%
RB2-2	2.64%	6.58%	0.57%	1.85%	12.50%
RB2-3	13.20%	13.40%	0.08%	30.88%	17.47%
RB2-4	79.21%	50.49%	15.55%	62.67%	97.36%
LB1-2	2.43%	1.78%	0.49%	4.20%	1.95%
LB1-3	4.06%	1.91%	0.48%	5.53%	3.82%
LB1-4	71.84%	55.11%	24.89%	155.31%	92.81%
LB1-5	1.86%	1.62%	0.87%	2.01%	0.50%
RMB-3	8.83%	12.25%	2.55%	6.97%	5.21%
RB4-1	1.08%	2.06%	1.63%	0.50%	0.64%
RB4-2	15.51%	0.75%	4.43%	16.04%	8.03%
RB4-3	33.40%	20.72%	13.09%	49.83%	12.67%
LB4-1	0.10%	0.52%	0.16%	0.46%	0.04%
LB4-2	3.64%	3.30%	9.75%	7.36%	5.51%
LB4-3	1.04%	7.18%	14.90%	6.46%	16.40%
RB6	22.03%	11.44%	0.64%	26.58%	15.48%
LMB-5	0.82%	1.15%	3.86%	0.26%	1.59%
LB6	5.84%	3.39%	2.49%	7.78%	6.22%
LMB-6	0.82%	0.44%	8.73%	0.26%	5.87%
RMB-6	15.37%	1.38%	5.17%	14.83%	13.25%
RB7	19.78%	46.93%	31.25%	80.56%	77.44%
RMB-7	4.02%	18.63%	8.30%	17.94%	17.88%
RB8-1	3.88%	3.40%	0.29%	6.94%	4.25%
RB8-2	12.86%	9.10%	14.40%	21.66%	23.50%
RB8-3	29.43%	34.39%	20.80%	55.60%	47.23%
LB8-1	3.44%	29.19%	0.61%	34.88%	20.20%
LB8-2	0.82%	2.16%	0.36%	1.14%	0.87%
LB8-3	42.35%	21.93%	30.49%	70.92%	63.65%

Table 10—continued.

Subject 40191, Percent Error Comparison of 0.74 mGy and 14.98 mGy					
Airway	MinD	MajD	IA	WT	OA
T2	1.23%	0.53%	0.57%	1.78%	1.32%
RB1-1	25.58%	38.04%	3.61%	36.69%	25.32%
RB1-2	3.95%	3.07%	0.65%	1.66%	0.57%
RB1-3	54.94%	46.14%	20.01%	77.56%	84.08%
RMB	0.92%	0.04%	1.46%	0.10%	0.28%
LMB	0.47%	1.06%	5.42%	0.32%	1.52%
RB2-1	1.16%	1.51%	8.71%	2.20%	4.81%
LB1-1	6.55%	1.96%	5.64%	0.19%	2.43%
RB2-2	9.46%	5.53%	1.89%	17.08%	9.68%
RB2-3	8.85%	7.02%	11.92%	14.48%	18.39%
RB2-4	8.53%	7.51%	0.80%	21.07%	9.53%
LB1-2	0.69%	0.42%	0.54%	2.81%	1.25%
LB1-3	21.64%	1.12%	15.97%	19.64%	23.77%
LB1-4	80.23%	66.50%	26.35%	67.20%	82.06%
LB1-5	3.29%	3.83%	0.69%	0.57%	0.03%
RMB-3	7.43%	12.60%	2.24%	7.08%	5.32%
RB4-1	0.54%	0.18%	0.95%	0.10%	0.68%
RB4-2	21.99%	2.23%	8.41%	35.46%	28.35%
RB4-3	1.37%	17.56%	24.77%	24.25%	30.90%
LB4-1	10.84%	19.65%	2.16%	35.73%	23.93%
LB4-2	9.84%	12.57%	10.04%	21.00%	19.25%
LB4-3	4.90%	3.90%	12.43%	7.77%	5.15%
RB6	20.27%	11.79%	2.04%	26.10%	17.37%
LMB-5	0.80%	1.84%	0.19%	0.77%	0.66%
LB6	0.80%	4.90%	4.70%	7.54%	0.46%
LMB-6	0.18%	0.49%	15.01%	1.92%	10.39%
RMB-6	8.76%	0.87%	6.51%	12.06%	12.06%
RB7	22.96%	44.94%	29.91%	80.67%	76.67%
RMB-7	0.21%	4.85%	9.84%	2.51%	4.08%
RB8-1	7.20%	6.75%	0.22%	12.03%	7.50%
RB8-2	2.61%	6.57%	1.03%	11.01%	7.19%
RB8-3	23.64%	30.02%	16.11%	47.31%	39.89%
LB8-1	1.05%	4.19%	12.21%	4.56%	7.31%
LB8-2	1.09%	3.15%	0.17%	3.53%	2.73%
LB8-3	45.88%	20.02%	30.78%	77.16%	67.64%

Table 10—continued.

Subject 40383, Percent Error Comparison of 6.00 mGy and 14.98 mGy					
Airway	MinD	MajD	IA	WT	OA
T2	5.62%	3.86%	0.58%	9.39%	7.65%
RB1-1	0.74%	8.38%	0.33%	2.08%	2.47%
RB1-2	3.27%	3.43%	0.41%	8.47%	5.40%
RB1-3	0.90%	8.24%	0.96%	9.41%	5.29%
RMB	10.49%	18.62%	3.75%	29.58%	19.81%
LMB	3.46%	4.28%	0.18%	5.89%	4.33%
RB2-1	3.49%	4.05%	2.16%	6.52%	3.34%
LB1-1	23.71%	7.57%	8.82%	24.58%	21.48%
RB2-2	0.62%	8.06%	0.74%	7.76%	3.79%
RB2-3	7.14%	3.77%	0.26%	7.68%	5.28%
RB2-4	16.05%	12.00%	2.09%	7.06%	4.65%
LB1-2	5.59%	4.07%	0.23%	9.20%	6.08%
LB1-3	0.32%	0.72%	0.01%	1.40%	0.80%
LB1-4	8.93%	2.12%	12.53%	4.44%	7.55%
LB1-5	11.64%	0.54%	6.41%	9.21%	10.08%
RMB-3	3.76%	2.98%	60.30%	5.05%	20.51%
RB4-1	1.76%	0.69%	0.16%	0.36%	0.11%
RB4-2	2.39%	2.91%	0.56%	5.83%	2.60%
RB4-3	1.68%	1.57%	0.08%	2.52%	1.53%
LB4-1	3.52%	0.11%	0.14%	3.08%	2.08%
LB4-2	3.33%	0.44%	0.38%	3.20%	1.13%
LB4-3	3.74%	0.08%	0.31%	4.26%	2.65%
RB6	3.20%	3.10%	0.54%	6.12%	3.75%
LMB-5	0.08%	0.16%	15.86%	0.33%	7.56%
LB6	11.66%	10.31%	0.65%	22.82%	13.88%
LMB-6	5.49%	5.62%	10.34%	10.80%	13.38%
RMB-6	0.44%	1.69%	0.12%	1.95%	1.49%
RB7	5.23%	3.75%	0.47%	0.60%	0.70%
RMB-7	0.81%	0.58%	12.25%	2.93%	3.82%
RB8-1	1.58%	1.68%	7.36%	3.43%	6.69%
RB8-2	0.27%	1.47%	0.24%	0.27%	0.25%
RB8-3	27.85%	35.52%	16.56%	51.30%	43.04%
LB8-1	2.75%	1.27%	1.06%	2.27%	2.13%
LB8-2	1.29%	0.50%	0.12%	0.34%	0.26%
LB8-3	2.62%	5.96%	1.52%	9.96%	6.52%

Table 10—continued.

Subject 40383, Percent Error Comparison of 0.74 mGy and 14.98 mGy					
Airway	MinD	MajD	IA	WT	OA
T2	4.36%	3.18%	1.39%	7.15%	6.49%
RB1-1	8.95%	15.15%	1.33%	18.58%	11.59%
RB1-2	4.03%	0.72%	0.22%	1.31%	1.01%
RB1-3	0.72%	0.16%	0.33%	0.87%	0.46%
RMB	10.34%	18.58%	3.94%	29.10%	19.18%
LMB	2.26%	2.21%	1.85%	4.46%	4.44%
RB2-1	1.88%	1.75%	1.39%	1.22%	0.42%
LB1-1	16.48%	1.99%	7.68%	18.07%	16.39%
RB2-2	6.73%	5.13%	1.08%	3.39%	2.49%
RB2-3	2.38%	3.86%	0.22%	5.31%	3.55%
RB2-4	9.21%	3.24%	0.08%	6.84%	4.32%
LB1-2	1.31%	5.36%	0.31%	4.80%	2.73%
LB1-3	0.94%	0.46%	0.18%	0.57%	0.13%
LB1-4	6.41%	1.19%	0.83%	6.24%	4.46%
LB1-5	5.19%	1.33%	5.92%	6.82%	8.38%
RMB-3	2.92%	4.80%	0.01%	6.27%	5.02%
RB4-1	2.08%	0.37%	0.15%	3.01%	1.90%
RB4-2	0.71%	3.60%	0.39%	4.15%	2.93%
RB4-3	2.83%	0.24%	0.33%	2.64%	1.74%
LB4-1	4.15%	1.46%	0.34%	5.27%	3.44%
LB4-2	0.86%	3.19%	0.49%	1.25%	0.32%
LB4-3	1.00%	1.75%	0.27%	0.24%	0.12%
RB6	2.60%	2.19%	0.00%	6.15%	3.81%
LMB-5	1.29%	1.93%	16.81%	3.01%	5.80%
LB6	15.34%	17.34%	0.76%	28.80%	17.22%
LMB-6	3.46%	1.89%	5.99%	3.23%	0.79%
RMB-6	1.50%	0.38%	0.05%	1.23%	0.96%
RB7	1.74%	3.86%	0.18%	1.42%	0.65%
RMB-7	1.06%	0.94%	15.67%	3.97%	4.44%
RB8-1	0.85%	2.15%	0.28%	3.13%	2.04%
RB8-2	1.77%	0.05%	0.28%	0.31%	0.26%
RB8-3	28.06%	32.44%	10.25%	50.66%	39.58%
LB8-1	1.85%	3.14%	4.16%	3.02%	0.03%
LB8-2	8.78%	3.86%	0.47%	13.22%	9.12%
LB8-3	1.32%	6.31%	0.22%	4.62%	2.07%

Table 10—continued.

Subject 40470, Percent Error Comparison of 6.00 mGy and 14.98 mGy					
Airway	MinD	MajD	IA	WT	OA
T2	0.84%	0.23%	0.10%	0.36%	0.21%
RB1-1	30.73%	44.34%	2.92%	35.67%	25.86%
RB1-2	0.86%	0.09%	3.76%	1.55%	3.49%
RB1-3	1.43%	0.50%	3.32%	0.44%	2.57%
RMB	5.88%	12.71%	2.27%	45.09%	52.52%
LMB	0.18%	0.28%	0.40%	0.67%	0.55%
RB2-1	0.60%	1.36%	2.73%	1.70%	0.70%
LB1-1	4.78%	1.21%	3.55%	1.44%	1.53%
RB2-2	0.01%	0.04%	0.02%	0.57%	0.20%
RB2-3	0.59%	4.54%	0.92%	3.37%	1.67%
RB2-4	5.37%	8.06%	0.14%	13.31%	7.83%
LB1-2	0.88%	0.47%	1.02%	0.93%	1.31%
LB1-3	19.83%	22.02%	12.69%	39.33%	33.84%
LB1-4	2.70%	0.59%	0.28%	2.56%	1.81%
LB1-5	3.02%	0.23%	2.11%	2.94%	1.09%
RMB-3	3.04%	0.27%	0.08%	1.43%	1.14%
RB4-1	2.48%	0.32%	0.79%	2.01%	0.86%
RB4-2	0.69%	0.70%	1.83%	1.29%	1.04%
RB4-3	0.72%	0.06%	0.01%	1.45%	0.78%
LB4-1	0.34%	0.56%	5.58%	1.69%	5.32%
LB4-2	4.01%	3.90%	1.16%	7.74%	3.09%
LB4-3	1.59%	0.51%	0.17%	2.30%	1.44%
RB6	4.56%	4.57%	7.71%	10.39%	2.82%
LMB-5	0.53%	0.32%	10.14%	0.67%	3.72%
LB6	1.27%	2.15%	0.25%	3.18%	1.71%
LMB-6	0.02%	2.69%	2.02%	0.01%	1.17%
RMB-6	1.76%	0.11%	0.22%	0.31%	0.30%
RB7	10.77%	12.82%	0.11%	19.61%	13.66%
RMB-7	1.57%	1.64%	13.33%	0.17%	6.82%
RB8-1	0.17%	1.35%	0.06%	1.14%	0.84%
RB8-2	1.01%	0.07%	0.03%	0.45%	0.34%
RB8-3	8.20%	12.17%	1.00%	20.34%	10.09%
LB8-1	2.79%	1.26%	2.74%	3.48%	1.26%
LB8-2	0.97%	0.05%	1.27%	1.57%	0.04%
LB8-3	2.85%	7.49%	0.34%	11.00%	6.53%

Table 10—continued.

Subject 40470, Percent Error Comparison of 0.74 mGy and 14.98 mGy					
Airway	MinD	MajD	IA	WT	OA
T2	0.36%	0.03%	3.98%	0.02%	0.92%
RB1-1	32.33%	5.53%	5.21%	20.78%	19.02%
RB1-2	2.08%	1.55%	5.37%	1.39%	4.45%
RB1-3	2.18%	1.07%	0.21%	0.71%	0.69%
RMB	9.28%	8.01%	2.98%	9.17%	5.79%
LMB	1.16%	0.23%	2.46%	1.01%	1.68%
RB2-1	0.46%	1.84%	0.12%	4.94%	3.20%
LB1-1	2.76%	0.25%	2.51%	0.76%	2.34%
RB2-2	1.96%	1.01%	0.52%	4.30%	3.04%
RB2-3	2.58%	0.15%	1.69%	4.26%	2.10%
RB2-4	7.47%	8.00%	0.48%	14.79%	8.68%
LB1-2	1.39%	1.07%	1.27%	2.13%	2.07%
LB1-3	23.06%	22.22%	13.04%	41.10%	34.96%
LB1-4	9.40%	9.04%	13.50%	20.31%	22.41%
LB1-5	0.48%	0.63%	5.97%	1.24%	3.74%
RMB-3	0.89%	0.66%	0.09%	0.88%	0.67%
RB4-1	1.72%	0.30%	0.05%	0.88%	0.54%
RB4-2	3.35%	2.82%	1.68%	8.58%	6.56%
RB4-3	2.17%	1.34%	0.06%	4.94%	3.31%
LB4-1	0.07%	2.92%	10.05%	3.21%	8.76%
LB4-2	51.26%	87.29%	8.00%	92.82%	84.07%
LB4-3	3.48%	0.25%	0.48%	4.43%	2.91%
RB6	4.36%	8.33%	1.26%	10.48%	6.58%
LMB-5	0.20%	0.43%	16.71%	1.25%	5.94%
LB6	4.35%	16.14%	1.03%	21.88%	10.21%
LMB-6	1.98%	1.89%	7.86%	1.37%	3.07%
RMB-6	0.39%	0.00%	0.05%	1.47%	1.13%
RB7	1.36%	3.14%	0.01%	2.99%	1.97%
RMB-7	1.55%	0.40%	1.81%	1.51%	2.02%
RB8-1	1.80%	2.88%	0.12%	1.58%	0.85%
RB8-2	5.21%	2.47%	0.15%	6.35%	4.41%
RB8-3	31.03%	24.78%	16.17%	48.94%	41.58%
LB8-1	0.15%	1.73%	7.69%	2.55%	1.93%
LB8-2	0.45%	0.80%	1.53%	0.01%	1.14%
LB8-3	9.87%	7.41%	2.36%	17.39%	12.85%

Table 11. Percent error values for in- to ex-vivo comparison. Each table compares the 14.98 mGy scans using the in-vivo as ground truth with values < 0.05 emphasized.

Subject 40016, Percent Error Comparison of 14.98 mGy ex-vivo and 14.98 mGy in-vivo					
Airway	MinD	MajD	IA	WT	OA
T2	21.12%	4.28%	22.98%	9.00%	13.98%
RB1-1	69.35%	45.64%	20.14%	81.63%	75.84%
RB1-2	8.95%	8.90%	6.89%	19.43%	16.23%
RB1-3	13.99%	5.81%	2.14%	17.05%	11.86%
RMB	21.55%	5.25%	14.26%	13.19%	15.01%
LMB	1.64%	4.62%	0.58%	9.14%	7.21%
RB2-1	38.07%	1.68%	8.99%	30.29%	23.87%
LB1-1	35.32%	2.55%	14.22%	29.90%	26.36%
RB2-2	48.63%	27.70%	3.16%	82.97%	47.31%
RB2-3	28.82%	25.04%	14.21%	61.51%	19.91%
RB2-4	17.96%	14.41%	32.05%	31.75%	39.38%
LB1-2	7.19%	8.56%	13.77%	16.74%	19.80%
LB1-3	41.22%	17.19%	14.96%	49.32%	39.66%
LB1-4	47.62%	59.97%	18.82%	45.76%	90.96%
LB1-5	3.44%	7.33%	13.23%	10.03%	14.64%
RMB-3	13.26%	1.38%	1.86%	11.91%	9.67%
RB4-1	18.02%	1.02%	5.57%	15.22%	12.46%
RB4-2	44.28%	27.73%	27.54%	59.21%	52.47%
RB4-3	29.65%	34.34%	2.44%	72.73%	43.16%
LB4-1	6.97%	2.00%	2.37%	5.30%	4.16%
LB4-2	54.08%	43.31%	17.91%	77.64%	70.47%
LB4-3	4.01%	7.24%	12.72%	8.06%	12.14%
RB6	17.51%	24.60%	0.50%	52.52%	27.87%
LMB-5	6.32%	1.56%	0.78%	9.12%	6.83%
LB6	42.30%	34.33%	14.64%	61.40%	46.45%
LMB-6	5.05%	0.87%	11.20%	8.31%	11.85%
RMB-6	5.48%	5.47%	1.05%	2.16%	1.72%
RB7	75.31%	44.67%	2.48%	77.71%	37.71%
RMB-7	5.52%	4.15%	2.88%	10.99%	8.51%
RB8-1	10.76%	4.60%	1.15%	6.09%	2.80%
RB8-2	27.34%	27.89%	16.66%	47.45%	40.78%
RB8-3	7.21%	8.74%	7.69%	19.96%	16.56%
LB8-1	48.79%	34.76%	5.55%	96.76%	63.06%
LB8-2	15.77%	38.77%	9.49%	56.38%	42.86%
LB8-3	67.21%	65.62%	36.77%	88.13%	81.18%

Table 11—continued.

Subject 40189, Percent Error Comparison of 14.98 mGy ex-vivo and 14.98 mGy in-vivo					
Airway	MinD	MajD	IA	WT	OA
T2	16.80%	12.35%	0.53%	24.47%	17.71%
RB1-1	6.07%	207.61%	31.98%	241.66%	166.85%
RB1-2	4.71%	6.69%	27.48%	1.72%	24.48%
RB1-3	16.03%	7.84%	26.49%	7.86%	16.28%
RMB	18.92%	50.95%	9.04%	66.24%	58.21%
LMB	22.30%	6.94%	44.95%	15.87%	7.13%
RB2-1	25.04%	10.04%	7.45%	32.96%	18.46%
LB1-1	34.37%	0.23%	13.62%	33.67%	6.04%
RB2-2	21.09%	13.05%	17.68%	28.10%	26.39%
RB2-3	3.32%	5.53%	25.93%	4.13%	27.50%
RB2-4	45.35%	45.91%	24.64%	68.74%	56.96%
LB1-2	25.35%	1.92%	15.46%	18.87%	5.07%
LB1-3	1.63%	1.19%	4.19%	0.26%	1.14%
LB1-4	35.45%	42.38%	32.10%	56.16%	51.92%
LB1-5	39.58%	22.11%	1.89%	51.29%	30.11%
RMB-3	34.37%	12.50%	22.04%	40.72%	38.78%
RB4-1	11.30%	6.21%	7.07%	18.90%	4.83%
RB4-2	21.70%	31.51%	24.57%	47.43%	45.14%
RB4-3	9.57%	13.15%	9.27%	23.73%	7.96%
LB4-1	9.57%	3.27%	8.81%	4.15%	9.97%
LB4-2	26.24%	12.64%	33.12%	7.05%	22.18%
LB4-3	12.68%	10.61%	1.63%	20.78%	8.01%
RB6	11.77%	1.37%	6.62%	7.79%	0.70%
LMB-5	9.39%	5.50%	29.63%	14.50%	6.54%
LB6	32.12%	25.71%	17.25%	49.65%	41.14%
LMB-6	9.78%	4.50%	19.33%	14.16%	2.54%
RMB-6	4.10%	12.62%	23.07%	21.94%	6.49%
RB7	49.60%	30.42%	61.94%	76.74%	67.21%
RMB-7	8.96%	7.87%	27.24%	12.99%	9.20%
RB8-1	6.18%	4.97%	24.83%	13.67%	10.08%
RB8-2	7.89%	15.93%	15.62%	23.78%	2.67%
RB8-3	16.06%	16.95%	9.32%	36.69%	32.48%
LB8-1	2.00%	3.20%	6.77%	6.43%	3.28%
LB8-2	35.96%	33.96%	27.87%	57.26%	50.59%
LB8-3	6.29%	8.54%	19.54%	1.74%	8.71%

Table 11—continued.

Subject 40190, Percent Error Comparison of 14.98 mGy ex-vivo and 14.98 mGy in-vivo					
Airway	MinD	MajD	IA	WT	OA
T2	21.81%	11.03%	5.98%	27.77%	22.82%
RB1-1	12.30%	29.11%	35.09%	22.54%	2.61%
RB1-2	4.72%	7.31%	1.67%	12.01%	6.12%
RB1-3	9.09%	19.43%	16.86%	30.62%	35.18%
RMB	12.62%	57.38%	4.35%	61.53%	51.98%
LMB	40.95%	7.79%	19.54%	43.73%	38.52%
RB2-1	7.26%	2.54%	1.21%	3.51%	1.96%
LB1-1	27.10%	6.87%	0.72%	32.61%	15.61%
RB2-2	74.80%	44.32%	4.28%	68.50%	73.79%
RB2-3	23.67%	24.28%	9.69%	55.43%	28.93%
RB2-4	15.75%	6.58%	4.52%	26.92%	17.74%
LB1-2	38.93%	15.57%	15.02%	16.47%	14.52%
LB1-3	2.21%	12.94%	21.85%	11.64%	21.33%
LB1-4	7.40%	10.47%	25.86%	15.73%	9.56%
LB1-5	6.71%	5.67%	1.86%	10.00%	3.17%
RMB-3	1.87%	2.86%	23.85%	0.16%	11.79%
RB4-1	9.77%	5.89%	5.41%	2.39%	5.24%
RB4-2	18.92%	16.10%	19.22%	29.32%	27.35%
RB4-3	11.31%	0.82%	5.18%	12.82%	9.88%
LB4-1	7.51%	1.57%	1.05%	10.26%	10.92%
LB4-2	0.49%	15.57%	29.42%	12.39%	28.01%
LB4-3	92.67%	47.20%	3.24%	88.30%	91.81%
RB6	15.43%	5.88%	18.05%	23.23%	1.35%
LMB-5	22.37%	18.43%	17.78%	38.62%	21.36%
LB6	17.37%	10.65%	9.32%	32.27%	22.65%
LMB-6	5.20%	6.64%	27.53%	14.93%	3.95%
RMB-6	3.78%	4.17%	30.25%	0.69%	16.24%
RB7	14.75%	8.09%	5.68%	23.87%	11.04%
RMB-7	12.38%	38.94%	30.30%	54.85%	67.46%
RB8-1	2.58%	7.97%	1.93%	3.67%	4.12%
RB8-2	16.95%	17.72%	5.75%	31.71%	18.67%
RB8-3	12.56%	5.76%	11.41%	20.74%	4.52%
LB8-1	6.17%	20.06%	24.21%	31.52%	42.12%
LB8-2	3.47%	14.38%	5.86%	23.71%	14.73%
LB8-3	36.59%	43.15%	35.41%	88.73%	95.57%

Table 11—continued.

Subject 40191, Percent Error Comparison of 14.98 mGy ex-vivo and 14.98 mGy in-vivo					
Airway	MinD	MajD	IA	WT	OA
T2	18.90%	3.93%	9.22%	19.95%	18.72%
RB1-1	4.03%	53.75%	8.01%	62.30%	52.68%
RB1-2	30.09%	23.06%	17.60%	46.12%	37.39%
RB1-3	86.66%	72.15%	28.24%	46.01%	55.37%
RMB	11.83%	48.59%	4.47%	69.86%	45.19%
LMB	9.97%	50.72%	24.30%	63.63%	28.59%
RB2-1	6.79%	5.62%	3.53%	11.12%	9.95%
LB1-1	21.48%	12.82%	23.01%	5.09%	17.57%
RB2-2	32.36%	16.74%	3.40%	63.80%	38.84%
RB2-3	53.47%	86.72%	17.75%	78.58%	49.03%
RB2-4	12.97%	2.87%	27.65%	19.03%	11.16%
LB1-2	2.31%	0.31%	5.88%	2.68%	0.28%
LB1-3	10.34%	5.09%	15.49%	13.46%	15.97%
LB1-4	58.78%	68.65%	11.40%	80.88%	59.40%
LB1-5	7.99%	5.60%	0.54%	0.42%	3.15%
RMB-3	7.09%	8.54%	17.90%	17.91%	4.81%
RB4-1	8.89%	1.79%	7.36%	3.99%	4.92%
RB4-2	24.15%	7.74%	4.38%	29.54%	13.94%
RB4-3	33.92%	17.86%	20.86%	49.82%	8.05%
LB4-1	5.77%	12.05%	6.51%	12.86%	16.07%
LB4-2	6.78%	10.66%	24.08%	17.16%	28.01%
LB4-3	29.25%	26.06%	18.99%	63.08%	58.20%
RB6	27.28%	24.95%	16.92%	41.76%	33.83%
LMB-5	28.34%	24.77%	11.20%	44.28%	29.43%
LB6	1.48%	0.74%	99.19%	1.31%	35.61%
LMB-6	17.63%	19.07%	2.42%	34.13%	22.25%
RMB-6	18.52%	7.02%	16.46%	23.52%	7.13%
RB7	3.01%	60.87%	22.83%	68.21%	75.10%
RMB-7	16.39%	4.01%	13.91%	11.88%	2.59%
RB8-1	29.33%	2.07%	3.81%	30.02%	19.39%
RB8-2	28.33%	5.68%	33.13%	30.47%	37.59%
RB8-3	31.40%	37.31%	37.72%	58.03%	57.74%
LB8-1	25.96%	62.09%	10.17%	51.61%	74.95%
LB8-2	19.07%	14.34%	29.73%	27.86%	34.70%
LB8-3	22.28%	14.77%	7.45%	48.52%	36.39%

Table 11—continued.

Subject 40383, Percent Error Comparison of 14.98 mGy ex-vivo and 14.98 mGy in-vivo					
Airway	MinD	MajD	IA	WT	OA
T2	6.02%	21.42%	11.55%	14.53%	4.92%
RB1-1	30.70%	75.50%	0.74%	46.23%	55.02%
RB1-2	11.88%	13.29%	1.31%	24.10%	13.51%
RB1-3	10.63%	19.37%	2.25%	34.47%	22.58%
RMB	11.78%	31.99%	5.56%	12.93%	12.69%
LMB	15.44%	7.99%	30.67%	6.42%	19.88%
RB2-1	16.96%	8.03%	1.57%	7.67%	2.97%
LB1-1	22.62%	17.61%	13.66%	4.00%	7.13%
RB2-2	1.79%	2.35%	6.99%	4.18%	10.41%
RB2-3	1.29%	4.83%	12.39%	5.48%	4.07%
RB2-4	11.61%	3.70%	13.82%	15.95%	19.80%
LB1-2	7.65%	6.13%	17.81%	2.11%	15.26%
LB1-3	2.44%	0.72%	4.08%	3.81%	5.07%
LB1-4	9.00%	1.58%	0.63%	10.88%	5.51%
LB1-5	2.76%	0.52%	10.82%	5.57%	10.51%
RMB-3	9.28%	0.98%	18.14%	7.85%	1.17%
RB4-1	10.48%	15.33%	17.99%	28.82%	31.86%
RB4-2	13.70%	9.76%	2.75%	26.65%	19.44%
RB4-3	24.53%	17.90%	19.06%	49.61%	45.61%
LB4-1	8.61%	15.90%	17.81%	23.77%	29.13%
LB4-2	17.77%	2.46%	16.13%	18.37%	26.50%
LB4-3	14.53%	7.58%	18.16%	24.97%	29.42%
RB6	12.98%	5.59%	3.96%	19.62%	14.16%
LMB-5	7.17%	2.80%	24.56%	13.16%	1.77%
LB6	12.77%	3.94%	17.33%	13.65%	6.38%
LMB-6	7.93%	0.97%	22.59%	1.54%	10.15%
RMB-6	0.24%	1.63%	14.61%	0.44%	7.24%
RB7	20.92%	11.85%	18.69%	34.86%	36.36%
RMB-7	3.92%	0.61%	11.37%	2.05%	7.22%
RB8-1	5.99%	0.11%	15.14%	3.40%	7.14%
RB8-2	7.24%	12.43%	18.61%	21.77%	28.58%
RB8-3	23.07%	29.32%	1.98%	42.59%	25.98%
LB8-1	4.40%	2.50%	27.00%	2.46%	13.02%
LB8-2	4.14%	10.89%	17.86%	14.29%	22.63%
LB8-3	49.39%	52.05%	22.33%	133.14%	92.69%

Table 11—continued.

Subject 40470, Percent Error Comparison of 14.98 mGy ex-vivo and 14.98 mGy in-vivo					
Airway	MinD	MajD	IA	WT	OA
T2	11.81%	6.15%	16.58%	17.86%	19.66%
RB1-1	24.53%	61.44%	20.46%	73.97%	64.46%
RB1-2	11.08%	12.86%	14.87%	26.93%	26.58%
RB1-3	10.99%	8.02%	8.74%	20.51%	19.15%
RMB	5.18%	65.94%	12.28%	87.18%	59.48%
LMB	19.52%	3.88%	16.61%	19.46%	21.19%
RB2-1	14.37%	20.86%	7.81%	31.01%	26.58%
LB1-1	26.44%	12.60%	13.36%	30.78%	28.52%
RB2-2	8.55%	6.17%	9.68%	3.73%	8.91%
RB2-3	10.85%	3.94%	10.06%	12.48%	14.54%
RB2-4	77.73%	80.23%	3.11%	63.07%	47.02%
LB1-2	16.94%	3.37%	11.02%	17.36%	18.25%
LB1-3	8.23%	7.89%	21.17%	14.69%	25.09%
LB1-4	23.73%	20.65%	23.53%	40.03%	40.72%
LB1-5	2.16%	1.45%	13.61%	1.01%	9.66%
RMB-3	4.51%	4.65%	9.25%	5.76%	8.26%
RB4-1	3.91%	4.39%	9.36%	1.50%	4.31%
RB4-2	5.37%	14.26%	7.08%	10.47%	1.13%
RB4-3	3.12%	2.64%	8.99%	3.98%	3.64%
LB4-1	4.10%	0.02%	15.44%	3.63%	8.09%
LB4-2	31.88%	27.31%	8.91%	63.15%	22.81%
LB4-3	18.65%	22.00%	8.85%	43.50%	18.95%
RB6	47.08%	48.29%	8.59%	73.19%	59.01%
LMB-5	5.22%	4.56%	7.09%	7.06%	8.62%
LB6	4.80%	3.84%	8.21%	1.93%	7.16%
LMB-6	0.66%	6.44%	10.55%	3.68%	2.55%
RMB-6	4.72%	1.35%	10.30%	2.95%	6.41%
RB7	21.29%	2.21%	10.97%	13.72%	15.20%
RMB-7	4.89%	0.94%	23.15%	0.72%	12.56%
RB8-1	7.19%	8.44%	3.65%	13.61%	6.20%
RB8-2	0.58%	0.35%	9.16%	0.08%	5.97%
RB8-3	27.44%	26.24%	20.26%	47.95%	43.31%
LB8-1	5.63%	7.06%	10.68%	13.06%	15.06%
LB8-2	9.03%	0.58%	10.03%	5.93%	2.88%
LB8-3	0.90%	7.24%	8.43%	8.08%	11.50%

Table 12. Output values from the full-width half-maximum calculation on the ex-vivo airways. Each of the five locations is shown for each of the thirteen cubes.

Cube	Location	MinD (mm)	MajD (mm)	WT (mm)	IA (mm)	OA (mm)
B8L7C2R3	High Dose	0.98	5.38	2.01	57.09	161.67
	Medium Dose	1.00	5.69	1.72	64.08	144.05
	Low Dose	1.00	5.24	2.06	60.30	155.40
	CT Cube	1.00	6.44	1.92	101.01	160.49
	μCT Cube	0.64	6.08	1.13	108.65	170.93
B8L7C2R4	High Dose	1.32	3.25	0.93	10.68	32.44
	Medium Dose	1.00	3.01	1.08	10.36	32.76
	Low Dose	1.17	3.25	1.16	10.84	42.91
	CT Cube	1.00	2.56	0.58	18.77	50.38
	μCT Cube	0.77	3.80	0.64	38.27	65.97
B8L7C2R5	High Dose	1.00	1.86	0.41	4.40	14.34
	Medium Dose	1.00	1.88	0.62	4.70	15.26
	Low Dose	1.00	2.12	0.72	5.21	18.26
	CT Cube	0.90	2.20	1.53	65.45	88.97
	μCT Cube	0.50	4.31	1.34	74.36	72.84
B8L7C5R3	High Dose	1.00	2.91	1.37	16.79	46.75
	Medium Dose	0.98	3.19	1.29	15.88	44.03
	Low Dose	1.00	2.73	1.45	15.07	47.50
	CT Cube	1.00	1.37	1.28	23.50	97.63
	μCT Cube	0.87	1.61	0.93	27.62	81.89
B8L7C5R4	High Dose	1.31	3.35	1.22	11.51	67.83
	Medium Dose	1.31	3.73	1.15	14.50	61.37
	Low Dose	1.31	3.62	1.22	13.46	68.33
	CT Cube	1.00	3.53	0.97	42.23	108.25
	μCT Cube	0.66	3.45	0.88	38.48	112.17

Table 12—continued.

B11L10C1R3	High Dose	1.73	3.56	1.14	14.13	47.00
	Medium Dose	1.86	3.62	1.08	14.24	49.70
	Low Dose	1.99	3.60	1.11	14.38	59.65
	CT Cube	1.41	3.39	0.50	28.16	47.86
	μCT Cube	1.51	3.18	0.45	24.22	42.72
B11L10C2R2	High Dose	1.47	4.48	1.32	19.82	54.74
	Medium Dose	1.39	4.67	1.00	23.48	52.20
	Low Dose	1.61	4.47	1.11	19.68	48.94
	CT Cube	1.00	4.83	0.88	77.35	85.91
	μCT Cube	0.84	4.98	0.66	57.44	94.29
B11L10C3R2	High Dose	1.40	6.80	1.32	42.44	105.67
	Medium Dose	1.51	6.84	1.31	44.82	107.60
	Low Dose	1.25	6.53	1.35	40.62	109.77
	CT Cube	2.00	7.03	1.16	89.00	110.24
	μCT Cube	2.47	7.06	0.72	110.12	119.93
B11L10C3R3	High Dose	1.19	3.04	1.20	11.09	40.43
	Medium Dose	1.18	3.04	1.02	10.86	32.48
	Low Dose	1.22	3.03	1.09	12.64	37.20
	CT Cube	1.20	3.55	0.92	27.47	55.26
	μCT Cube	1.11	3.41	0.73	26.14	60.35
B11L10C5R2	High Dose	1.13	2.55	1.08	6.56	32.97
	Medium Dose	1.29	2.50	1.13	6.75	42.08
	Low Dose	1.05	2.42	1.23	8.12	40.42
	CT Cube	2.36	4.84	0.57	66.81	130.94
	μCT Cube	2.12	5.82	0.72	75.38	132.68
B11L10C5R3	High Dose	1.00	2.58	1.07	19.47	66.14
	Medium Dose	1.02	2.61	1.12	20.02	63.09
	Low Dose	1.01	2.95	1.08	20.37	68.38
	CT Cube	1.00	2.50	0.96	14.73	56.71
	μCT Cube	0.97	2.49	0.57	14.67	38.85

Table 12—continued.

B14L13C2R1	High Dose	1.00	2.07	1.02	5.32	45.11
	Medium Dose	1.00	2.44	1.12	6.79	51.86
	Low Dose	1.00	2.67	0.89	6.11	32.54
	CT Cube	1.07	2.32	1.59	36.33	105.27
	μCT Cube	1.10	3.16	1.17	47.78	111.62
B14L13C3R2	High Dose	1.43	2.85	0.97	8.56	27.88
	Medium Dose	1.29	2.96	1.02	9.18	29.83
	Low Dose	1.39	2.98	0.97	9.45	29.11
	CT Cube	1.00	3.40	1.25	22.48	44.04
	μCT Cube	1.27	3.29	0.51	21.93	43.70

Table 13. Output values from the full-width half-maximum calculation on the in-vivo airways. Each of the five locations is shown for each of the five.

Cube	Location	MinD (mm)	MajD (mm)	WT (mm)	IA (mm)	OA (mm)
B8L7C2R3	High Dose	0.98	5.38	2.01	57.09	161.67
	Medium Dose	1.00	5.69	1.72	64.08	144.05
	Low Dose	1.00	5.24	2.06	60.30	155.40
B8L7C2R4	High Dose	1.32	3.25	0.93	10.68	32.44
	Medium Dose	1.00	3.01	1.08	10.36	32.76
	Low Dose	1.17	3.25	1.16	10.84	42.91
B8L7C2R5	High Dose	1.00	1.86	0.41	4.40	14.34
	Medium Dose	1.00	1.88	0.62	4.70	15.26
	Low Dose	1.00	2.12	0.72	5.21	18.26
B8L7C5R3	High Dose	1.00	2.91	1.37	16.79	46.75
	Medium Dose	0.98	3.19	1.29	15.88	44.03
	Low Dose	1.00	2.73	1.45	15.07	47.50
B8L7C5R4	High Dose	1.31	3.35	1.22	11.51	67.83
	Medium Dose	1.31	3.73	1.15	14.50	61.37
	Low Dose	1.31	3.62	1.22	13.46	68.33

Table 14. Post-registration layering. Examples of the registered images are showed layered over one another. Note the distinct appearance of the μ CT cube airway in the images as opposed to the appearance of the CT cube airway.


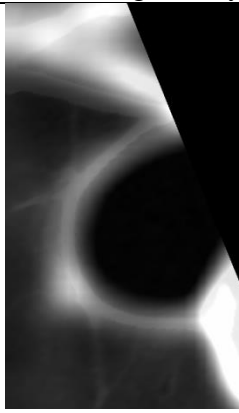
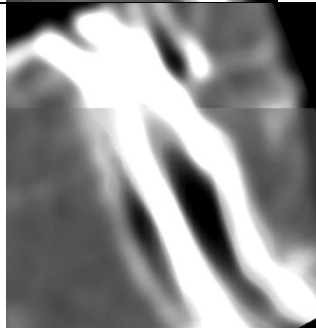
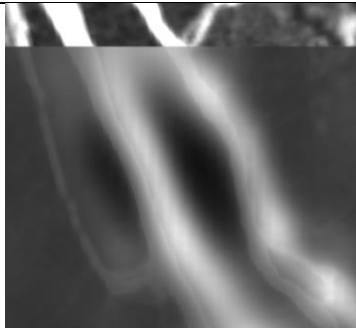
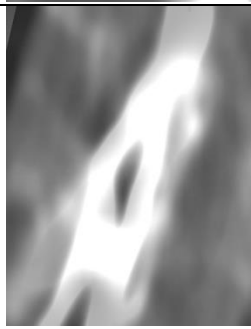
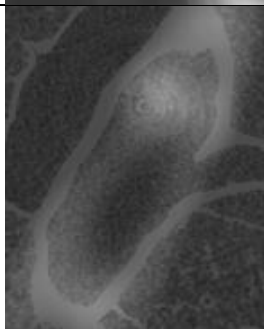


	CT cube airway and high dose whole lung airway	μ CT cube airway and high dose whole lung airway
B8L7C2R3		
B8L7C2R4		
B8L7C2R5		
B8L7C5R3		

Table 14—continued.

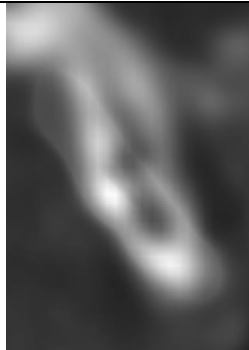
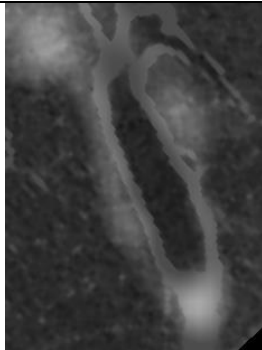
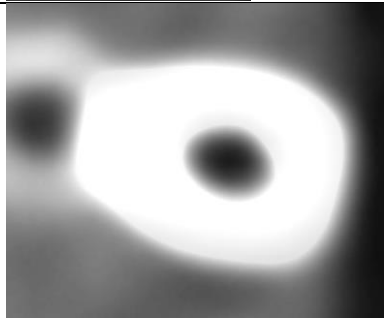
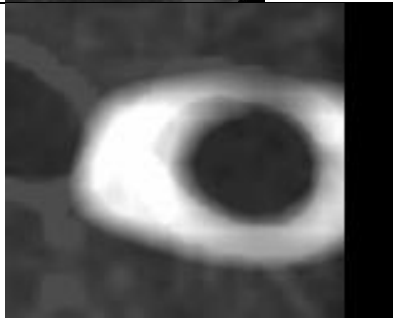
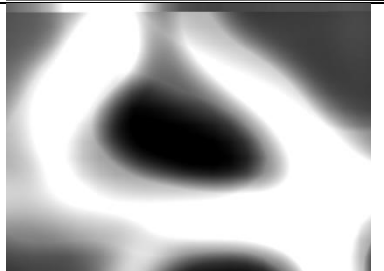
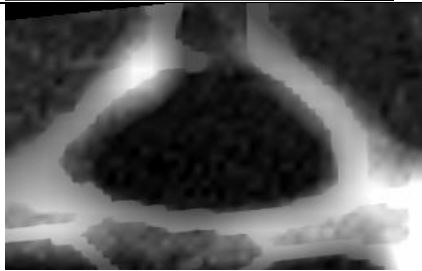
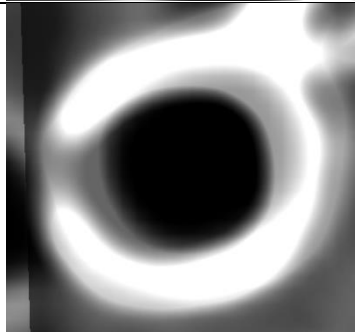
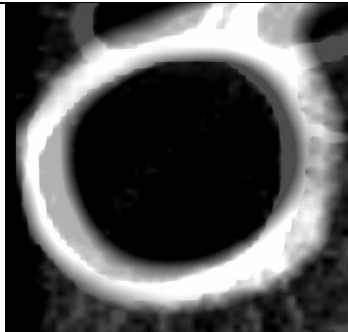


B8L7C5R4		
B11L10C1R3		
B11L10C2R2		
B11L10C3R2		
B11L10C3R3		

Table 14—continued.

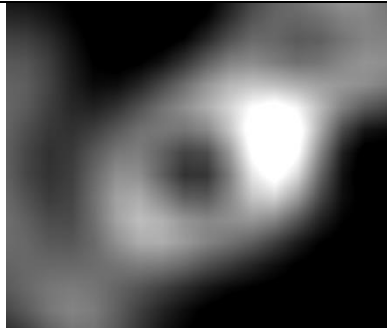
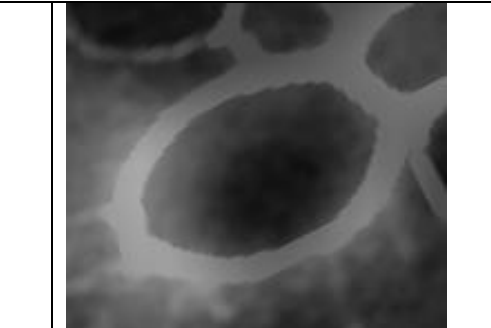
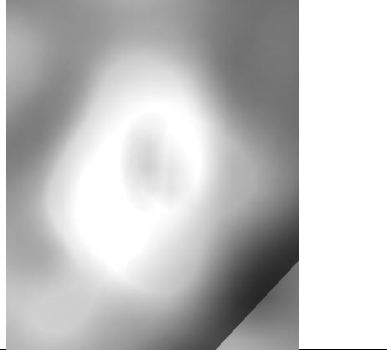
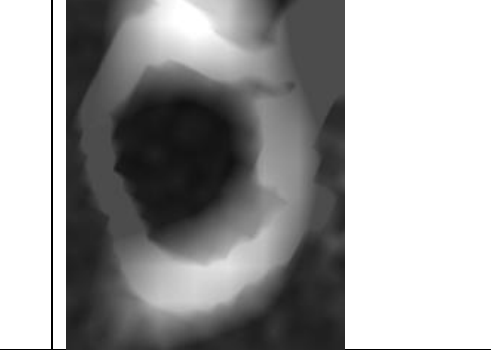
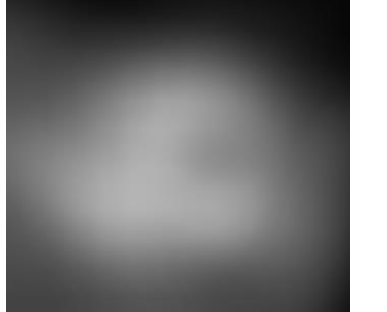

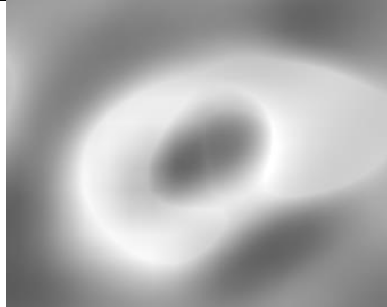

B11L10C5R2		
B11L10C5R3		
B14L13C2R1		
B14L13C3R2		

Table 15. Fiducial alignment pre- and post-registration. The images in the left column are aligned by their centers. The images in the right column are aligned according to the final registration transform.

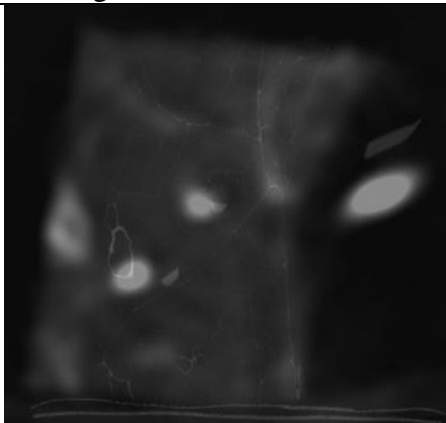
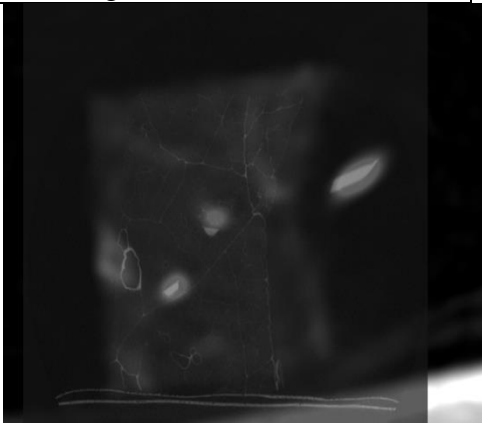

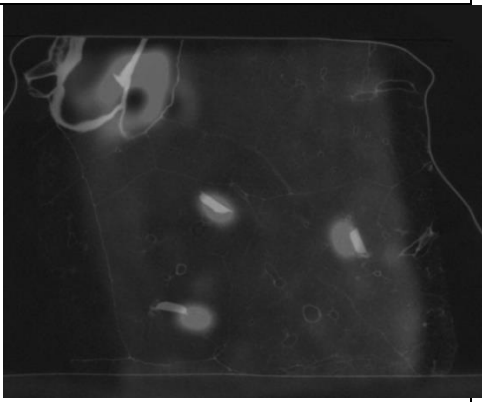
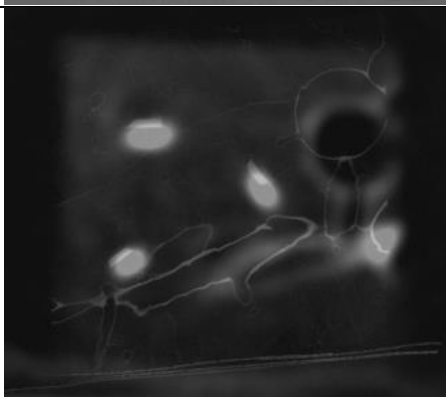
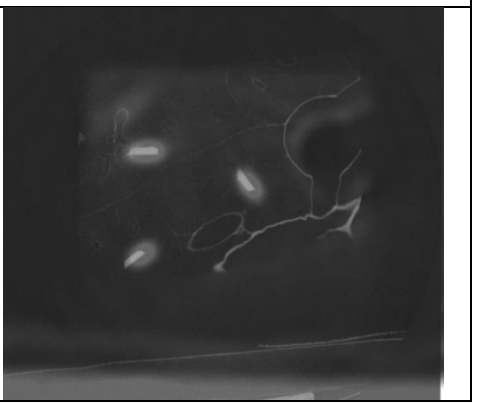
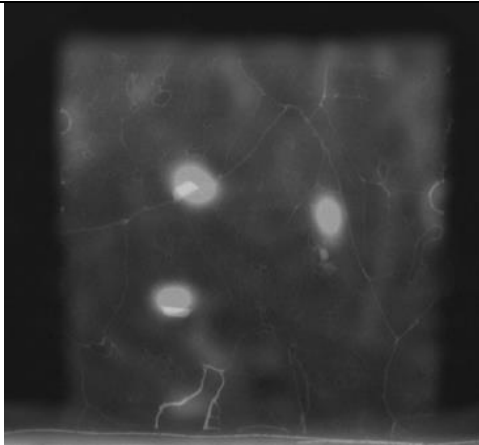
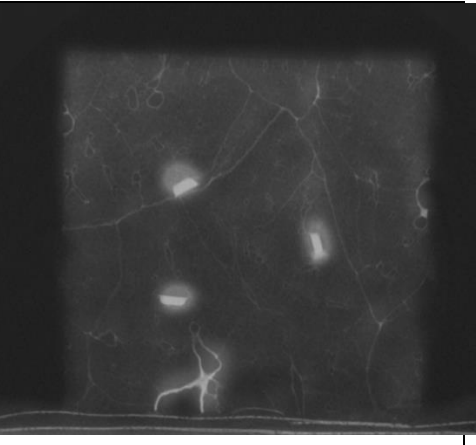
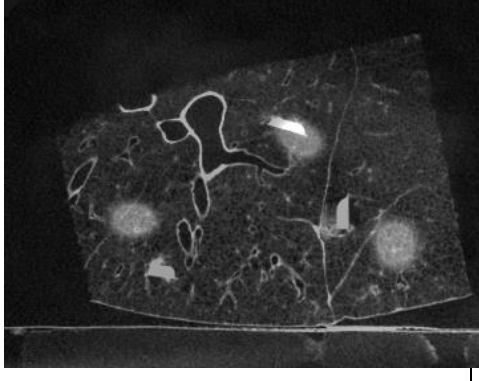
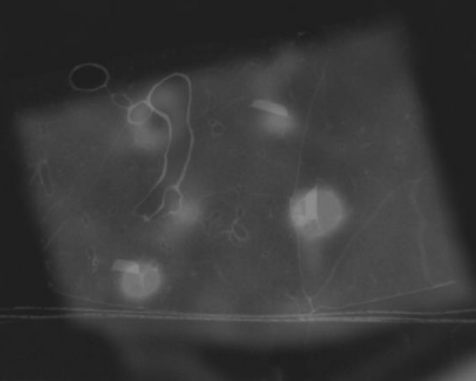
Cube ID	Pre-Registration	Post-Registration
B8L7C2R5		
B8L7C5R3		
B11L10C2R2		

Table 15—continued.

B11L10C5R3		
B14L13C2R1		

REFERENCES

1. *Disease Statistics*. 2012; Available from: <http://www.nhlbi.nih.gov/about/documents/factbook/2012/chapter4>.
2. West, J.B., *Respiratory Physiology: The Essentials*. 9 ed. 2012, Baltimore, MD: Lippincott Williams & Wilkins.
3. *What Is COPD?* 2015; Available from: <http://www.nhlbi.nih.gov/health/health-topics/topics/copd>.
4. *Understanding Chronic Bronchitis*. 2015; Available from: <http://www.lung.org/lung-disease/bronchitis-chronic/understanding-chronic-bronchitis.html>.
5. *Cystic fibrosis*. 2014; Available from: <http://ghr.nlm.nih.gov/condition/cystic-fibrosis>.
6. Hogg, J.C., et al., *The Nature of Small-Airway Obstruction in Chronic Obstructive Pulmonary Disease*. *New England Journal of Medicine*, 2004. **350**(26): p. 2645-2653.
7. Coxson, H.O. and R.M. Rogers, *Quantitative Computed Tomography of Chronic Obstructive Pulmonary Disease I*. *Academic Radiology*. **12**(11): p. 1457-1463.
8. Hruban, R.H., et al., *High Resolution Computed Tomography of Inflation-fixed Lungs: Pathologic-Radiologic Correlation of Centrilobular Emphysema*. *American Review of Respiratory Disease*, 1987. **136**(4): p. 935-940.
9. McDonough, J.E., et al., *Small-Airway Obstruction and Emphysema in Chronic Obstructive Pulmonary Disease*. *New England Journal of Medicine*, 2011. **365**(17): p. 1567-1575.
10. Remy-Jardin, M., et al., *Lung parenchymal changes secondary to cigarette smoking: pathologic-CT correlations*. *Radiology*, 1993. **186**(3): p. 643-651.
11. Stern, E.J. and M.S. Frank, *CT of the lung in patients with pulmonary emphysema: diagnosis, quantification, and correlation with pathologic and physiologic findings*. *American Journal of Roentgenology*, 1994. **162**(4): p. 791-798.
12. Takahashi, M., et al., *Classification of Centrilobular Emphysema Based on CT-Pathologic Correlations*. *The Open Respiratory Medicine Journal*, 2012. **6**: p. 155-159.
13. Washko, G.R., G. Parraga, and H.O. Coxson, *Quantitative Pulmonary Imaging Using Computed Tomography and Magnetic Resonance Imaging*. *Respirology (Carlton, Vic.)*, 2012. **17**(3): p. 432-444.
14. Nicholas, J.S., et al., *Closed-Loop Perfusion Fixation For The Validation Of Quantitative Computed Tomography (QCT) Metrics*, in *C36. IMAGING AND THE LUNG: A RAPIDLY EVOLVING FIELD*. 2014, American Thoracic Society. p. A4309-A4309.
15. Hsia, C.C.W., et al., *An Official Research Policy Statement of the American Thoracic Society/European Respiratory Society: Standards for Quantitative Assessment of Lung Structure*. *American Journal of Respiratory and Critical Care Medicine*, 2010. **181**(4): p. 394-418.
16. Jiang, S., et al., *Tri-linear interpolation-based cerebral white matter fiber imaging*. *Neural Regeneration Research*, 2013. **8**(23): p. 2155-2164.

17. Matsuoka, S., et al., *Quantitative CT Assessment of Chronic Obstructive Pulmonary Disease*. RadioGraphics, 2010. **30**(1): p. 55-66.
18. Guo, J., et al. *Integrated system for CT-based assessment of parenchymal lung disease*. in *Biomedical Imaging, 2002. Proceedings. 2002 IEEE International Symposium on*. 2002.
19. Knudsen, L., et al., *Assessment of air space size characteristics by intercept (chord) measurement: an accurate and efficient stereological approach*. J Appl Physiol (1985), 2010. **108**(2): p. 412-21.
20. Vasilescu, D.M., et al., *Stereological assessment of mouse lung parenchyma via nondestructive, multiscale micro-CT imaging validated by light microscopic histology*. Journal of Applied Physiology, 2013. **114**(6): p. 716-724.